Leveraging Molecular Pharmacological Principles for the Design of Novel Treatments for Drug Addiction and Mood Disorders

Carlie Neiswanger

A dissertation

submitted in partial fulfillment of the

requirements for the degree of

Doctor of Philosophy

University of Washington

2024

Reading Committee:

Charles Chavkin, Chair

Benjamin Land

Susan Ferguson

Program Authorized to Offer Degree:

Pharmacology

University of Washington

Abstract

Leveraging Molecular Pharmacological Principles for the Design of Novel Treatments for Drug Addiction and Mood Disorders

Carlie Neiswanger

Chair of the Supervisory Committee:

Charles Chavkin

Department of Pharmacology

The dynorphin/Kappa opioid receptor (KOR) system has been implicated in the regulation of stress, anxiety, depression, and substance use disorders. KOR antagonists have great potential as a therapeutic for these disorders, but the culmination of preclinical work over the last two decades has made for very little success in the clinic. The work here aims to identify and design a repeated dosing regimen to use with partial and G-biased KOR agonists. These agonists, specifically nalfurafine and nalmefene, activate the G-protein mediated JNK-ROS pathway that leads to long-term inactivation seen with norBNI and JDTic. Using a new tool, oROS-Gr, ROS generation was detected in ex vivo slice and in vivo fiber photometry with the treatment of these agonists. Repeated dosing caused significant KOR inactivation and blocked stress-induced aversion and aversion during opioid-withdrawal mediated by the dyn/KOR system. Low dosing combined with

previously demonstrated high degree of safety profiles for nalfurafine and nalmefene make them promising new options for the treatment of substance use and mood disorders in humans.

ACKNOWLEDGEMENTS

Thanks to Dr. Charles Chavkin for teaching me the important traits needed for success in science and demanding excellence while also making room for understanding.

Thanks to Dr. Ben Land for being the voice of reason during my panic moments and the voice of irrationality when I got too uptight.

Thanks to Katie Reichard, Harrison Fontaine, and Antony Abraham for welcoming me into the lab so that I never felt like an outsider.

Thanks to Kandace Kimball and Mickey Ruiz for letting me teach you what I knew and teaching me in return. You are the best students and friends anyone could ask for.

Thanks to my committee members and the NAPE center for supporting my work and allowing me to grow in this community.

Thanks to Lusine Eyde, Selena Schattauer, and Charles Zhou for listening to my thoughts, problems, fears, and successes with such love and understanding.

Thanks to my family, my husband, and my daughter for the unending support in my endeavors.

DEDICATION

To my daughter, Kiara Rex.

May my success be yours and inspire you to let passion lead your every step.

TABLE OF CONTENTS

Chapter 1

Why is norBNI long-lasting?

It has been four decades since the start of characterization of the kappa opioid receptor (KOR) and its endogenous ligand dynorphin (Chavkin et al., 1982; Han & Xie, 1984; Martin et al., 1976; Meng et al., 1993). Since then, KOR has been implicated in the regulation of stress, anxiety, depression, and substance-use disorders (Lalanne et al., 2014). This body of work is almost entirely preclinical and uses either gene knock-out models or the KOR antagonist, norbinaltorphimine (norBNI). NorBNI is selective for KOR with a long-lasting block of signaling for days to weeks (Horan et al., 1992; Jones & Holtzman, 1992). It appeared in the literature not long after it was made obvious that KOR offered its own regulation of neurobiological systems, separate from the mu and delta opioid receptors (Sayre et al., 1983; Shippenberg & Herz, 1986). The long-lasting, selective inactivation of KOR makes it a near-perfect tool for studying the effects of endogenous dynorphin as well as exogenous ligands. But what happens when norBNI is introduced into a biological system? The field has been either split, confused, or indifferent in terms of norBNI action for arguably too long. Because **this thesis aims to address both a continued characterization of KOR action and the ability to mimic the effects of norBNI for the treatment of mood and substance use disorders**, it is important to have as complete an understanding of the action as possible. Further, the exploration and identification of the intricacies of norBNI action are required for the advancement of KOR regulation and modulation for therapeutic use in humans.

As mentioned above, norBNI shows up in the literature not long after the delineation of opioid receptor subtypes (Martin et al., 1976) to address the need for a KOR selective antagonist as opposed to naloxone and naltrexone that act nonselectively for opioid receptors (Portoghese et al., 1987). While norBNI's receptor selectivity in vivo was not entirely agreed on (Birch et al., 1987), it became clear that its antagonistic action at KOR, while somewhat delayed, lasted on the scale of days instead of hours (Endoh et al., 1992; Jones & Holtzman, 1992). Indeed, it was indicated that KOR blockade was evident for an astounding 56 days after a single dose given i.c.v., with the simple assumption that norBNI physically remained in the brain for as long (Horan et al., 1992). To this day, there are some in the field that still assert that this is the case. However, there is more evidence to support a different explanation - irreversible inactivation of KOR via biased signaling.

During the 1980s, the concepts of "message-address" and "induced fit" were starting to be explored more readily (Nagase et al., 1998). These early ideas eventually led to the pharmacological principle of functional selectivity or biased signaling. Functional selectivity refers to the process in which a receptor undergoes different conformation changes based on the type of ligand bound to it. This leads to various signal transduction events that ultimately cause distinct biological responses (Urban et al., 2007). Possibly the best example of this is the characterization of the beta-blocker medication, Carvedilol. This drug, when compared to others of its class, can preferentially stimulate beta-arrestin-mediated signaling without increasing Gs-dependent adenylyl cyclase activity. This causes the treatment to be especially effective

since it does not create a push-and-pull stimulation versus inhibition and leans heavily toward just inhibition (Wisler et al., 2007).

Functional selectivity has shifted the Receptor Theory dogmas in the field of pharmacology. Traditional Receptor Theory suggests streamlined definitions of agonists (full or partial) that activate all downstream effectors. In contrast, classical antagonists block endogenous or exogenous ligands from further activating the receptor or decreasing typical receptor activity (also known as inverse agonists). Such definitions are great for teaching introductory pharmacology but fail to capture the true depth required to understand ligand-receptor interactions.

It's difficult to overstate how meaningful the principle of functional selectivity has been for opioid receptor pharmacology. Determining the downstream effects of biased mu-opioid receptor (MOR) ligands for example may hold promise for strong analgesics without the extremely debilitating side effects of respiratory depression, tolerance, and dependence. Thus far, however, it seems that the complexity of effects related to each major pathway (G-protein versus beta-arrestin dependent) remains unclear, with a strong possibility that the sought-after clinical effects and unwanted side effects are both mediated by the G-protein pathway (Kelly et al., 2023). Interestingly, even these major pathways have intricacies that suggest further complexity.

Functional selectivity also holds great promise for KOR ligands. It was suggested early in KOR research that agonists of the receptor offered an alternative to MOR agonists for

pain management since they did not cause the same euphoric effects as ligands like morphine or fentanyl. However, the ligand U50,488H, which had been used as the prototypical agonist to characterize KOR activation effects along with dynorphin, actually caused dysphoria along with analgesic effects (Shippenberg & Herz, 1986; Von Voigtlander & Lewis, 1982). Quickly, the need for a biased KOR agonist was identified, and compounds like TRK-820 (now known as nalfurafine) were designed for their selectivity and ability to cause analgesia without induction of dysphoria (Nagase et al., 1998). This is a great example of the early use of functional selectivity in drug design. Indeed, Nagase et al., (1998) knew that they wanted the “address” (in the “message-address concept) of norBNI to recreate its KOR selectivity, but with the “message” of an agonist. The fate of nalfurafine was to become an anti-itch drug restricted to the use in Japan (another KOR-mediated biological effect) for the treatment of uremic pruritus associated with kidney failure (Inui, 2015), but this won’t be the last we hear of it. To date, there has been little success in developing KOR analgesics for human use.

A unique aspect of KOR signaling was demonstrated by McLaughlin et al., in 2003 showing that immobility resulting from repeated force swim stress (rFSS) in mice could be blocked by norBNI and that the same rFSS could cause norBNI-sensitive potentiation of cocaine reward. This finding essentially changed norBNI from a tool used to elucidate KOR functionality to a possible antagonist of stress-related behavior and gave rise to the proposal that KOR antagonism had therapeutic potential for the treatment of addiction and depression. Following this, studies identified a whole host of

stress, depression, anxiety, and drug abuse behaviors that are KOR-mediated. (More on this topic will be covered in Chapter 5.)

Focusing on the molecular mechanisms of KOR-mediated behaviors, it was determined that sustained activation results in G protein-coupled receptor kinase (GRK3) activation and recruitment of beta-arrestin 2, which was responsible for the aversive properties of KOR (unbiased) agonists. This cascade is considered the G protein-independent pathway, meaning that it does not occur through direct interaction with the G protein subunits. In contrast, KOR-mediated analgesic and anti-pruritic effects occur through the G-protein dependent pathway through activation of the Gi-alpha subunit and dissociation of the βγ subunit, leading to activation of G-protein activated inwardly rectifying potassium (GIRK) channels and inhibition of voltage-gated calcium channels. These two pathways, resulting in analgesia and aversion, are the basis for our understanding of the biological effects of KOR activation. However, the complexity increases from there.

In the early 2000s, evidence was emerging that KOR activation stimulates mitogen-activated protein kinase (MAPK) pathways. Specifically extracellular signal-regulated kinase (ERK1/2), p38 MAPK, and c-Jun N-terminal kinase (JNK) (Bruchas et al., 2006; Kam et al., 2004). These downstream effectors held promise for a better explanation of what may be causing the long-term block of KOR signaling seen with antagonists like norBNI, JDTic, and GNTI. As mentioned above, the predominant explanation at the time was that norBNI and similar antagonists physically persisted for the 3-4 weeks that

inhibition was observed. However, these antagonists were reversible and noncompetitive, failing to covalently bond to KOR (Smith et al., 1990). Using receptor protection assays, Bruchas et al., (2007b) showed that pretreatment with readily reversible opioid antagonist naloxone and buprenorphine could inhibit long-lasting norBNI action, indicating that norBNI did not persist at the site of action. Furthermore, after in vivo treatment with norBNI, the agonist site of the receptor remained intact, suggesting that a different functional disruption may occur due to these antagonists. They were then able to show that JNK phosphorylation could be stimulated by both norBNI and JDTic in a KOR-dependent manner and that direct inhibition of JNK attenuated norBNI long-term antagonism (Bruchas et al., 2007b). This pointed to JNK being the primary mediator for the long-acting effects of norBNI-like functional antagonists. It also suggested that instead of norBNI being a classical antagonist, it was instead a “collateral” agonist, causing activation of a specific pathway that eventually led to downstream inactivation. Still to be determined though was how JNK might be interacting with KOR to cause receptor inactivation. It was hypothesized that a hypothetical substrate of JNK (called “Jammer” or JNK Modulated Regulator (JMR)) was sterically blocking the G protein association (Figure 1.1) (Bruchas & Chavkin, 2010).

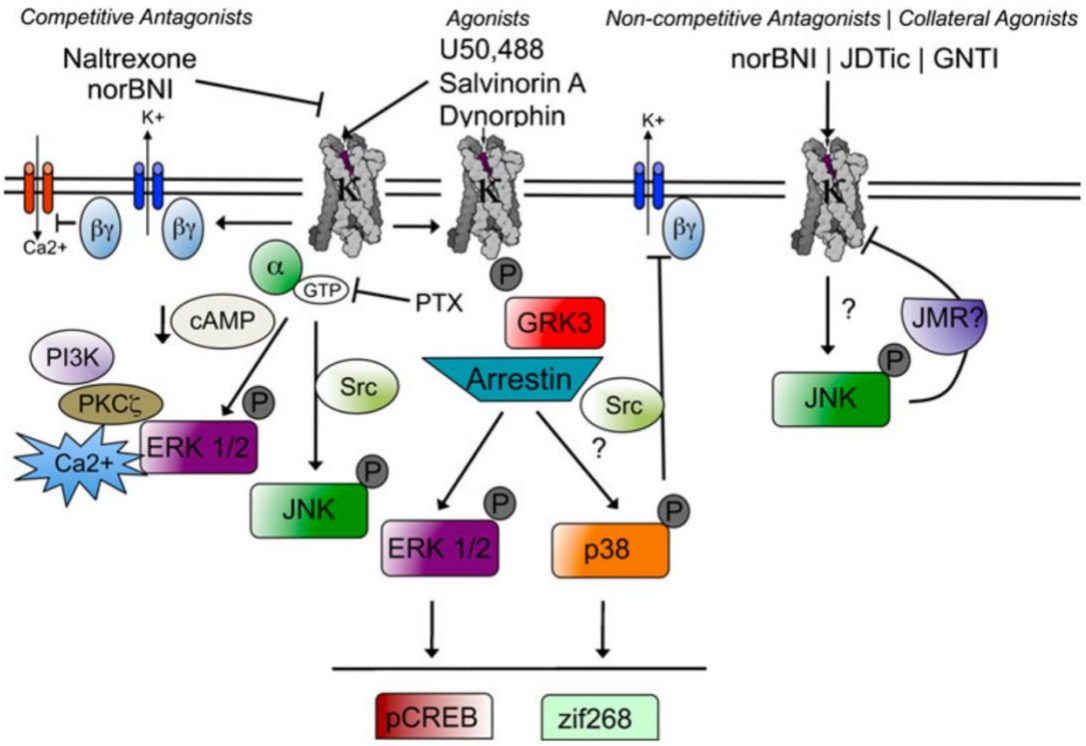

Figure 1.1. KOR-mediated signal transduction highlighting the hypothetical missing piece "JMR". (from (Bruchas & Chavkin, 2010).)

As more exploration into MAPK pathways activated by opioid signaling was underway, it was determined that ERK1/2 had an “early” and “late” stage activation in KOR. The early stage of this bi-phasic effect was arrestin-independent while the late stage was arrestin-dependent (Bruchas et al., 2006; Schattauer et al., 2012), suggesting tight MAPK control in response to signaling. It was also demonstrated that p38 MAPK was responsible for the aversive properties of KOR activation, shown by lack of effect when inhibited or knocked out of either the VTA (DA cells) or DRN (5-HT cells) (Bruchas et al., 2011; Ehrich et al., 2015). In MOR, JNK was shown to have pathway specificity as well. Acute tolerance due to the administration of morphine could be blocked by JNK inhibition while fentanyl could be blocked by GRK3 knock-out, but not the other way around (Melief et al., 2010). In addition, the duration of KOR antagonism of various ligands was positively correlated with JNK activation (Melief et al., 2011). These data further suggested that JNK activation is both ligand-dependent and responsible for KOR long-term inactivation.

In 2017, Schattauer et al. published an important study identifying the elusive “Jammer” that was proposed previously (Bruchas & Chavkin, 2010). In this work, iterative, discovery-based proteomics was employed to identify the pJNK-dependent recruitment of peroxiredoxin 6 (PRDX6) to the opioid receptor complex. Then, using a CellROX Green detection assay, the study determined that reactive oxygen species (ROS) were generated by treatment with norBNI in KOR-expressing cells, and by morphine, but not fentanyl, in MOR-expressing cells. This was consistent with the specificity for JNK phosphorylation using morphine that had been previously shown (Melief et al., 2010).

The generation of ROS by norBNI in KOR could be blocked by inhibition of ROS, PRDX6, or JNK. Similarly, the generation of ROS could be blocked in MOR cells with inhibition of JNK. These effects were also shown in vivo using KOR- and MOR-mediated analgesia. The ability of norBNI to block KOR-mediated analgesia long-term was reversed by the PRDX6 inhibitor MJ33 and partially reversed by antioxidant treatment. Acute analgesic tolerance to morphine, but not fentanyl, could also be reversed by pretreatment of MJ33. Lastly, it was shown that the same block of ROS generation and acute tolerance could be achieved in D2 dopamine receptors when pretreatment with MJ33 and that JNK-mediated cross-tolerance was observed in cells co-expressing KOR and D2 dopamine receptors. The hypothesis generated based on these findings was that ROS generated from increased NADPH-oxidase activity oxidizes a palmitoylated cysteine residue (Cys3) on the $G\alpha_i$, depalmitoylating it and causes a tighter association between the G-protein and the receptors. This would prevent the exchange of GDP and GTP necessary for conformational change and subsequent Gβγ subunit release (Schattauer, et al., 2017).

Together, the results of this study suggested several important aspects of GPCR signaling. Firstly, it identified the downstream regulators of JNK-mediated long-lasting KOR inactivation and acute MOR tolerance to morphine-like drugs. After phosphorylation of JNK, PRDX6 is recruited to the receptor complex, PLA2 activity is increased, and NADPH-oxidase activity is increased leading to the generation of reactive oxygen species. Secondly, the study demonstrated that this mechanism is not limited to opioid signaling but can be shown in D2 dopamine receptors and has been

suggested for other GPCRs as well (Chatterjee et al., 2011). Lastly, the effects of JNK-mediated generation of ROS may not be localized to the receptor responsible for the generation and instead may be able to cause cross-tolerance or cross-inactivation with nearby receptors. In a follow-up study, it was shown that there is a biphasic activation of JNK following treatment of U50,488 and that early phase JNK phosphorylation, but not late phase, is arrestin-independent and causes ROS generation. U50,488 elicited an inverted U-shaped dose-response curve of ROS generation. Genetic modification of the receptor to prevent the GRK3/arrestin binding or inhibition of p38 MAPK caused U50,488 to instead dose-dependently increase ROS generation (Schattauer et al., 2019). This study helped to complete our understanding of how this pathway is responsible for long-term inactivation with norBNI and JDTic and why those same inactivating effects are absent with endogenous dynorphin signaling. It can be concluded from this work that sufficient activation of the GRK3/arrestin-dependent pathway and downstream phosphorylation of p38 MAPK inhibits ROS generation and receptor inactivation.

One of the remaining intricacies of norBNI action and KOR signaling as a whole lies in observed sex differences. Studies have suggested decreased KOR-mediated analgesic efficacy in female humans and animals that may be linked to genetic difference or, more likely, sex specific hormones (Craft, 2008; Mogil et al., 2003; Stoffel et al., 2005). We know from the previously mentioned work that KOR analgesia is a G-protein pathway-mediated effect. Consistent with that, it was demonstrated that male and female mice show similar KOR-mediated aversion (GRK/arrestin pathway), but KOR-mediated

analgesia was only present in males. This insensitivity to analgesic effects was reversed by ovariectomy, GRK2/3 inhibition, and the low estrogen estrous cycle state (estrus). The phosphorylated, inhibitory form of GRK2 was found to be elevated in female mice and estradiol increased the association of GRK2 and Gβγ (Abraham, et al., 2018). Taken together, these results suggest that estrogen increases the phosphorylation of GRK2, which then interacts with Gβγ to inhibit the G-protein dependent pathway. Similarly, it was found that female mice are insensitive to the long-lasting KOR antagonism of norBNI, and that this insensitivity can be overcome by a block of GRK2 or by repeated low-dose administration of norBNI (Chavkin et al., 2019; Reichard et al., 2020). These findings corroborate the previous results that show norBNI action as being G-protein pathway-mediated.

The evidence presented here (summarized in Table 1), especially that of the last two decades, has shaped our understanding of norBNI action. With this extensive characterization, I believe that we can leverage the concepts of functional selectivity and JNK-ROS-dependent KOR inactivation to design novel treatments for dyn/KOR induced anhedonia associated with drug addiction and mood disorders.

Table 1.1

Evidence of proposed mechanism of norBNI	**Publications**
ERK1/2 early phase activation and p38 late phase activation	Bruchas et al., 2006; Schattauer et al., 2012
Protection from long-term inactivation with short-acting, competitive inhibition	Bruchas et al., 2007
G-protein pathway-dependent JNK phosphorylation and correlation with duration of inhibition	Melief et al., 2011
JNK-, PRDX6-dependent ROS generation and subsequent long-term inactivation	Schattauer et al., 2017
Arrestin-dependent pathway/p38 MAPK block of JNK activation	Schattauer et al., 2019
Inconsistent KOR agonist effects in females due to GRK2-estrogen interaction during acute high estrogen state	Abraham et al., 2018; Reichard et al., 2020
Accumulation of effect	Chavkin et al., 2019; Reichard et al., 2020

Chapter 2

Microdosing G-biased Partial Agonists Inactivates Kappa Opioid Receptors - an alternative strategy for human therapeutics.

Authors: Carlie Neiswanger, Micaela V. Ruiz, Kandace Kimball, Justin D. Lee, Benjamin Land, Andre Berndt, and Charles Chavkin

This chapter is currently being prepared for submission for publication in a peer-reviewed journal.

Introduction

An essential role for endogenous dynorphin opioids in regulating mood and addiction risk has been suggested by extensive preclinical studies during the last two decades (Chavkin, 2011, 2013; Knoll & Carlezon, 2010; Schwarzer, 2009; Zhang et al., 1998). Pharmacological and genetic disruption of dynorphin actions in the rodent brain block depression-like and anxiety-like behaviors (Bruchas et al., 2009; Carr et al., 2010; Chartoff et al., 2012). Stress-induced release of endogenous dynorphins potentiates the rewarding effects of addictive drugs (e.g. cocaine, ethanol, nicotine, and morphine) (Ehrich et al., 2014; Schindler et al., 2012; J. S. Smith et al., 2012; Walker & Koob, 2008). Stress-induced reinstatement of drug self-administration is blocked by kappa opioid receptor (KOR) antagonists (Beardsley et al., 2005), and KOR antagonists block the dysphoric effects evident during opioid, nicotine, and ethanol abstinence (Chavkin, 2018; Jackson et al., 2010, 2015). Stress exposure has been shown to increase the risk of mood and substance use disorders in humans (Calabrese et al., 2009; Lijffijt et al.,

2014), and these preclinical studies strongly suggest that KOR antagonists could be therapeutically useful in promoting stress resilience in vulnerable people. However selective, safe, and effective KOR antagonists for human studies are still being developed, and the role of dynorphin in human pathophysiology is not yet established.

The majority of the preclinical studies cited have been done using the selective KOR antagonists norbinaltorphimine (norBNI) or JDTic (Lalanne et al., 2014). Although these drugs are competitive KOR antagonists in vitro, they both have the unusual properties of delayed onset of action and very long durations of effect when given in vivo; for example, a single injection of norBNI in rodents or nonhuman primates can block KOR activation for weeks (Endoh et al., 1992). The mechanism for this long duration was initially unclear and attributed to the very slow clearance of the drug from the brain (a pharmacokinetic mechanism) (Horan et al., 1992). However, a detailed analysis of the molecular pharmacology revealed that both norBNI and JDTic are not conventional antagonists; rather they are functionally selective KOR agonists that activate cJun N-terminal Kinase (JNK) which recruits the phospholipase peroxiredoxin 6 (PRDX6) to the plasma membrane; PRDX6 bound to KOR stimulates NADPH to locally generate reactive oxygen (ROS) which oxidizes the sulfhydryl in cysteine residues and depalmitoylated the G-protein, Gαi. The depalmitoylated Gαi binds more tightly to KOR and prevents receptor activation (Figure 1; (Schattauer et al., 2019)). Pharmacological inhibition of the JNK or PRDX6 components in this signaling pathway or genetic deletion of *JNK-1* blocked the long duration of norBNI action (Bruchas et al., 2006; Melief et al., 2010; Schattauer, Land, et al., 2017). In this context, the agonist or antagonist label is

confusing, and norBNI-like ligands are better described as ***KOR-inactivating agents***. This series of molecular characterization studies helped establish that there are four different types of functionally selective KOR ligands (Fig. 2.1).

A. Highly efficacious agonists

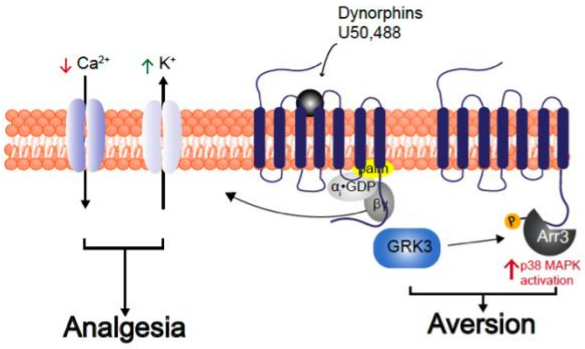

B. Competitive antagonists

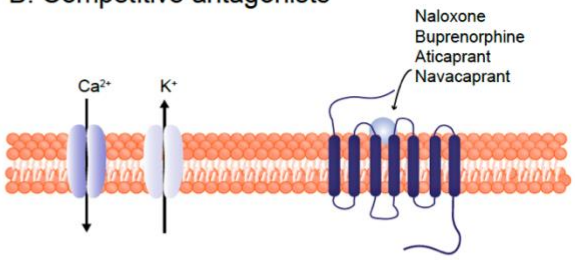

C. Functionally selective, G-biased partial agonists

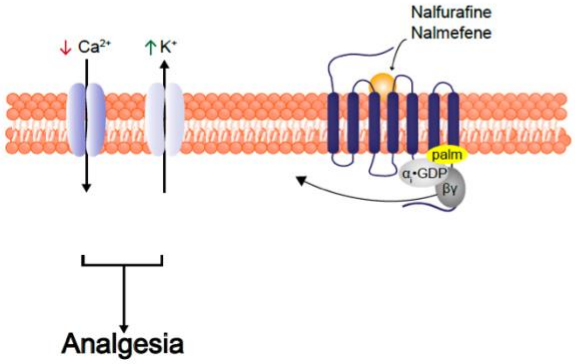

D. Long-lasting, functionally selective antagonists

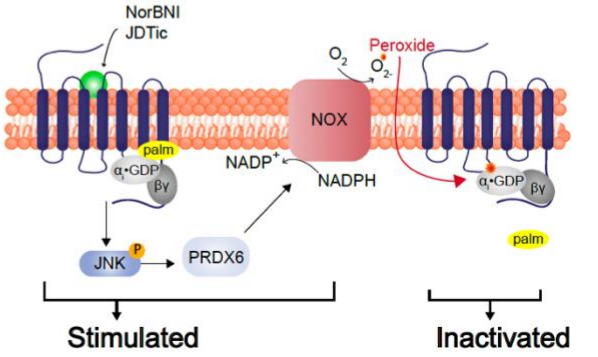

Figure 2.1: An overview of major pathways in the functionally selective signaling cascade of the kappa opioid receptor. **A)** Highly efficacious agonists like U50,488, and the endogenous peptide dynorphin cause analgesic effects through a G-protein dependent pathway and dysphoric effects through a G-protein independent, beta-arrestin/GRK3 pathway. p38 MAPK is required for this dysphoria. **B)** Competitive antagonists such as naloxone bind to the active site of the receptor and prevent agonists from binding. **C)** Biased and partial agonists cause conformational changes that lead to the g-protein pathway being activated preferentially or the GRK3/arrestin pathway being activated weakly. **D)** Long–lasting functional antagonists like norBNI activate the G-protein pathway preferentially but do not elicit analgesia. Instead, they activate a cascade that leads to the phosphorylation of c-Jun N-terminal kinase (JNK), recruitment of PRDX6, increased activity of NADPH oxidase, and generation of reactive oxygen species (ROS). ROS then causes the oxidation of cys-3 on the Gα subunit and blocks repalmitoylation of the residue, causing inactivation from the lack of ability to exchange GDP for GTP. This inactivation is irreversible and the receptor has to be resynthesized before it can be activated again, leading to the ~3-week antagonist effect of norBNI and JDTic. The functional selectivity of drugs binding to G protein-coupled receptors (GPCRs) is now a well-established pharmacological principle (Urban et al., 2007), but the functional selectivity of KOR ligands are particularly impressive. Highly efficacious KOR agonists (e.g. dynorphins, U50,488, salvia divinorum, and others) produce their responses by activating Gαi/o-protein signaling to produce analgesia, sedation, inhibition of itch, and psychotomimetic effects (Dalefield et al., 2022). Sustained receptor activation by high-efficacy KOR agonists results in G-protein receptor kinase (GRK3) activation and β-arrestin binding to the C-terminally phosphorylated KOR (McLaughlin et al., 2003). β-Arrestin binding to the cytoplasmic face of KOR sterically inhibits G-protein activation (causing acute receptor desensitization and receptor internalization) and receptor-bound β-arrestin acts as a scaffold to enable KOR activation of mitogen-activated kinases (MAPKs) (Bruchas & Chavkin, 2010; McLaughlin, Xu, et al., 2003). GRK3/arrestin-dependent activation of p38α MAPK results in the dysphoric effects of high-efficacy KOR agonists through mechanisms involving the inhibition of serotonin and dopamine signaling (Bruchas et al., 2011; Ehrich et al., 2015). In contrast, competitive KOR antagonists bind to the receptor with little or no signaling efficacy (Fig. 2.1B). Competitive KOR antagonists include drugs lacking receptor selectivity (e.g. naloxone, naltrexone, buprenorphine) and the recently developed receptor-selective KOR antagonists Aticaprant and Navacaprant (Hampsey et al., 2024; Kormos et al., 2018).

A fourth group of functionally selective KOR ligands includes nalfurafine, which is a highly efficacious but G-biased KOR agonist (Huskinson et al., 2022; Schattauer, Kuhar, et al., 2017), and nalmefene, which is a low-efficacy KOR partial agonist (Browne et al., 2020; Windisch et al., 2021) (Fig. 1C). Neither nalfurafine nor nalmefene efficiently activate GRK3/arrestin-dependent desensitization mechanisms (Liu et al., 2019; Windisch et al., 2018). In consequence, neither produces the dysphoric effects of highly efficacious KOR agonists at analgesic doses. Another important distinction is that the activation of p38α MAPK by the highly efficacious KOR agonists inhibits cJun Kinase and prevents long-lasting receptor inactivation (Schattauer et al., 2019). Based on this insight, we hypothesized that nalfurafine and nalmefene which do not efficiently activate either GRK3 or p38α MAPK might produce a norBNI-like long-lasting inactivation of KOR. The results presented in this study support this prediction. Because both nalfurafine and nalmefene have long histories of safe use in humans (Chick et al., 2021; Inui, 2015), they could conceivably be repurposed as medications to block KOR and promote stress resilience for the adjunctive treatment of mood disorders and drug addiction.

Methods

Animals

C57BL/6 wild-type (WT) male and female mice 8-24 weeks of age were used for behavioral experiments (Charles River). KOR-cre mice were ear punched at least 21 days after birth and genotyped using Transnetyx genotyping services. PCR screening was performed for the presence of cre recombinase. Surgeries performed on KOR-cre

mice occurred between 5 and 7 weeks of age. All animal studies were approved by the University of Washington IACUC.

Drugs

Nalfurafine (NIDA Drug Supply Program), nalmefene (Tocris), norBNI (NIDA Drug Supply Program), U50,488 (Tocris), naloxone (Tocris), and MJ33 (Sigma Aldrich) were dissolved in saline and administered intraperitoneally. Estradiol (50ug/kg; Cayman Chemical) was dissolved following a previously described procedure (Abraham et al, 2018) in 0.1% ethanol/ 0.1% Cremophor EL/ 99% saline and administered subcutaneously in a volume of 10ml/kg. Progesterone (5 mg/kg; ThermoFisher) was dissolved in 0.1% ethanol/ 0.1% Cremophor EL/ 99% saline and administered subcutaneously in a volume of 10 ml/kg.

Stereotaxic injection

Male KOR-cre mice between 5-7 weeks were anesthetized with 2.5% isoflurane and head fixed on a Kopf Model number stereotaxic alignment system. After the incision to expose the skull, bregma was determined and a drill was used at the appropriate coordinates (see below) to allow for needle entry. A 2.0uL model 7002 KH Neuros Syringe (Hamilton, NV, USA) was lowered for viral injection of 0.5 uL of AAV1-FLEX-oROS-mCherry. For in vitro brain slice experiments, bilateral injection into the VTA using coordinates: ML: +/- 0.5mm, AP: -3.28mm, DN: -4.5mm, and for fiber photometry experiments, unilateral injection using coordinates AP: -3.28 mm, ML: -1.71 mm, DV: -4.67 mm at a 15-degree angle. An implantable fiber optic cannula (400/430 core, 0.57

NA; Doric Lenses, Quebec, CA) was placed at the same coordinates as the viral injection site, and then C&B meta bond was used to secure the cannula to the skull. After injection, the needle was kept at the injection site for 5 minutes before removal. All mice were monitored and given carprofen (dose) daily for 7 days for post-surgical analgesia.

Fiber photometry

Briefly, a real-time signal processor (RZ5P; Tucker-Davis Technologies) was connected to Synapse Software (Fiber Photometry) to set the frequency of light stimulation and record input from photodetectors as described (Abraham 2021). The RZ5P was connected to a light-emitting diode (LED) driver (Doric Lenses) that controlled the power of a 465 nm and 560 nm Doric LED. A low autofluorescence patch cord (400/430 nm) was attached to the LED, to a fluorescent MiniCube (Doric Lenses) with dichroic mirrors. Connected optical patch cords to the MiniCube with pigtailed rotary joining (FRJ; Doric Lenses) allowed free animal movement during data collection. Patch Cords were bleached with light before photometry sessions to minimize autofluorescence. The power of the LED at the fiber tip was set to ~30 μW and was tested before the start of each session. Fluorescent signals were collected at a sampling frequency of 1017 Hz. Each of the sessions was down-sampled by a factor of 100 and normalized to a fifteen-minute baseline period at the beginning of the recording. The sessions were then smoothed using a moving average filter (100s window) to remove high-frequency noise and detrended to remove linear drift. The isobestic channel (405 nm) was fitted to the 470 nm channel using a least-squares method and subtracted to remove motion

artifacts. Each session started with a 15-minute baseline recording period before pharmacological experiments to calculate fluorescent change from baseline (ΔF/F; Change in fluorescence from baseline fluorescence/baseline fluorescence). For in vivo experiments, mice were run with all conditions on separate days. Mice received Saline, 100 µg/kg Nalfurafine, and 10 mg/kg Naloxone. For 100 µg/kg Nalfurafine experiments, after baseline, the recording session lasted for 45 minutes. For 10 mg/kg naloxone pretreatment to 100 µg/kg Nalfurafine experiments, after baseline, mice were given administration of naloxone, and after 15 minutes 100 µg/kg Nalfurafine was administered. Mice were allowed to freely explore the chamber during in vivo experiments.

Estrous cycle determination

Vaginal lavage for the estrous cycle stage determination was done following behavioral testing. 50 µL of DI water was pipetted to collect cells and placed on glass slides for cytology. The estrous cycle stage was classified using the estrous cycle identification tool (Byers et al., 2012) and then quantified by the relative ratio of nucleated epithelial cells, cornified epithelial cells, and leukocytes. Cytology was determined with the investigator blind to treatment.

Hormone treatment

Female mice were injected subcutaneously with progesterone or estradiol. 3 days after, the mice were tethered for fiber photometry (as described above) and given an intraperitoneal injection of Nalfurafine (100 µg/kg) to measure oROS response. Estrous

states were determined after the recording session. Following lavage, mice were given a second subcutaneous injection of the treatment they received prior and 3 days after, repeated the assessment of their estrous state and fiber photometry experiments. Both treatment groups had a two-week recovery period with no treatment. Following the recovery period, the treatment groups switched. Data analyses were done by an investigator blinded to treatment.

Slicing

Brains were collected 2-4 weeks after viral injection and 200 μm horizontal sections were obtained using a vibratome in NMDG cutting solution (92 mM NMDG, 2.5 mM KCl, 1.25 mM NaH_2PO_4, 30 mM $NaHCO_3$, 20 mM HEPES, 25 mM Glucose, 2 mM Thiourea, 5 mM Na-ascorbate, 3 mM Na-pyruvate, pH to 7.4, 0.5 mM CaCl•4H2O, 10 mM MgSO4•7H2O). Sections are then placed in NMDG solution at 32^{o} C for 15 minutes then incubated for an hour in room temperature HEPES solution (92 mM NaCl, 2.5 mM KCl, 1.25 mM NaH_2PO_4, 30 mM $NaHCO_3$, 20 mM HEPES, 25 mM Glucose, 2 mM Thiourea, 5 mM Na-Ascorbate, 3 mM Na-Pyruvate).

Imaging

Image collection was done on a Bruker Investigator 2-photon microscope, with software Prairie View 5.5, simultaneously collecting both the mCherry (1040 nM fixed) and GFP (920 nM tunable) signals with a Nikon 16X water immersion objective, as well as a z-stack spanning 60 μm across an hour time course. During this collection time a baseline is established for 7 minutes in ACSF buffer solution (124 mM NaCl, 3 mM KCl, 2 mM

$MgSO_4$, 1.25 mM NaH_2PO_4, 2.5 mM $CaCl_2$, 26 mM $NaHCO_3$, 10 mM Glucose) or ACSF with (1 uM) naloxone, (10 uM) MJ33, or (1 uM) JNK-IN-8 at 32oC followed by wash on the treatment with 100 nM nalfurafine, 10 uM nalmefene, or those in addition to previously mentioned inhibitors for 30 min, followed by H_2O_2 (590 uM) for 5 minutes. Analysis was completed by creating a hyperstack in ImageJ and then creating a Z-projection for both signal channels. Regions of interest (ROIs) were drawn broadly over the entire slice and values were collected using ImageJ for each channel with the same ROI. The mCherry signal value was subtracted from the GFP signal value and the resulting data were fit so that the lowest value was adjusted to be 1. Then a ΔF/F was calculated using the average value of the baseline (7 minutes of buffer solution, or 7 minutes of only inhibitor treatment) for the rest of the time course.

Confocal images

Horizontal images were collected using slices that underwent 2Photon imaging and were put into 10% formalin after the H_2O_2 wash. Confocal images are taken with the Leica SP8x Confocal microscope located in the Keck Center at UW.

Warm water tail withdrawal

Mice were tested for U50,488 analgesic response using a warm water tail withdrawal test as previously described (Bruchas et al., 2007). Briefly, a water bath is brought to 52.5^{o}C and maintained. Mice were wrapped in paper towels and roughly ⅓ to ½ of their tail was submerged in the water. The latency for tail removal was taken by stopwatch and recorded to 1/100th of a second. This was performed for 3 trials separated by no

less than 8 seconds. After the initial trials, mice were treated with U50,488 (10 mg/kg) i.p., and the 3 trials were repeated at 30 minutes post U50,488 injection. Scores were calculated as the difference of the before and after trials, reflecting a positive number for increase. This assay was performed on mice after 7 days of daily norBNI, nalfurafine, nalmefene, or saline treatment and was repeated 7 days post-last treatment for 7-day recovery experiments or on days 0, 3, 7, 14, 21, and 28 post-treatment for 28-day recovery experiments.

Odorant-paired repeated forced swim stress

Mice were treated with saline, norBNI, nalfurafine, or nalmefene daily for 7 days. 7 days after their last treatment day mice were exposed to one 15-minute swim on day 1 and four 6-minute swims on day 2, in 30°C water, without opportunity for escape. Two minutes before each swim, Nestlets with 20 µl of imitation almond extract (Kroger, Cincinnati, OH) were placed in their home cage. During the forced swim test, each animal was simultaneously exposed to a Nestlett with 20 µl of almond extract 5–10 cm above the swim chamber. Each mouse experienced 5 odorant-swim pairings; control mice were exposed to the odorant without the swim pairing. Odorant-aversion test followed 24 hours after the last swim.

Odorant-paired precipitated fentanyl withdrawal

Mice were treated with saline, norBNI, nalfurafine, or nalmefene daily for 7 days. On day 4 of the 7-day treatment, Alzet$^{(R)}$ micro-osmotic pumps (Model 1007D) filled with either saline or fentanyl (2 mg/kg/day) were implanted under the skin between the scapula to

induce dependence. The pumps were removed after 7 days and mice were allowed recover for 2 days. On day 3 post-pump removal, they were given injections of 1 mg/kg naloxone, once in the morning and once in the afternoon, in the presence of a Nestlet containing 20 µl of imitation almond extract. Odorant-aversion test followed 24 hours and 7 days after naloxone pairing.

Odorant-aversion test

Mice underwent two types of odorant pairing; stress-odorant pairing in which almond scent was paired with repeated forced swim stress and withdrawal-odorant pairing in which almond scent was paired with two instances of naloxone-precipitated withdrawal (outlined above). Mice were pre-exposed to a 3-chamber Plexiglas box for 3 min before odorant pair conditioning. For the odorant-aversion test, mice were placed in a Plexiglas 3-chamber box with a quarter Nestlet containing 20 µl of almond extract placed on one far side of the chamber, and a quarter Nestlet with no scent placed on the far side of the other chamber. The session in the 3-chamber box was video recorded for 14 min and analyzed using Ethovision for the time spent in each zone. The odorant score was calculated by the time spent in the odor-paired chamber minus the time spent in the opposite chamber.

Statistical analysis

All data were analyzed using either one- or two-way ANOVA appropriate for variables. Post-hoc tests for multiple comparisons were performed to determine differences from controls.

Results

The novel sensor oROS-Gr detects increases in ROS generation in the presence of nalfurafine and nalmefene

We previously determined that nalfurafine stimulated cJun Kinase phosphorylation in KOR-expressing HEK293 cells by western blot analysis (Schattauer et al., 2019) and showed that nalfurafine could stimulate the KOR/JNK/PRDX6 pathway in KOR-expressing neurons in live slices of the ventral tegmental area (VTA) using the ROS sensor HyPerRed (Reichard et al., 2020). These responses required KOR expression and were blacked by KOR antagonists. However, HyPerRed has low sensitivity and slow kinetics; thus, we started by optimizing the ROS sensor using structure-based design as described (Lee et al., 2024 *in review)*. The resulting sensor oROS-Gr performed better in its enhanced “off” kinetics (Suppl figure) and was used to characterize ROS generation by nalfurafine and nalmefene in this study. Adult male KOR-cre mice were bilaterally injected in the Ventral Tegmental Area (VTA) with AAV1-DIO-oROS-Gr-mCherry virus (Fig. 2.2A). Horizontal ventral tegmental area slices were taken 2-4 weeks post viral injection to allow for expression. Live slice imaging was performed using 2-photon microscopy over a 50-minute time interval at 1 frame per minute. Both nalfurafine and nalmefene significantly increased oROS fluorescence by 45-50% (Fig. 2.2D-E). The fluorescence increase was blocked by the competitive opioid receptor antagonist naloxone (10 uM), the PRDX6 inhibitor MJ33, and the JNK inhibitor JNK-IN-8 (Fig 2.2D). The advantage of the 2-photon imaging in the in vitro slice

preparation is the single cell resolution (Fig 2.2C) and ability to control the drug and inhibitor concentrations in the perfusion buffer (Fig 2.2E).

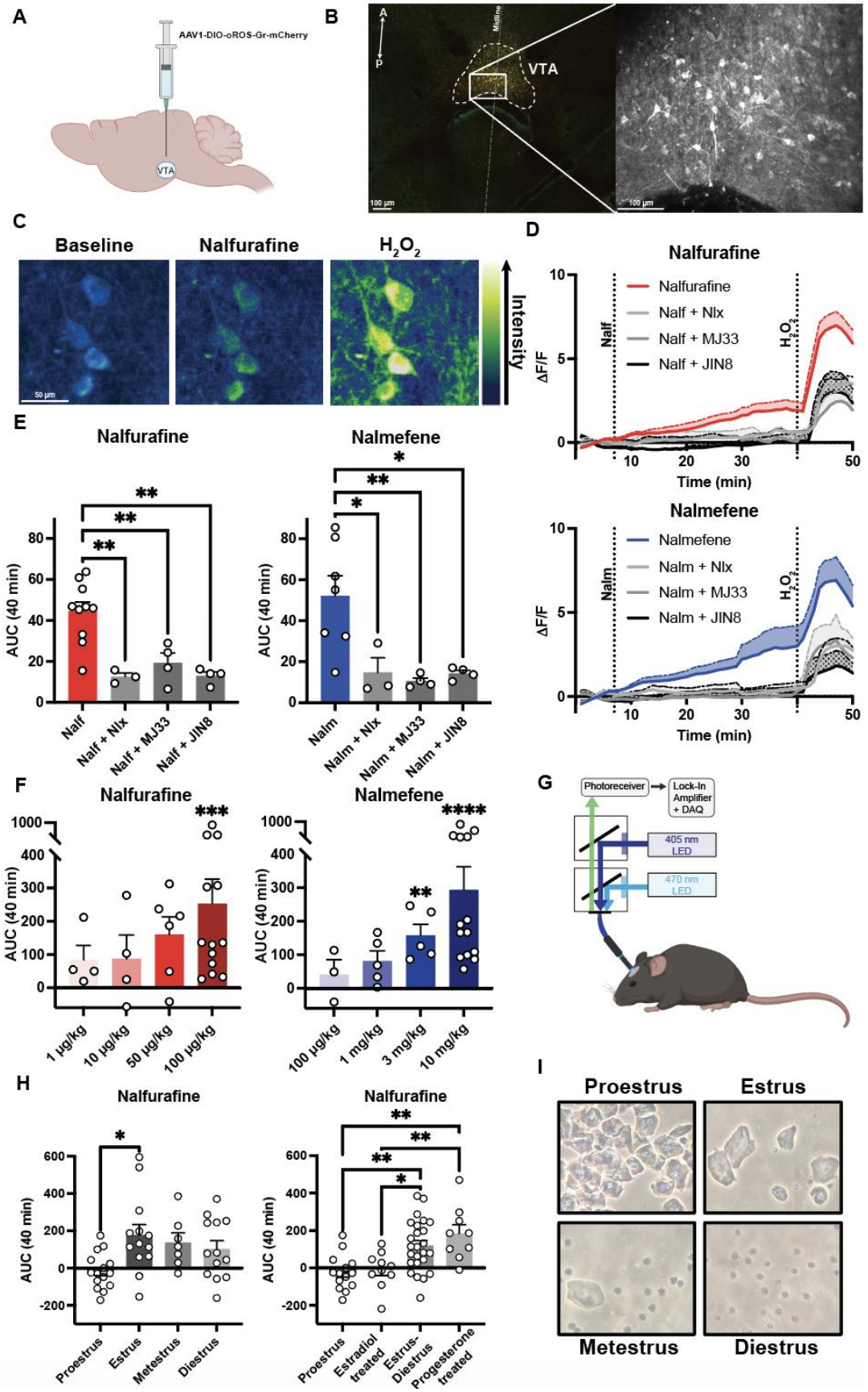
A
AAV1-DIO-oROS-Gr-mCherry
VTA
B
A
P
Midline
VTA
100 µm
100 µm
C
Baseline
Nalfurafine
H2O2
Intensity
50 µm
D
Nalfurafine
Nalfurafine
Nalf + Nlx
Nalf + MJ33
Nalf + JIN8
Nalf
H2O2
ΔF/F
Time (min)
Nalmefene
Nalmefene
Nalm + Nlx
Nalm + MJ33
Nalm + JIN8
Nalm
H2O2
ΔF/F
Time (min)
E
Nalfurafine
Nalmefene
AUC (40 min)
Nalf
Nalf + Nlx
Nalf + MJ33
Nalf + JIN8
Nalm
Nalm + Nlx
Nalm + MJ33
Nalm + JIN8
F
Nalfurafine
Nalmefene
AUC (40 min)
1 µg/kg
10 µg/kg
50 µg/kg
100 µg/kg
100 µg/kg
1 mg/kg
3 mg/kg
10 mg/kg
G
Photoreceiver
Lock-In Amplifier + DAQ
405 nm LED
470 nm LED
H
Nalfurafine
Nalfurafine
AUC (40 min)
Proestrus
Estrus
Metestrus
Diestrus
Proestrus
Estradiol treated
Estrus-Diestrus
Progesterone treated
I
Proestrus
Estrus
Metestrus
Diestrus

Figure 2.2: Nalfurafine and nalmefene cause ROS generation in a KOR-specific manner A) Cartoon visual of viral expression of oROS-Gr in the VTA of KOR-cre mice. **B)** *Left* Confocal image a horizontal VTA slice showing merged channels of the GFP sensor (green) and the mCherry tag (red). *Right* Representative 2-photon image of the same slice. **C)** Representative images using 2-photon microscopy of KOR+ cell bodies in the VTA with oROS expression under buffer only condition, with nalfurafine washed on for 20 min, followed by H_2O_2 for positive control **D)** Delta-F/F values for 50 min imaging sessions. Wash on of 100 nM nalfurafine (red) and 10 uM nalmefene (blue) both show clear increases in oROS fluorescence that can be blocked by naloxone, MJ33, or JNK-IN-8. Wash on of H_2O_2 at 40 min shows the sensor was adequately active by the end of the time course. **E)** AUC quantification of time course data from 0-40 min. **F)** AUC quantification of fiber photometry time course for 40 min after injection of various doses of nalfurafine and nalmefene in freely behaving male mice. Both drugs dose-dependently caused the generation of ROS. **G)** Cartoon visual of the fiber photometry setup used in (F). **H)** *Left* AUC quantification of time course data from 0-40 min after injection of 100 µg/kg nalfurafine in female mice measured at various points in the estrus cycle. Female mice show no response to nalfurafine at the high estrogen stage (proestrus). *Right* AUC 0-40 min in female mice pretreated with estradiol or progesterone compared to the cycle collapsed into high estrogen stage (proestrus) and low estrogen stages (estrus-diestrus). Pretreatment with estradiol mimics the proestrus stage and pretreatment with progesterone keeps the animals in the low estrus state, mimicking the low estrogen stages. **I)** Representative images of histology from vaginal lavage to determine estrus cycle stage.

Expression of oROS-Gr in the VTA was also imaged using in vivo fiber photometry (Fig 2.2F). Similar to the ex vivo slice results, we see an increase in oROS fluorescence with both nalfurafine and nalmefene and in a dose-dependent manner (Fig. 2.2G). The in vivo increase in oROS fluorescence was blocked by pretreatment with 10 mg/kg naloxone. These results confirm that both nalfurafine and nalmefene generate ROS through the KOR/JNK/PRDX6 signaling cascade in KOR-expressing VTA neurons.

KOR-induced ROS generation increase is estrus cycle dependent in female mice

It has been previously reported that female rodents have estrus state-dependent insensitivity to KOR activation because estrogen stimulates GRK2 to block G**βγ** signaling. Through this mechanism, estrogen blocked the long-lasting effects of norBNI (Abraham 2018, Reichard 2020). To determine if the activation of oROS was similarly affected, we expressed oROS-Gr in VTA neurons of adult female KOR-Cre mice and measured the fluorescence responses to nalfurafine during different estrus stages. Nalfurafine significantly increased oROS fluorescence during estrus (lowest estrogen state) but had no effect during proestrus (highest estrogen state) (Fig. 2H), consistent with what has been reported. To mimic these states, we pretreated females with either exogenous estradiol or progesterone and repeated the in vivo fiber photometry with the same dose of nalfurafine. Female mice pretreated with estradiol had no ROS response to nalfurafine, whereas female mice pretreated with progesterone had a robust increase in fluorescence after nalfurafine injection (Fig. 2I). These results confirm that female mice have estrus state-dependent insensitivity to KOR activation by nalfurafine

(comparable to norBNI) and that this can be overcome by progesterone. These findings have important implications as we advance to human trials with women subjects.

Repeated administration of nalfurafine and nalmefene blocks U50-induced analgesia in a JNK-pathway-specific manner

A single injection of 10 mg/kg norBNI completely inactivates KOR for weeks in mice (Bruchas et al., 2007). A single injection of a 100-fold lower dose of norBNI was ineffective, but daily injection of 0.1 mg/kg norBNI for 3 weeks produced KOR inactivation in both male and female mice (Chavkin, 2019). Presumably, the lower dose is able to inactivate a small percentage of the receptors and because recovery takes weeks, the inactivation accumulates. Reducing a drug dose by 100-fold reduces the risk of adverse and off-target effects and would be potentially advantageous in human trials. To determine the ability of nalfurafine and nalmefene to produce nor-BNI-like cumulative KOR inactivation, we injected various doses daily for 7-days then waited for 7 days to allow drug clearance before assessing the degree of KOR inactivation. Treatment of the mice for 7-days was chosen to simulate the future human Phase 1 clinical trial, however if the treatment advanced to therapeutics, we imagine that persons would continuously take the medication at an even lower dose (to be determined).

We used the tail-flick assay of KOR function as the initial measure of receptor inactivation. We utilized the warm water tail withdrawal paradigm in which mice have ⅓-½ of their tail dipped in 52.5^{o}C water and the latency for them to withdraw their tail was measured. Typically, the analgesic effect of U50,488 increases latency to withdraw by about 3-6 seconds (Bruchas, Land, et al., 2007; Chavkin et al., 2019)

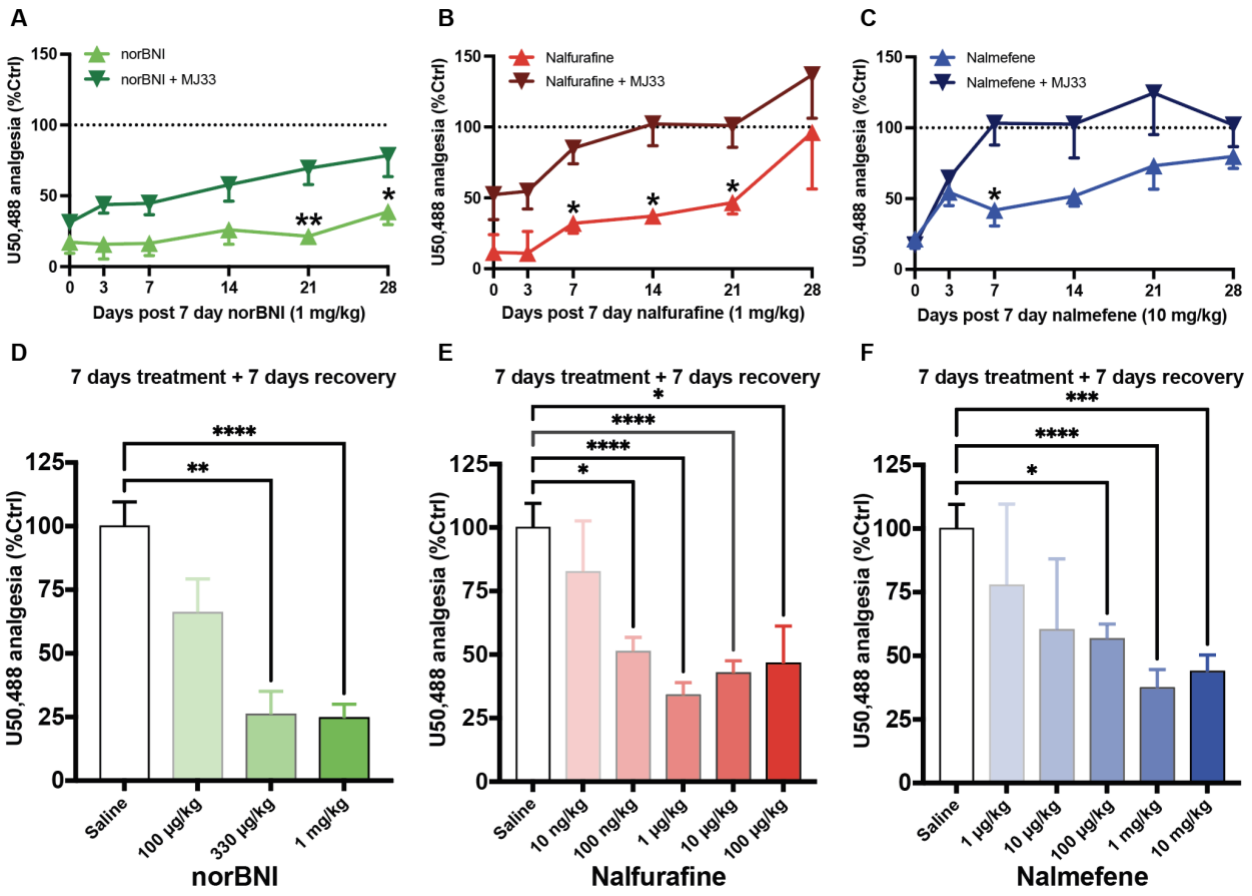

Figure 2.3: Repeated administration of nalfurafine and nalmefene blocks KOR-induced analgesic response through the JNK pathway. A-C) Tail withdrawal latency is shown as a percent of the baseline of the normal increase elicited by U50,488 administration. Treatments of norBNI (1 mg/kg), nalfurafine (1 mg/kg), and nalmefene (10 mg/kg) were given once daily for 7 days. Time points are shown as days after the last administration of treatment measured out to 28 days. Saline or saline with MJ33 pretreatment shows no change from the normal baseline (Supplemental Fig. 3). Repeated treatment with norBNI, nalfurafine, and nalmefene blocks U50,488-induced latency increase. Pretreating with MJ33 1 hour before each daily dose caused KOR function to recover more rapidly. D-F) The same dosing regimen as in A-C showing 7 days post-last treatment norBNI (100 µg/kg - 1 mg/kg), nalfurafine (10 ng/kg - 100 µg/kg), and nalmefene (1 µg/kg - 10 mg/kg). All 3 treatments dose-dependently block U50,488-induced analgesia.

and we consider that response 100% effect and compare each back to their maximal effect (Fig. 2.3).] Mice were injected i.p. with saline, norBNI (1 mg/kg), nalfurafine (1 mg/kg), or nalmefene (10 mg/kg) once daily for 7 days then the analgesic response to the kappa opioid agonist U50,488 (10 mg/kg) was assessed in the standard warm-water (52.5^{o}C) tail withdrawal assay. Treatment for 7-days with low doses of norBNI (330 µg/kg), nalfurafine (100 ng/kg), or nalmefene (100 µg/kg) significantly inhibited the antinociceptive effects of U50,488 (Fig 3A-C). The inactivation was long-lasting: norBNI-treated mice (1 mg/kg) showed only partial recovery after 28 days (Fig 3D). Nalfurafine-treated mice recovered only after 21 days (Fig 3E), and nalmefene-treated mice required more than 14 days to recover (Fig 3F). When PRDX6 was inhibited by injection with MJ33 (1.25 mg/kg) prior to each injection of norBNI, nalfurafine or nalmefene, the rates of recovery of the U50488 analgesic response were significantly increased. These results support the prediction that microdosing with nalfurafine or nalmefene can inactivate KOR in a norBNI-like manner through the JNK/PRDX6 cascade.

Repeated administration of nalfurafine and nalmefene block stress-paired cue aversion

The therapeutic utility of KOR antagonists would presumably be to promote stress-resilience. To determine if microdosing nalfurafine or nalmefene would block dynorphin-induced stress responses, we used two different assays of dysphoria. In mice, dysphoria typically measured as aversion conditioned to a cue associated with the stressful experience (Land et al., 2009). In the first assay, mice were subjected to a

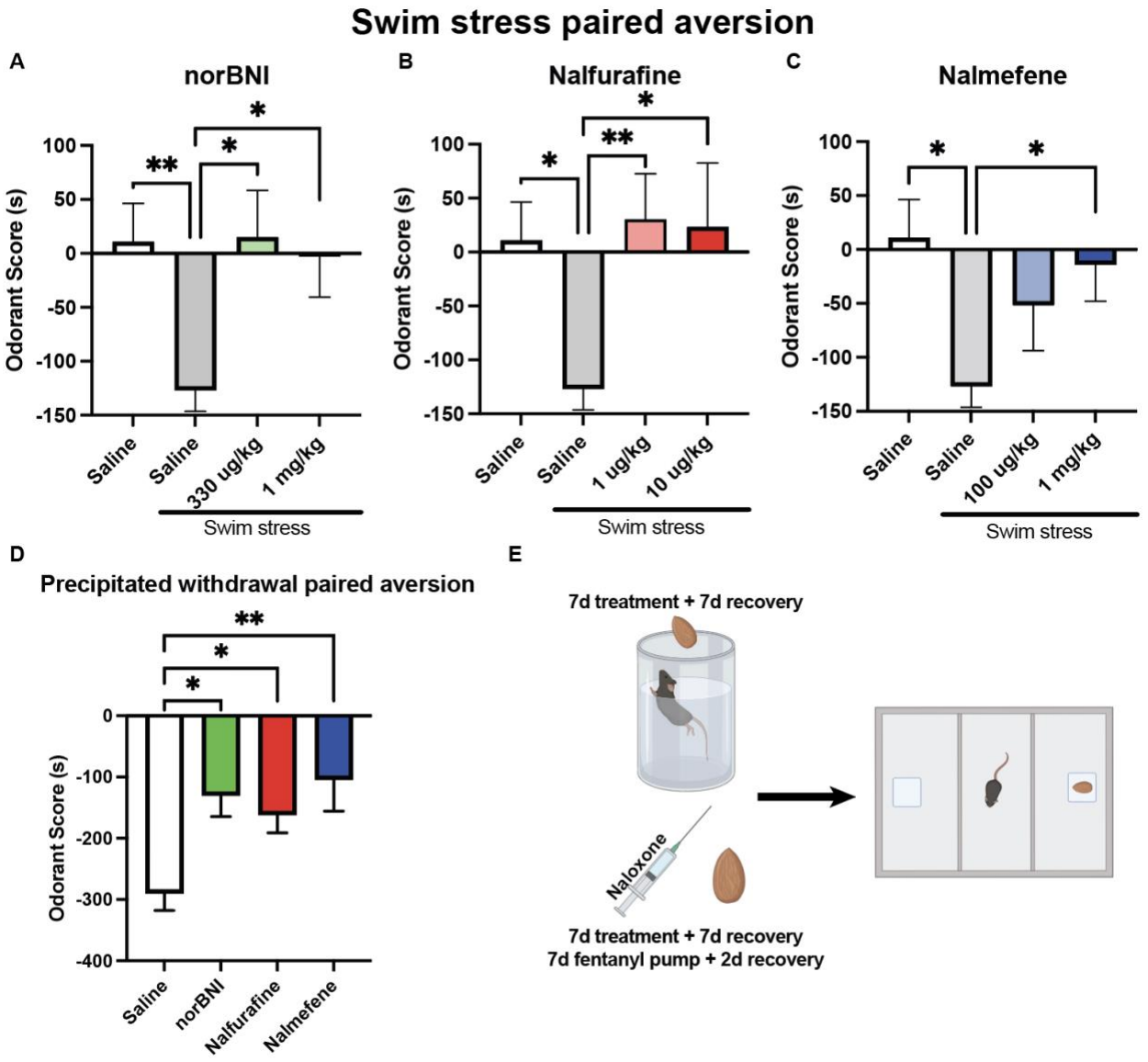

Figure 2.4: Repeated administration of nalfurafine and nalmefene block stress-paired cue aversion. A-C) Odorant scores were determined by the amount of time spent in the null odorant side subtracted from the paired odorant side (a negative score representing aversion). Unstressed animals had neutral scores while stressed animals pretreated with saline showed an aversion of over 100 seconds. Repeated low-dose treatments of nalfurafine (1 µg/kg) and nalmefene (1 mg/kg) fully blocked this aversion. Unstressed animals have no aversion to the almond scent while animals that had the almond scent-swim stress pairing showed an aversion (calculated by time in the odor zone – time spent in the null zone). 7 daily injections of norBNI (330 µg/kg or 1 mg/kg), nalfurafine (1 µg/kg or 10 µg/kg), and nalmefene (1 mg/kg) blocked stress-odor paired aversion. D) Mice were started on daily treatments of saline, norBNI (1 mg/kg), nalfurafine 5 µg/kg), or nalmefene (5 mg/kg). 4 days into treatment, they were implanted with osmotic pumps delivering 2mg/kg/day of fentanyl for 7 days. 2 days after pump removal, the almond scent was paired with an injection of naloxone (1 mg/kg) to

precipitate withdrawal, once in the morning and once in the evening. Mice were tested for aversion to the almond scent 15 days post-pump removal. Mice treated daily for 7 days with saline showed a strong aversion to the almond scent which was greatly attenuated in groups receiving daily injections of norBNI, nalfurafine, or nalmefene. E) Schematic of almond pairing with either repeated force swim-stress or naloxone precipitated withdrawal, followed 24 hours later by 3-chamber aversion assay with the scent on one of the far sides.

repeated forced swim paradigm previously shown to release dynorphin (Land et al., 2008; McLaughlin, Marton-Popovici, et al., 2003) in the presence of a neutral odorant cue (almond scent). Following conditioning, mice were introduced to a 3-chamber place preference apparatus with the almond scent present in only one compartment. Control mice exposed to the almond scent in the absence of the stress-pairing show no aversion to the almond scent-containing compartment. In contrast, mice experiencing the stress-pairing show robust aversion (Fig 2.4). Pretreatment of the mice for 7 days with norBNI (either 330 µg/kg or 1 mg/kg) followed by 7-days of recovery before repeated swim stress exposure in the presence of the cue did not develop aversion to the almond scent (Fig 2,4A). Mice pretreated daily with nalfurafine (1 µg/kg or 10 µg/kg) for 7 days did not develop aversion to the almond scent (Fig 2,4B). Similarly, pretreated daily with nalmefene (100 µg/kg or 1 mg/kg) for 7 days did not develop aversion to the almond scent (Fig 2,4C). The drug potencies in the swim-odorant assay were comparable to the tail-flick analgesia assay. Because the place aversion assay requires conditioning, it is important to determine if treatment affects learning and memory processing. When a different set of mice were injected with cocaine in the presence of the almond scent, they developed robust place preference to the almond-scent paired compartment. NorBNI (10 mg/kg) treatment prior to cocaine conditioning did not block almond-scent preference (Land et al., 2008).

The second stress assay we used paired almond scent during naloxone precipitated withdrawal in opioid-dependent mice. Acute abstinence to opioids causes dynorphin release and includes a profound dysphoria response (Abraham et al., 2021).

Mice were implanted with osmotic mini-pumps containing fentanyl (2 mg/kg/day) to produce opioid dependence. After 7 days, the pumps were removed and 2 days later mice were injected twice with 1 mg/kg naloxone in the presence of the almond scent, once in the morning and once in the evening to precipitate withdrawal. Fentanyl-dependent mice developed robust place aversion (Fig 2.4D). In contrast, control mice with saline-filled minipumps did not develop aversion when injected with naloxone in the presence of almond scent.

Fentanyl-dependent mice that were pretreated for 7 days with either norBNI (100 µg/kg), nalfurafine (5 µg/kg), or nalmefene (5 mg/kg) showed significantly reduced odorant aversion when challenged with naloxone 2-days after pump removal (acute withdrawal). Naloxone-precipitation is not identical to spontaneous withdrawal from opioids - it is more intense and acute; however the symptoms are qualitatively similar (Schulteis et al., 1998). Although we are ultimately interested in the determining the role of dynorphin in humans experiencing opioid abstinence, the conditioning paradigm in mice works better if the cue and the stimulus are discrete and temporally associated. The 1 mg/kg dose of naloxone chosen will block mu opioid receptors but is insufficient to block KOR (Abraham et al., 2021). These results from both these stress assays suggest that repeated low-dose treatment with nalfurafine or nalmefene promotes stress resilience and supports their potential therapeutic utilities.

KOR agonists increase circulating prolactin in the blood and this physiological response can be blocked with the repeated dosing regimen

It has been previously reported that KOR activation increases prolactin and could be used as a biomarker for KOR agonists (Er & Mj, 2001; Kopruszinski et al., 2022). To determine the relative increases of prolactin at different doses of our treatments, we generated a dose-response with ng/ml of serum prolactin as our output measure, 1 hr post i.p. injection of each drug (Fig. 2.5A). These curves highlight the high potency of nalfurafine (left-shifted compared to U50,488) and the partial agonism of nalmefene (decreased maximal effect compared to U50,488). Pretreatment with norBNI (10 mg/kg, 7 days prior) blocks the increase in prolactin seen with U50, nalfurafine, and nalmefene (Fig. 2.5B).

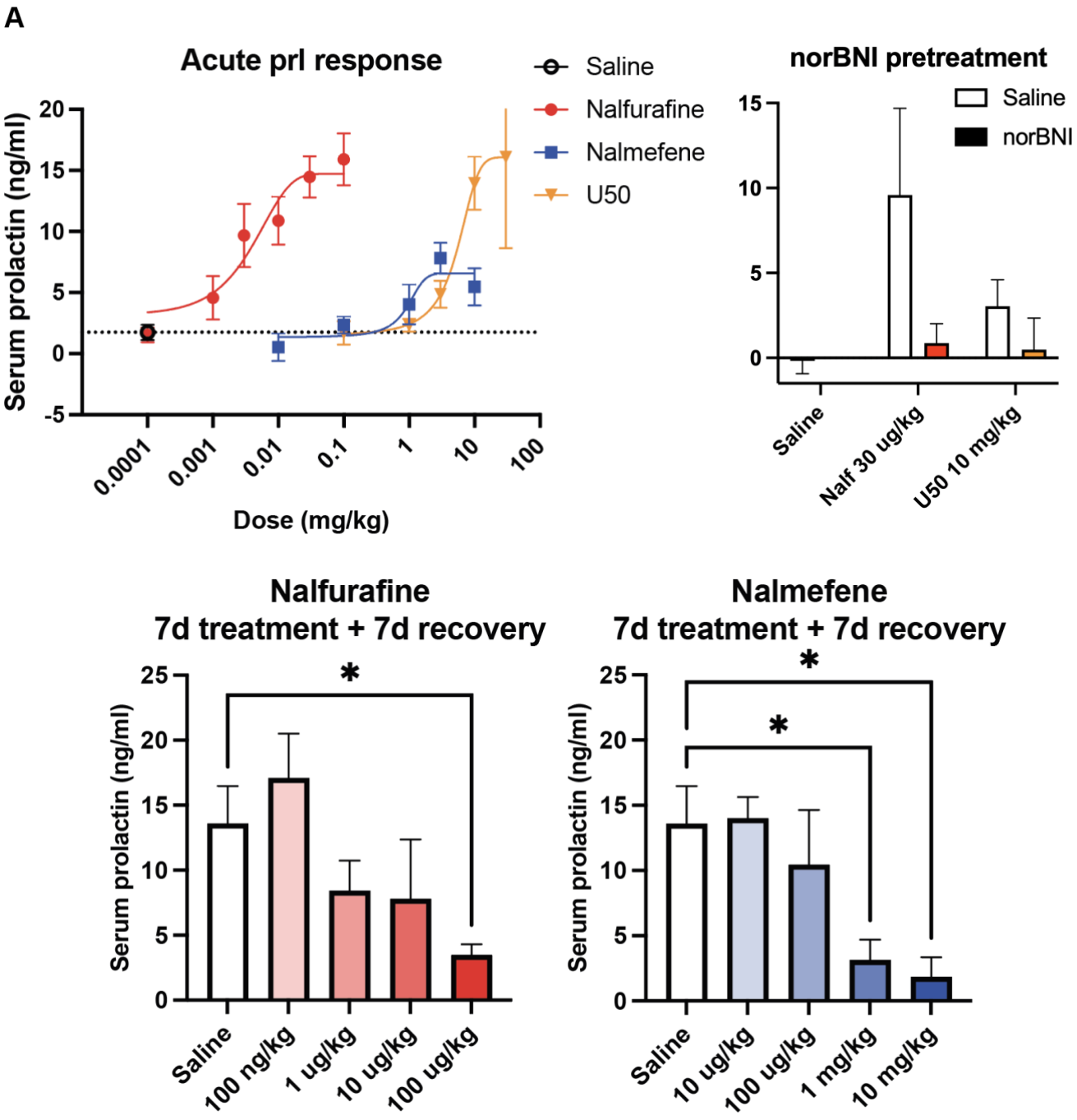

Figure 2.5: KOR agonists increase serum prolactin which can be blocked by nalfurafine and nalmefene A) Serum prolactin dose-response curves 60 min post administration of nalfurafine, nalmefene, and U50,488. Nalfurafine has increased potency compared to U50 while nalmefene has similar potency but reduced efficacy, highlighting its partial agonism. B) Pretreatment with norBNI blocked nalfurafine, and U50-induced increase in prolactin. C) Repeated doses of nalfurafine and nalmefene blocked nalfurafine-induced increase in serum prolactin

Long-term KOR antagonism is tissue-specific

The long-lasting KOR block that results from ROS generation and subsequent receptor inactivation has been previously shown to have specificity in where it acts. GNTI-induced scratching behavior, lack of ROS generation at NAc dopamine terminals. A single large dose of norBNI (10 mg/kg) blocks KOR-induced diuresis at 1hr and 24hr post administration but not 7 days post-administration. Similarly, we show here that repeated injections with varying nalfurafine doses nor norBNI pretreatment of the same block KOR-induced diuresis (Fig. 2.6A). These data, along with the previous data showing a lack of ROS generation in NAc dopamine terminals, suggest that the ROS-induced receptor inactivation with norBNI and now with repeated doses of nalfurafine and nalmefene are restricted to specific CNS areas.

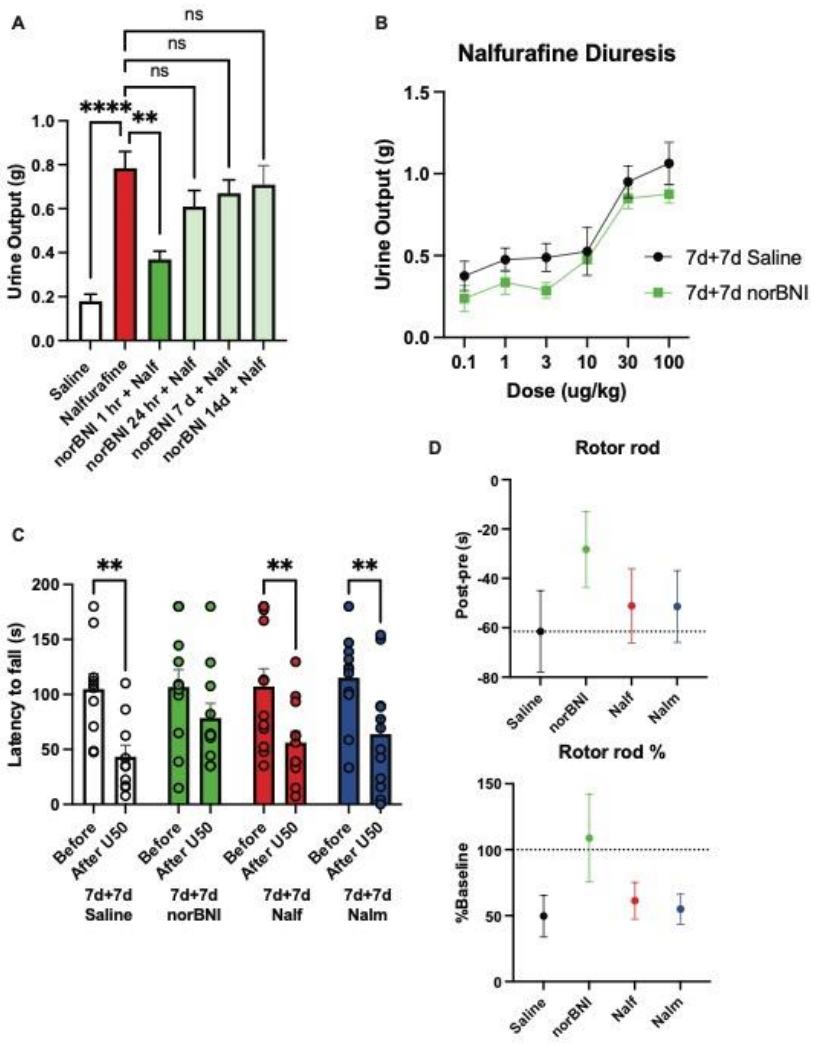

Figure 2.6: norBNI demonstrates short-acting antagonism in specific tissues. A) Administration of nalfurafine increases diuresis compared to saline control. This effect can be block acutely by norBNI (10 mg/kg, 1 hr pretreatment) but is not long lasting (10 mg/kg, 24 hr, 7d, and 14d pretreatment) B) Nalfurafine was given to mice each day for 6 days at varying doses with pretreatment of either saline or low-dose norBNI (1 mg/kg) for 7 days and 7 days of recovery. No differences were observed between saline and norBNI repeated dose pretreatment. Doses of nalfurafine were given each day and no tolerance effect was observed in its diuretic action. C) Mice treated with saline, norBNI (1 mg/kg), nalfurafine (5 µg/kg), or nalmefene (5 mg/kg) daily for 7 days. 7 days post last administration, they were tested on a rotor rod, rotating from 6-14 rpm (increased every 30 seconds). Latency to fall was measured in seconds. U50,488 administration caused a significant decrease in latency with saline, nalfurafine, and nalmefene 7+7 treated animals. D) Rotor rod scores expressed as latency post U50,488 minus pre U50,488 (top) or as a % of pre U50,488 score (bottom). No treatments significantly blocked U50,488-induced decrease in rotor rod performance.

Discussion

The results presented in this study highlight the potential of leveraging functional selectivity. With the identification and characterization of these 4 signaling pathways at KOR, we can expand past the more traditional idea of what a partial agonist is and continue to use these mechanisms to our advantage with drugs that are already available and shown to be safe and well tolerated in humans. In the case of nalfurafine and nalmefene in combination with repeated low-dosing regimens, KOR blockade can build slowly to promote stress-resilience.

Nalfurafine has been shown to be a G-protein-biased agonist (Schattauer et al., 2017), exhibiting 10-20-fold more selectivity for G$\beta\gamma$ in rodent KOR and 200-fold more in human KOR. Because of this, we were able to find an exceptionally large range of doses in which repeated administration caused KOR inactivation. Having such selectivity for the G-protein pathway allows for JNK to be activated without hindrance from p38 MAPK activation which occurs primarily through the GRK3-arrestin pathway. Nalmefene's partial agonist properties result in low efficacy in both the analgesic and aversive pathways, possibly allowing for it to build the ROS generated from the JNK pathway without enough p38 MAPK kinase to block it. Nalmefene is also a functional antagonist of opioid receptors at high doses, allowing for its use in the reversal of opioid overdose as well as treatment for alcohol use disorder, similar to that of naltrexone. However, at the range of doses we have shown here, combined with its ability to cause downstream generation of ROS, we are able to block KOR action long-term. This suggests for both nalfurafine and nalmefene, dosing could be adjusted as needed in

human patients in the event of psychological or physiological discomfort without loss of KOR inactivation.

There is now a large body of preclinical literature suggesting that KOR antagonists may prove useful in the treatment of the anhedonic component of many mental ailments. norBNI and JDTic, long-lasting KOR antagonists, have been shown to block stress-induced drug seeking and self-administration (Graziane et al., 2013; Redila & Chavkin, 2008; Walker et al., 2011). Dynorphin has been shown to be elevated in a host of preclinical models of stress and in the CSF of persons experiencing psychosis (Heikkilä et al., 1990). In this study, we show the ability of nalfurafine and nalmefene to block stress-cue-paired aversion. In the odor-swim stress pairing, there is a full block of odor aversion, consistent with what has been shown with a single large dose of norBNI (Land et al., 2008). In the odor-withdrawal pairing, the is a partial block of the aversion with norBNI, nalmefene, and nalfurafine. It is unclear why the aversion behavior is not fully blocked. However, we speculate that because withdrawal is multifaceted and we believe we are blocking the anhedonic component, other factors that are not KOR-mediated contribute to the whole effect.

There has been large variability in the response to KOR agonists in preclinical models using females. This phenomenon has been attributed to estrus cycle changes. Both the menstrual cycle in humans and the estrus cycle in rodents are controlled by fluctuations in ovarian steroid hormones. The mouse reproductive cycle is 4-6 days, with key fluctuations of estrogen and progesterone mimicking a condensed version of the human

menstrual cycle. Estrogen concentrations increase during peak ovulation during the early proestrus phase and drop rapidly during the rise of progesterone. Indeed, both previous data as well as the data presented here confirm that female mice have an extremely muted response to KOR agonism in the G-protein mediated pathway, including the collateral agonism of norBNI, during the peak estrogen phase, proestrus (Fig. 2.2H-I) (Abraham et al., 2018; Reichard et al., 2020). This is due to estrogen's ability to increase the phosphorylation of GRK2, a key regulator of the G-protein mediated signals, and the phosphorylated GRK2 may sequester the G$\beta\gamma$ subunit. This has implications for the treatment of human females with KOR agonists and the possibility of blunted responses to downstream activation of JNK. However, previous studies suggest that the repeated dosing we have proposed here has the potential to overcome this insensitivity issue (Chavkin et al., 2019). In addition, treatment using KOR inactivation may be more effective in females who are concurrently on progesterone in one form or another, a common method of contraception.

Aside from sex differences, there is also cell specificity in KOR activity. It has been shown that the ability of norBNI to block KOR inhibition of dopamine release NAc core is not long-lasting (Reichard et al., 2020). It may also be the case for different brain areas as well as for KOR in the periphery. In this study, KOR-induced diuresis was the same for both males and females, suggesting that nalfurafine is not subject to the same lack of sensitivity in females in this assay. However, a single injection of high-dose norBNI blocked this increase in diuresis a week post-administration in males but not females. This may indicate that the GRK2 interaction with estrogen is different in renal tissue

containing KOR. It has also been shown that GNTI, a KOR-antagonist that causes pruritic effects when injected subcutaneously can be blocked by acute treatment with nalfurafine (Schattauer et al., 2017). While the pruritic effect of GNTI is a KOR-independent, off-target effect, the nalfurafine block is KOR-meditated. Pretreatment with norBNI blocks nalfurafine inhibition of GNTI-induced pruritus 18-20 hours after injection (Inan et al., 2011), however, we showed that norBNI does not block the antipruritic effect of nalfurafine 7 days post-administration, suggesting yet another site that KOR long term antagonism is absent.

Our ability to identify the generation of ROS by nalfurafine and nalmefene in both ex vivo slice and in vivo fiber photometry was reliant on the development of the novel oROS sensor (Lee, 2024). This bacterial-derived sensor, modified from HyPerRed (Ermakova et al., 2014), allows for the detection of very low levels of ROS. It is important to note that while the absolute value of ROS concentration in oxidative stress compared to the low concentrations that can be used instead as physiological messengers has not been demonstrated. However, it is typically understood that the concentration differs by several magnitudes. The idea of ROS as an essential part of signal transduction is not new but it is understudied, especially in the context of GPCR inactivation.

The mechanism described here for KOR inactivation due to downstream ROS production is, in fact, the same mechanism that occurs in mu-opioid receptors (MOR) and may contribute to the tolerance seen when using some MOR agonists. The

difference in how this inactivation functions between MOR and KOR is due to the relative turnover rate of the receptor. We understand the inactivation caused by ROS-induced depalmitoylation to be irreversible in this context, meaning the receptor is taken offline and has to be resynthesized. This process takes 2-3 days for MORs (Messing et al., 1982) but 21+ days for KORs (Jones & Holtzman, 1992) and accounts for the long-lasting effect of antagonists like norBNI and JDTic. Our findings that the same can be achieved with repeated low dosing of KOR G-biased and partial agonists represent a brand new avenue for leveraging KOR modulation in the treatment of human disease.

REFERENCES

1. Abraham, A. D., Schattauer, S. S., Reichard, K. L., Cohen, J. H., Fontaine, H. M., Song, A. J., Johnson, S. D., Land, B. B., & Chavkin, C. (2018). Estrogen Regulation of GRK2 Inactivates Kappa Opioid Receptor Signaling Mediating Analgesia, But Not Aversion. Journal of Neuroscience, 38(37), 8031–8043.

2. Bruchas, M. R., Schindler, A. G., Shankar, H., Messinger, D. I., Miyatake, M., Land, B. B., Lemos, J. C., Hagan, C. E., Neumaier, J. F., Quintana, A., Palmiter, R. D., & Chavkin, C. (2011). Selective p38α MAPK Deletion in Serotonergic Neurons Produces Stress Resilience in Models of Depression and Addiction. *Neuron*, *71*(3),

3. Ehrich, J. M., Messinger, D. I., Knakal, C. R., Kuhar, J. R., Schattauer, S. S., Bruchas, M. R., Zweifel, L. S., Kieffer, B. L., Phillips, P. E. M., & Chavkin, C. (2015). Kappa Opioid Receptor-Induced Aversion Requires p38 MAPK Activation in VTA Dopamine Neurons. Journal of Neuroscience, 35(37), 12917–12931.

4. Beardsley, P. M., Howard, J. L., Shelton, K. L., & Carroll, F. I. (2005). Differential effects of the novel kappa opioid receptor antagonist, JDTic, on reinstatement of cocaine-seeking induced by footshock stressors vs cocaine primes and its antidepressant-like effects in rats. Psychopharmacology, 183(1), 118–126. https://doi.org/10.1007/s00213-005-0167-4

5. Bruchas, M. R., Land, B. B., Aita, M., Xu, M., Barot, S. K., Li, S., & Chavkin, C. (2007). Stress-Induced p38 Mitogen-Activated Protein Kinase Activation Mediates κ-Opioid-Dependent Dysphoria. Journal of Neuroscience, 27(43), 11614–11623. https://doi.org/10.1523/JNEUROSCI.3769-07.2007

6. Bruchas, M. R., Land, B. B., Lemos, J. C., & Chavkin, C. (2009). CRF1-R Activation of the Dynorphin/Kappa Opioid System in the Mouse Basolateral Amygdala Mediates Anxiety-Like Behavior. PLOS ONE, 4(12), e8528. https://doi.org/10.1371/journal.pone.0008528

7. Calabrese, F., Molteni, R., Racagni, G., & Riva, M. A. (2009). Neuronal plasticity: A link between stress and mood disorders. Psychoneuroendocrinology, 34, S208–S216. https://doi.org/10.1016/j.psyneuen.2009.05.014

8. Carr, G. V., Bangasser, D. A., Bethea, T., Young, M., Valentino, R. J., & Lucki, I. (2010). Antidepressant-Like Effects of κ-Opioid Receptor Antagonists in Wistar Kyoto Rats. Neuropsychopharmacology, 35(3), 752–763. https://doi.org/10.1038/npp.2009.183

9. Chartoff, E., Sawyer, A., Rachlin, A., Potter, D., Pliakas, A., & Carlezon, W. A. (2012). Blockade of kappa-opioid receptors attenuates the development of depressive-like behaviors induced by cocaine withdrawal in rats.

Neuropharmacology, 62(1), 167–176. https://doi.org/10.1016/j.neuropharm.2011.06.014

10. Chavkin, C. (2011). The Therapeutic Potential of κ -Opioids for Treatment of Pain and Addiction. Neuropsychopharmacology, 36(1), Article 1. https://doi.org/10.1038/npp.2010.137

11. Chavkin, C. (2013). Dynorphin–Still an Extraordinarily Potent Opioid Peptide. Molecular Pharmacology, 83(4), 729–736. https://doi.org/10.1124/mol.112.083337

12. Chavkin, C. (2018). Kappa-opioid antagonists as stress resilience medications for the treatment of alcohol use disorders. Neuropsychopharmacology, 43(9), 1803–1804. https://doi.org/10.1038/s41386-018-0046-4

13. Chavkin, C., Cohen, J. H., & Land, B. B. (2019). Repeated Administration of Norbinaltorphimine Produces Cumulative Kappa Opioid Receptor Inactivation. Frontiers in Pharmacology, 10, 88. https://doi.org/10.3389/fphar.2019.00088

14. Ehrich, J. M., Phillips, P. E. M., & Chavkin, C. (2014). Kappa Opioid Receptor Activation Potentiates the Cocaine-Induced Increase in Evoked Dopamine Release Recorded In Vivo in the Mouse Nucleus Accumbens. Neuropsychopharmacology, 39(13), Article 13. https://doi.org/10.1038/npp.2014.157

15. Er, B., & Mj, K. (2001). Kappa-Opioid receptor agonist-induced prolactin release in primates is blocked by dopamine D(2)-like receptor agonists. European Journal of Pharmacology, 423(2–3). https://doi.org/10.1016/s0014-2999(01)01121-9

16. Ermakova, Y. G., Bilan, D. S., Matlashov, M. E., Mishina, N. M., Markvicheva, K. N., Subach, O. M., Subach, F. V., Bogeski, I., Hoth, M., Enikolopov, G., & Belousov, V. V. (2014). Red fluorescent genetically encoded indicator for intracellular hydrogen peroxide. Nature Communications, 5(1), 5222. https://doi.org/10.1038/ncomms6222

17. Inan, S., Dun, N. J., & Cowan, A. (2011). Investigation of Gastrin-Releasing Peptide as a Mediator for 5′-Guanidinonaltrindole-Induced Compulsive Scratching in Mice. Peptides, 32(2), 286–292. https://doi.org/10.1016/j.peptides.2010.11.022

18. Jackson, K. J., Carroll, F. I., Negus, S. S., & Damaj, M. I. (2010). Effect of the selective kappa-opioid receptor antagonist JDTic on nicotine antinociception, reward, and withdrawal in the mouse. Psychopharmacology, 210(2), 285–294. https://doi.org/10.1007/s00213-010-1803-1

19. Jackson, K. J., Jackson, A., Carroll, F. I., & Damaj, M. I. (2015). Effects of orally-bioavailable short-acting kappa opioid receptor-selective antagonist LY2456302 on nicotine withdrawal in mice. Neuropharmacology, 97, 270–274. https://doi.org/10.1016/j.neuropharm.2015.05.023

20. Jones, D. N., & Holtzman, S. G. (1992). Long term kappa-opioid receptor blockade following nor-binaltorphimine. European Journal of Pharmacology, 215(2–3), 345–348. https://doi.org/10.1016/0014-2999(92)90055-9

21. Knoll, A. T., & Carlezon, W. A. (2010). Dynorphin, stress, and depression. Brain Research, 1314C, 56. https://doi.org/10.1016/j.brainres.2009.09.074

22. Kopruszinski, C. M., Watanabe, M., Martinez, A. L., de Souza, L. H. M., Dodick, D. W., Moutal, A., Neugebauer, V., Porreca, F., & Navratilova, E. (2022). Kappa opioid receptor agonists produce sexually dimorphic and prolactin-dependent hyperalgesic priming. PAIN, 10.1097/j.pain.0000000000002835. https://doi.org/10.1097/j.pain.0000000000002835

23. Land, B. B., Bruchas, M. R., Lemos, J. C., Xu, M., Melief, E. J., & Chavkin, C. (2008). The dysphoric component of stress is encoded by activation of the dynorphin kappa-opioid system. The Journal of Neuroscience: The Official Journal of the Society for Neuroscience, 28(2), 407–414. https://doi.org/10.1523/JNEUROSCI.4458-07.2008

24. Lijffijt, M., Hu, K., & Swann, A. C. (2014). Stress Modulates Illness-Course of Substance Use Disorders: A Translational Review. Frontiers in Psychiatry, 5, 83. https://doi.org/10.3389/fpsyt.2014.00083

25. Messing, R. B., Portoghese, P. S., Takemori, A. E., & Sparber, S. B. (1982). Antagonism of morphine-induced behavioral suppression by opiate receptor alkylators. Pharmacology, Biochemistry, and Behavior, 16(4), 621–626. https://doi.org/10.1016/0091-3057(82)90426-9

26. Reichard, K. L., Newton, K. A., Rivera, Z. M. G., Menezes, P. M. S. de, Schattauer, S. S., Land, B. B., & Chavkin, C. (2020). Regulation of Kappa Opioid Receptor Inactivation Depends on Sex and Cellular Site of Antagonist Action. Molecular Pharmacology, 98(5), 548–558. https://doi.org/10.1124/molpharm.120.000124

27. Schattauer, S. S., Kuhar, J. R., Song, A., & Chavkin, C. (2017). Nalfurafine is a G-protein biased agonist having significantly greater bias at the human than rodent form of the kappa opioid receptor. Cellular Signalling, 32, 59–65. https://doi.org/10.1016/j.cellsig.2017.01.016

28. Schindler, A. G., Messinger, D. I., Smith, J. S., Shankar, H., Gustin, R. M., Schattauer, S. S., Lemos, J. C., Chavkin, N. W., Hagan, C. E., Neumaier, J. F., & Chavkin, C. (2012). Stress Produces Aversion and Potentiates Cocaine Reward by Releasing Endogenous Dynorphins in the Ventral Striatum to Locally Stimulate Serotonin Reuptake. Journal of Neuroscience, 32(49), 17582–17596. https://doi.org/10.1523/JNEUROSCI.3220-12.2012

29. Schwarzer, C. (2009). 30 years of dynorphins—New insights on their functions in neuropsychiatric diseases. Pharmacology & Therapeutics, 123(3), 353–370. https://doi.org/10.1016/j.pharmthera.2009.05.006

30. Smith, J. S., Schindler, A. G., Martinelli, E., Gustin, R. M., Bruchas, M. R., & Chavkin, C. (2012). Stress-Induced Activation of the Dynorphin/κ-Opioid Receptor System in the Amygdala Potentiates Nicotine Conditioned Place Preference. The Journal of Neuroscience, 32(4), 1488–1495. https://doi.org/10.1523/JNEUROSCI.2980-11.2012

31. Walker, B. M., & Koob, G. F. (2008). Pharmacological Evidence for a Motivational Role of κ-Opioid Systems in Ethanol Dependence. Neuropsychopharmacology : Official Publication of the American College of Neuropsychopharmacology, 33(3), 643–652. https://doi.org/10.1038/sj.npp.1301438

32. Zhang, S., Tong, Y., Tian, M., Dehaven, R. N., Cortesburgos, L., Mansson, E., Simonin, F., Kieffer, B., & Yu, L. (1998). Dynorphin A as a Potential Endogenous Ligand for Four Members of the Opioid Receptor Gene Family. Journal of Pharmacology and Experimental Therapeutics, 286(1), 136–141.

Chapter 3

Stress decreases serotonin tone in the nucleus accumbens in male mice to promote aversion and potentiate cocaine preference via decreased stimulation of 5-HT$_{1B}$ receptors.

This chapter was formatted for this thesis from the following article previously published. "Stress decreases serotonin tone in the nucleus accumbens in male mice to promote aversion and potentiate cocaine preference via decreased stimulation of 5-HT$_{1B}$ receptors". Fontaine HM, Silva PR, Nesiwanger, C, Tran R, Abraham AD, Land BB, Neumaier JF, Chavkin C. (2021) *Neuropsychopharmacology*, **47**: 891–901.
My contribution to this work was to run portions of the cocaine-conditioned place preference tests in Figures 3.1-3.3.

The presented study investigates the role of KOR in stress-induced dysphoria and drug reward potentiation. We found that excising KOR from serotonergic (SERT-expressing) neurons in male mice blocked stress-induced potentiation of cocaine preference. Two distinct populations of KOR-expressing neurons were identified in the dorsal raphe nucleus (DRN): those expressing VGluT3 and SERT. Optogenetic inhibition of SERT+ neurons increased cocaine preference, while inhibition of VGluT3+ neurons reduced it. Inhibition of SERT+ neurons in the DRN projecting to the medial nucleus accumbens (mNAc) caused aversion whereas stimulation reduced stress responses and cocaine preference. The dynorphin afferents in the mNAc were required for stress-potentiated cocaine preference. Blocking dynorphin in the mNAc or transiently inhibiting 5-HT$_{1B}$

receptors blocked this potentiation. Stress caused increased 5-HT_{1B} receptor expression in mNAc dynorphin cells.

This work further elucidates the dyn/KOR signaling modulating serotonin activation of 5-HT_{1B} receptors in the NAc that influences stress responses, emotional states, and drug reward in this system. Our increased understanding of these circuits adds to a body of knowledge on the therapeutic potential of KOR regulation.

Introduction

Stress has profound effects on the risk of substance use disorders and relapse in humans and promotes drug seeking behaviors in animal models of addiction [1–4]. Animal studies have shown that the endogenous opioid dynorphin (Dyn) and its cognate receptor, the kappa opioid receptor (KOR), are critical to the enhancement of each stage in the progression towards drug addiction, from initial preference, to escalation, and ultimately reinstatement [2,5–7]. These have been shown to be mediated in part by stress-induced modulatory effects on the serotonin (5-HT) system; however, the contribution of serotonin (5-HT) to hedonic processing remains controversial [8–10]. In humans, polymorphisms in genes encoding dynorphin, KOR, and the serotonin transporter (SERT) have been linked to stress-induced depression and increased risk for addiction [11–14].

Stress-evoked release of neuropeptides including corticotropin-releasing factor (CRF) and the prodynorphin-derived peptides impinge on affective circuitry to orchestrate

changes in both neurophysiological state and observable behavior [15]. CRF-induced Dyn release and KOR activation is required for the dysphoric and anxiogenic properties of stress. Additionally, Dyn action at KOR on dopaminergic and serotonergic neurons is necessary for a stress-induced dysphoric state, which may underlie stress-potentiation of drug-seeking behaviors [15,16]. KOR activation within serotonergic neurons of the dorsal raphe nucleus (DRN), which is a hedonic hot spot and primary source of forebrain serotonin, results in somatic hyperpolarization and increases the surface expression of SERT in axon terminals projecting to the nucleus accumbens (NAc) [9,10,17,18]. Together, these findings suggest that stress-induced activation of the Dyn-KOR-5-HT axis reduces serotonin tone in the NAc to increase drug reward in mice.

Direct manipulation of serotonergic neuron activity in DRN via optogenetic and chemogenetic techniques, however, has resulted in conflicting conclusions concerning the role of 5-HT in mediating responses to rewarding, aversive, and stressful stimuli [19– 24]. These discrepancies may be due to the genetic and anatomical complexity of the DRN as well as the impact of different assay conditions and event timing on stress and reward processing [25,26]. In the present study, we resolved a KOR-expressing, serotonergic projection from the lateral aspect of the DRN to the medial NAc (mNAc) that controls 5-HT tone to regulate stress response, aversion, and reward potentiation. We further implicate presynaptic dynorphin and postsynaptic 5-HT1B receptors within the mNAc in mediating these effects.

Materials and Methods

Drugs

Cocaine-HCl, norbinaltorphimine-HCl (norBNI), and ±U50488 were provided by the National Institute on Drug Abuse Drug Supply Program (Bethesda, MD) and were dissolved in 0.9% saline. Sodium pentobarbital, Beuthanasia Special-D, and isoflurane were obtained from University of Washington Medical Center Drug Services. CP 94253-HCl, GR 127935-HCl, and GR 125487 were purchased from Tocris Bioscience and dissolved in artificial cerebrospinal fluid (ACSF).

Viral reagents

CAV2-DIO-ZsGreen was provided by Dr. Larry Zweifel (University of Washington). UNC Vector Core or Addgene provided: AAV5-DIO-EYFP (UNC/ Addgene #27056), AAV5-DIO-SwiChRCA-EYFP (UNC), AAV5-DIO-ChR2-EYFP (UNC/ Addgene #20298), AAV5-EGFP (#105547), AAV5-Cre-EGFP (Addgene #105545), and AAVrg-DIO-EYFP (Addgene #27056). Viral suspensions were stored at -80°C until use and injected undiluted (2×1012 - 3×1013 vg/ml).

Animals

Adult (8-20wk) male C57BL/6 mice and transgenic strains on C57BL/6 genetic background were group housed (2-5/cage), given access to food pellets and water ad libitum, and maintained on a 12hr light:dark cycle (lights on at 7AM). All animal procedures were approved by the University of Washington Institutional Animal Care and Use Committee and conformed to US National Institutes of Health guidelines. We obtained Slc6a4-Cre (SERT-Cre) mice from the GENSAT project (MMRRC:017260-

UCD), Oprk1-Cre (KOR-Cre) mice from Dr. Sarah Ross (University of Pittsburgh) [1], Pdyn-IRES-Cre (Pdyn-Cre) and Pdyn-lox/lox (Pdynflx) mice from Dr. Richard Palmiter (University of Washington), Slc17a8-Cre (VGluT3-Cre) and Oprk1-lox/lox (KOR-flx) from Jackson Labs (MGI:5823257, MGI:5316477). KORSERT conditional knockout (cKO) mice were generated as previously described [2].

General behavioral methods

Mice were kept in the same housing facility in which behaviors were assayed for at least 1 week prior to experimentation. For all optogenetic experiments, controls were Cre+ mice injected with AAV-DIO-EYFP instead of the active opsin. Cage changes were conducted no less than 3 days prior to behavioral testing to minimize confounding effects of environmental stress exposure. Mice were habituated to handling daily for 3 days prior to the initiation of each experiment. All experiments were conducted on mice naïve to prior treatment, except for the optical stimulation during rFSS and social approach assays, which were conducted 2 weeks after the completion of cocaine CPP. EthoVision Software (Version 3.0 & 11.0, Noldus Information Technology) was used to assess movement and generate path heatmap graphics. Experiments were conducted in sound-attenuating behavioral rooms with medium-intensity lighting.

Stereotaxic Surgery

For aseptic surgery, mice were anesthetized in an induction chamber with 4% isoflurane before placement into a stereotaxic frame (David Kopf Instruments Model 1900) where they received 1-2% isoflurane as described previously [2]. Viral injections were

performed using Hamilton Neuros syringe (Sigma-Aldrich) at a rate of 100nl/min (500nl for all behavioral studies, 750nl for tracing studies). The syringe was left in place for 5min following the injection. Injection sites were as follows: DRN (AP -4.35, ML 0, DV-2.7; 20° angle) or NAc (AP+1.35, ML +-0.7, DV -4.6) and optic fibers (Doric) were placed 0.5mm above the target site. All NAc viral injections for behavioral studies and optical stimulation were bilateral and unilateral for retrograde tracing. For drug microinfusion, guide cannula (Plastics One #C235G/SPC-1.4mm) were placed above the NAc (AP +1.35, ML +-0.7, DV -4.1), with internal cannula projecting 0.5mm past the guide cannula. Implants were secured using Metabond (Parkell) and dental cement (Stoelting). Following surgeries, mice were given carpofen for 5 days to reduce inflammation and pain and allowed time for recovery and viral expression (10 days for infusion studies, 4 weeks for somatic optical stimulation, and 5 weeks for terminal optical stimulation and anatomical tracing studies).

Forced Swim Stress

Mice were subjected to a modified Porsolt forced swim stress (rFSS) as described previously [3]. All swim sessions were conducted in 31±1ºC water. On day 1, mice received a 15min initial swim, followed 22hr later by four 6min swims, each separated by 6min. After each swim, mice were removed from the water, towel dried, and returned to their home cage.

Optogenetic stimulation during rFSS

Mice were connected to the optical tether 1min prior to swim sessions on day 1 and 2, and they remained tethered throughout the swim session. Mice were visually monitored during swim sessions. Mice that submerged due to impaired swimming were removed from the water and excluded from subsequent analysis (3 EYFP-injected and 2 ChR2-injected mice were excluded). Optical stimulation was delivered 1min prior to the initial swim and 6min prior to the second and fourth swim on the day 2.

Cocaine conditioned place preference

Mice were assayed in a balanced place conditioning apparatus with distinct visual and tactile cues in each chamber as previously described [2,4]. On day 1, an initial preference test was conducted for place preference bias. Conditioning occurred on days 2 and 3, consisting of cocaine administration and 30min confinement to the drug-paired chamber in the morning (15mg/kg, IP) and saline administration (10ml/kg, IP) and confinement to the other chamber 4hr later. On day 4, mice were allowed to freely explore the apparatus for a postconditioning assessment in the absence of drug. Preference tests and conditioning sessions lasted for 30min and were conducted in sound attenuating chambers.

Manipulations prior to cocaine conditioning

Repeated forced swim stress prior to cocaine conditioning: mice were subjected to rFSS (as described above) 30min after the initial preference test on day 1 and before cocaine conditioning on day 2, terminating 10min prior to cocaine administration.

Optogenetic inhibition of DRN subtypes prior to cocaine conditioning

VGluT3-Cre and SERT-Cre mice expressing EYFP or SwiChR were tethered to fiber optic cables coupled to a 473-nm laser in an empty cage bottom and received optical stimulation (0.33 Hz, 15ms pulse duration) for 30min on each conditioning day. Following optical stimulation, mice were returned to their home-cage 30min prior to each cocaine conditioning session.

Optogenetic excitation of SERTDRN-NAc terminals during U50488 pretreatment

Mice received the selective KOR agonist U50488 (5mg/kg, IP) 1hr prior to cocaine conditioning and were immediately tethered to optical fibers providing 473-nm stimulation (15Hz, 10ms pulse duration) in an empty cage bottom. Mice were untethered 5min before each cocaine conditioning session.

Local infusion of 5-HT receptor antagonists prior to cocaine conditioning

Wild-type (WT) mice with guide cannula placed in the NAc received infusions of the 5-HT1B antagonist GR 127935 or 5-HT4 antagonist GR 125487 (1µg/0.2µl in ACSF, 0.1µl/min) 135min and/or 75min prior to each cocaine conditioning session. Following infusions, mice were returned to their home cage.

Conditioned place aversion

Cannulated SERT-Cre mice expressing EYFP or SwiChR were assayed in a balanced place conditioning apparatus with distinct visual and tactile cues as previously described [2]. An initial preference test was performed on day 1 to assess baseline preference. On

days 2 & 3 optogenetic conditioning was performed, comprising a tethering session with confinement to the less-preferred chamber in the morning and optical stimulation (0.33 Hz, 15ms pulse duration) with confinement to the more-preferred chamber 4hr later. On the 4th day, mice were allowed to freely explore the apparatus for a final preference test in the absence optical stimulation.

Social approach

Social interaction was assessed as described previously using a three-chambered apparatus with two clear internal partitions [5]. The day prior to the experiment, age-matched target mice were habituated to confinement in an inverted pencil cup (Spectrum Diversified Designs) for 1hr. WT mice with cannula placed in the NAc received infusions of 5HT1B antagonist GR 127935 (1µg/0.2µl in ACSF; 0.1 µl/min), and 125min later were allowed to freely explore the social interaction apparatus for a 10min habituation period. The mouse was then briefly removed to a holding cage, and two inverted pencil cups were placed in the far corners of the apparatus, with one cup containing a target mouse. The experimental mouse was then reintroduced and allowed to explore for an additional 10min. Time spent in an interaction zone adjacent to each cup was recorded.

Local infusion of 5-HT1B ligands prior to histology

WT mice with guide cannula placed in the NAc received norBNI (10mg/kg, IP) 24hr prior to the experiment to minimize the effects of infusion-induced stress on pERK-IR [6]. Mice received control infusions (ACSF, 0.2µl) in the right hemisphere and drug infusions

(GR 127935 or 5 CP94253; 1µg/0.2µl, 0.1µl/min) in the left hemisphere. Drug infusions consisted of CP 94253 alone or following infusions of GR127935 135min or 75min prior. 15min after infusion of CP 94253, mice were deeply anesthetized, transcardially perfused, and brains were prepared for histology as described below.

Immunohistochemistry

Mice were transcardially perfused with 4% paraformaldehyde in 0.1M phospho-buffered saline (PBS) as reported previously [7]. Brains were then dissected, cryoprotected with 30% sucrose at 4°C overnight, frozen, cut into 40µm sections (Leica microtome, SM200R), and stored in 0.1M PBS containing 0.1% sodium azide at 4°C until further processing. Standard immunohistochemical procedures were used to stain NAc sections as described previously [6]. Briefly: floating sections were washed 3x5min in PBS, then blocked for 1hr in 5% normal goat serum (Vector Labs), 0.3% Triton-X in PBS before 24hr at room temperature incubation with primary antibodies: 1:400 rabbit anti-pERK antibody (CS4370, Cell Signaling) for phospho-ERK detection or 1:1000 Chicken anti-GFP (AB12970, Abcam) to enhance detection of anterograde and retrograde tracing. Sections were washed again 4x5min in PBS before incubation with the 1:500 goat anti-rabbit 488 or goat anti-chicken 488 (Life Technologies) for 2hr at room temperature. Lastly, sections were washed 4x5 in PBS, then once with 0.5X PBS before mounting on Fisher Superfrost slides (Sigma-Aldrich) and coverslipped using Vectashield (Vector Laboratories).

Fluorescent in situ hybridization (ISH) using RNAscope

Brains were rapidly dissected and flash frozen on dry ice. For stress experiments, brain dissection was performed either 30min or 24hr following the last swim session of the rFSS protocol or unhandled (no rFSS) controls. Thin (14µm) coronal sections containing the NAc or DRN were collected and mounted onto Superfrost plus slides using a cryostat (Leica CM 1850) maintained at -20ºC. RNAscope ISH was performed according to the Advanced Cell Diagnostics as previously reported [8]. Each set of staining included a negative control, in which probes were omitted from the process. Probes were discriminated using tyramide signal amplification (TSA) fluorophores (NEL744001, NEL745001, NEL741001; Akoya Biosciences).

Characterization of DRN subpopulations

Probes for Oprk1 (mm-Oprk1), Slc6a4 (mmSlc6a4), and Slc17a8 (mm-Slc17a8) were used to label tissue from the central DRN (AP +4.34.5) of unstressed mice. NAc Htr1b distribution: sections containing the central NAc (AP 1.1-1.3) were obtained from stressed and unstressed mice, and separate sets of tissue were stained with probes to Htr1b(mm-Htr1b)/Chat (mm-Chat) and Htr1b/Pdyn (mm-Pdyn)/Adora2a (mmAdora2a).

Microscopy and Image Quantification

All images used for quantitation were taken using a confocal microscope (SP8X, Leica Microsystems), except for initial determination of expression in retrograde tracing studies and confirmation of viral expression in behavioral studies, in which a scanning widefield microscope was used (DMI6000, Leica Microsystems).

Anterograde tracing

Two brain sections containing the NAc (AP +1.3 and AP +1.0) were imaged at 10x magnification for each SERTDRN ChR2 and VGluT3DRN ChR2 mouse. Boundaries of the mNAc were determined using the Paxinos atlas [9]. Terminal density was determined using Image J software (NIH) by binarizing the images and calculating the density of positive pixels within the mNAc as described previously [10].

Retrograde tracing

For KOR retrograde tracing from the mNAc, every sixth section within the DRN (AP -4.0 to AP -5.0) was mounted and imaged at 10x magnification following anti-GFP staining to enhance detection of labeled cell bodies. For Pdyn retrograde tracing from the mNAc, every 12th section throughout the collected tissue (AP +2.5 to AP -5.5) was mounted to survey across all brain regions and imaged at 10x on a scanning widefield microscope. These were visually inspected for signal by an observer blind to treatment. Subsequently, confocal images were taken of the medial NAc at 10x magnification.

E*ffects of 5-HT1B drug infusion on pERK in the NAc*

The left and right medial NAc of two sections (AP +1.3 and AP +1.0) were imaged for each animal. Z-stacks (5µm thick, 7 steps) were taken at 60x magnification and an average projection was generated using LASX software (Leica Microsystems). A detection threshold for each section was set according to the brightest 5% of pixels in the ACSF image and positive cells (more than half of cell above threshold) for each image were quantified manually by an observer blind to treatment using ImageJ

software (NIH). Average counts of two sections for the ACSF and drug treated hemispheres were taken for each animal. Percent increase of NAc pERK-IR+ cells in the drug-treated hemisphere was calculated as (pERKDrug-pERKACSF)/ pERKACSF.

Fluorescent ISH: DRN subpopulations

The entire DRN was imaged at 20x magnification from one section (AP 4.4) of each subject. Images were taken during the same imaging session, and capture settings were adjusted such that no signal was observed in negative controls and kept constant for all subsequent images. For DRN subregion analysis, an observer blind to staining conditions determined subregion boundaries and selected a rectangular region within each DRN subregion for colocalization analysis. Cells that contained signal brighter than threshold were counted as positive or overlapping. NAc Htr1b distribution: a region immediately medial and ventral to the anterior commissure (ac) was imaged at 20x magnification, with capture settings adjusted to ensure no signal in the negative controls. Two bilateral images from two sections were taken. Images were processed using custom MATLAB scripts (available upon request) for positive cells, co-expressing cells, and levels of RNA detected per cell; these values were averaged for each subject animal and then group averages were calculated. Cells that contained signal brighter than threshold were counted as positive or overlapping. Within positive cells, RNA levels were calculated by determining the percent of area within positive cells that was above threshold. For all analyses, total cells were determined by the number of DAPIstained nuclei.

Data Analysis

Sample sizes were based on prior studies but were not predetermined by statistical methods. All aspects of histology and histological analysis were performed by an experimenter blind to genotype and treatment. Prior to further analysis, outliers in data sets were excluded using Grubb's Test for statistical outliers. The assumption of normal distribution was tested for each data set and was statistically corrected for (welch's correction) when this criterion was not met. Post-hoc tests used were Sidak's, except for the analysis of antagonist pretreatment on cocaine CPP, where Dunnet's T3 was used due to statistical correction. Alpha was set at 0.05 for all analyses.

Results

KOR expression in SERT neurons is required for stress potentiation of cocaine reward

Slc6a4-Cre ('SERT-Cre') and Oprk1-lox/lox ('KOR-flx') mice were crossed as previously described [16], resulting in conditional excision of KOR in SERT+ cells ('KORSERTcKO') (Figure 3.1A). These mice and their littermate controls were subjected to a modified Porsolt repeated forced swim stress (rFSS), which consisted of a 15 min initial swim, followed 22hr later by four 6min swims that terminated 10 min prior to cocaine conditioning (Figure 3.1B). Cocaine place preference of the unstressed KORSERTcKO mice was not significantly different from that of littermate controls (two-way ANOVA; $F_{1, 34} = 0.27$, $P = 0.604$), indicating that excision of KOR in SERT-expressing neurons does not regulate basal cocaine preference (Figure 3.1C). There was a significant main effect of stress ($F_{1, 34} = 8.87$, $P = 0.005$) and a marginal

interaction (F1, 34= 3.45, P= 0.072). Comparison of cocaine preference within each genotype revealed a significant effect of stress in controls (Sidak post-hoc, P= 0.004) that was absent in the KORSERT cKO group (P= 0.664) (Figure 3.1C). Normalized data revealed that stress increased cocaine preference in controls by more than twofold, significantly more than in KORSERT cKO group (t test, welch-corrected, P= 0.036) (Figure S1A). These data demonstrate that global deletion of KOR in SERT expressing neurons blocks stress-induced potentiation of cocaine CPP.

Inhibition of SERT neurons in the DRN is aversive

KOR activation by stress hyperpolarizes serotonergic neurons in the DRN [18], but stress exposure also broadly affects brain physiology. To assess the effect of selective inhibition of DRN neurons, we optogenetically inhibited SERT neurons in the DRN (SERTDRN) by injecting an inhibitory opsin (AAV5-DIO-SwiChR-EYFP) into the DRN of SERT-Cre mice (Figure 3.1D). SwiChR is a channel rhodopsin variant that conducts Cl- ions and has been utilized to generate long-term, reversible inhibition, while avoiding photic damage [30,31]. We conducted a CPP assay by confining the mice to an optically-paired chamber during SwiChR-mediated inhibition of SERT neurons in the DRN for two days, following and preceding preference tests (Figure 3.1E). SwiChR-mediated inhibition of SERT neurons in the DRN induced a robust and significant aversion to the optically-paired chamber (t test, P< 0.001) (Figure 3.1F). These results reflect the necessity of KOR expression within SERT neurons for KOR-mediated aversion [16] and support the conclusion that inhibition of SERT-DRN neurons produces place aversion.

KOR is expressed in SERT and VGluT3 subpopulations in the DRN

DRN serotonin neurons are anatomically and phenotypically heterogeneous and have been suggested to form functional subsystems regulating diverse stress-sensitive processes [32–36], but the distribution of KOR within DRN serotonin neurons has not been evaluated. RNAscope was used to probe for co-expression of transcripts for KOR (Oprk1), SERT (Slc6a4), and the vesicular glutamate transporter type III (VGluT3DRN; Slc17a8) (Figure 3.1G, S1B). SERT and VGluT3-expressing neurons within the DRN comprise largely serotonergic populations that overlap extensively yet may have distinct roles in driving reward-related behaviors [19,20,22]. Most Slc6a4 neurons expressed Slc17a8, indicating substantial overlap of SERT and VGluT3 populations in the DRN (Figure 3.1H). Oprk1 was present in nearly all Slc17a8+ or Slc6a4+ cells (Figure 3.1H). The expression of KOR transcript in the majority of SERT+ and VGluT3+ cells indicates a potential for direct regulation of these subsystems by KOR.

Next, the percentages of SERT+ (Slc6a4+) neurons in each subregion that co-expressed KOR transcript (Oprk1+/Slc6a4+) were determined. The percentage of Slc6a4+ neurons that co-expressed both Oprk1 and Slc7a18 (Oprk1+/Slc17a8+/Slc6a4+) was significantly higher in the dorsal and ventral DRN than in the lateral DRN (DRL), where Slc17a8 was nearly absent (two-way ANOVA; Interaction, $F_{2,8}= 61.1$, $P< 0.001$; Sidak post-hoc $P= 0.036$, $P< 0.0001$, respectively) (Figure 1I). These data indicate that unlike the majority of SERTDRN neurons, SERT+ neurons in the lateral DRN are almost exclusively KOR+/ VGluT3-.

SERT+ projections from the DRN innervate the medial NAc, but VGluT3+ projections neurons do not

To assess the projections of these SERT-DRN and VGluT3DRN populations to the NAc, AAV5-DIO-ChR2-EYFP was injected into the DRN of SERT-Cre and VGluT3-Cre mice. Labeled terminals in the medial NAc (mNAc; a region including medial aspect of NAc shell and core) revealed that SERT+ projection terminals in the mNAc were denser than VGluT3+ terminals, which were nearly absent (t test, welch corrected, P= 0.044) (Figure 3.2A, 3.2B). In contrast, VGluT3+ and SERT+ terminal density was similar in other regions (Figure S2A). These data are consistent with previous reports of different projection biases of these populations [19,32,37].

NAc-projecting KOR neurons are restricted to the lateral DRN

To confirm that KOR is expressed within the DRN-NAc projection, a retrograde virus (AAVretro-DIO-EYFP) was injected into the NAc of KOR-Cre mice [38]. We observed a population of KOR-expressing, NAc-projecting neurons that was concentrated in the lateral aspect of DRN (Figure 3.2C). This indicates that DRN KOR neurons projecting to the NAc define an anatomically segregated subpopulation. To validate these findings, AAV5DIO-ChR2-EYFP was injected into the DRN of KOR-Cre mice, and examination of the mNAc showed robust terminal expression of the fluorophore (Figure 3.2D). Together, these findings demonstrate that KOR is expressed in a subpopulation of DRN neurons that project to the mNAc, indicating a potential for direct regulation of this DRN-NAc projection by Dyn/KOR.

Inhibition of SERT+ neurons in the DRN recapitulates KOR-mediated potentiation of cocaine preference, but inhibition of VGluT3+ neurons does not

Although prior work has demonstrated an association between KOR activation, somatic hyperpolarization of DRN neurons, increased serotonin reuptake, and potentiation of cocaine preference, a causal link between decreased 5-HT tone and increased cocaine preference has not been established. We mimicked previous studies of KOR-agonist induced potentiation of cocaine preference but substituted KOR-agonist administration with optogenetic inhibition of DRN subpopulations (Figure 3.2E). SERT-Cre mice received DRN viral injections delivering inhibitory opsin (AAV5-DIO-SwiChR-EYFP) or control
(AAV5-DIO-EYFP), and an optical fiber was placed above the site of viral expression (Figure 3.2F). These mice received 30min of SERT+ neuron inhibition that terminated 30 min prior to cocaine conditioning. Comparing cocaine preference scores following SERTDRN SwiChR pretreatment to controls revealed a significant potentiation of subsequent cocaine CPP (t test, welch-corrected, P= 0.037) (Figure 3.2G). These findings indicate that prior inhibition of SERT+ neurons in the DRN is sufficient to potentiate cocaine CPP thereafter.

In parallel studies, VGluT3-Cre mice were injected with AAV5-DIO-SwiChR-EYFP or AAV5-DIO-EYFP in the DRN, and an optical fiber was placed above the site of viral expression (Figure 3.2H). Surprisingly, VGluT3DRN SwiChR pretreatment significantly attenuated subsequent cocaine preference (t test, welch-corrected, P= 0.050) (Figure

3.2I). Normalizing preference scores of the groups receiving pretreatment inhibition of SERT+ or VGluT3+ neurons to their corresponding controls illustrates divergent consequences on subsequent cocaine preference (Figure 3.2J). Thus, inhibition of different DRN populations exerted bidirectional control of subsequent cocaine preference, and inhibition of SERTDRN neurons (but not VGluT3DRN neurons) was sufficient to replicate the consequences of stress on subsequent cocaine CPP.

Increased 5-HT tone in the mNAc decreases rFSS immobility and cocaine preference following KOR activation

To probe the hypothesis that a KOR-mediated decrease in serotonin tone within the mNAc may be necessary for potentiation of subsequent cocaine preference, we optogenetically stimulated SERTDRN-NAc terminals during KOR activation. SERT-Cre mice were injected an excitatory opsin (AAV5-DIO-ChR2-EYFP) in the DRN, and a bilateral optical fiber was placed above the mNAc (Figure 3.3A). One hour before each cocaine conditioning session, these mice and their controls received pretreatment that included the selective KOR agonist U50488 (5mg/kg) as well as optical stimulation of SERT+ terminals (to counteract KOR-induced decreases in serotonin tone) that terminated 5 min before cocaine conditioning (Figure 3.3B). Concurrent stimulation in the SERTDRN-NAc ChR2 group reduced cocaine preference compared to EYFP controls (t test, $P = 0.029$). This indicates that increasing serotonin tone in the mNAc during KOR activation decreases subsequent cocaine preference (Figure 3.3C).

Next, SERT+ terminals were stimulated during a rFSS assay to determine if decreased NAc 5-HT is required for rFSS-induced immobility (Figure 3D). Immobility was analyzed, showing an escalation of immobility in EYFP controls but not in the SERTDRN-NAc ChR2 group (two-way ANOVA; Interaction, $F_{3,33}=1.050$, $P=0.384$; Sidak post-hoc, $P=0.0483$, $P=0.998$, respectively) (Figure 3.3E, S3A, S3B). Comparing immobility during the final swim shows that ChR2-stimulated mice spent significantly less time immobile (t test, $P=0.021$) (Figure 3.3F). These results suggest that stress-induced changes in mNAc serotonergic terminals are required for passive coping and potentiation of subsequent cocaine preference.

Pdyn+ neurons in the NAc are required for stress potentiation of cocaine preference

The role of dynorphin acting on KOR expressed in DRN-NAc projections has been demonstrated by the effects of global prodynorphin gene deletion and local KOR antagonism [1,8], but the neuronal source of dynorphin responsible for stress-induced potentiation of cocaine CPP is unknown. To identify candidate sources of dynorphin to the NAc, two different retrograde viral constructs (AAVretro-DIO-EYFP or CAV2-DIOZsgreen) were injected into the NAc of Pdyn-Cre mice. Examining regions for labeled neurons revealed signal only in the mNAc (Figure 3.3G, S3C). Distinct tropisms of these viruses have been documented that may cause either construct to undercount input populations [38]. However, because both show signal exclusively in the mNAc, we conclude that local neurons within the mNAc likely represent the principal source of endogenous dynorphin for this region.

To assess the necessity of these PdynNAc neurons in stress potentiation of cocaine CPP, AAV5-Cre-EGFP or AAV5-EGFP was injected into the NAc of Pdyn-lox/lox (‘Pdyn-flx’) mice to generate ‘PdynNAc cKO’ or ‘Ctl’ mice (Figure 3.3H). Examining the NAc of these mice demonstrated viral expression that was confined to the NAc (Figure 3.3I). These PdynNAc cKO mice were subjected to a rFSS potentiation of cocaine CPP assay. Cocaine preference scores indicated a main effect of Pdyn excision from the NAc (two-way ANOVA, $F_{1, 54} = 4.73$, $P = 0.034$), indicating that dynorphin within the NAc regulates basal cocaine preference (Figure 3.3I). There was also a significant main effect of stress ($F_{1, 54} = 13.1$, $P = 0.001$) but no significant interaction ($F_{1,54} = 2.437$, $P = 0.124$). Stress significantly potentiated cocaine preference in Cre- controls (Sidak post-hoc, $P = 0.015$) but not in the PdynNAccKOs ($P=0.901$). We have routinely observed cocaine preference scores higher than the ~500 s preference in the unstressed PdynNAccKO group, which suggests that the lack of stress potentiation is likely not due to a ceiling effect on expressed preference. To isolate the effect of stress on potentiation of cocaine preference, we normalized rFSS cocaine preference scores in each group to the cocaine preference of their unstressed counterparts (Figure S3D). This revealed a stress potentiation of cocaine preference of nearly two-fold in controls that was absent in PdynNAccKOs. This finding supports a central role of the dynorphinergic population within the NAc in regulation of both basal cocaine preference and stress potentiation of that preference.

Blockade of mNAc 5-HT1B receptors recapitulates KOR-mediated potentiation of cocaine preference and increases social preference

These findings suggest that a reduction in 5-HT tone in NAc is responsible for stress-induced potentiation of cocaine CPP, but the specific 5-HT receptor type that mediates the consequences of decreased serotonin tone is not known. An especially plausible candidate receptor was 5-HT1B, which is heavily expressed in the nucleus accumbens [39,40]. 5-HT1B receptors regulate stress-enhancement of psychostimulant effects and have been proposed to mediate a compensatory response to the negative hedonic properties stress [40–42]. To mimic the transient decrease in serotonin at 5-HT1B receptors caused by stress, 5-HT1B antagonist GR 127935 was infused into the NAc of WT mice (Figure 3.4A). Histological data measuring pERK-IR (Figure S4) demonstrated that 5-HT1B receptor blockade was present 75min, but not 135min, after GR 127935 infusion. GR 127935 produced a transient decrease in signaling at this receptor (Figure S3). GR 127935 was infused at 135min and/or 75min prior to each cocaine conditioning session (Figure 4B). Preference scores indicated that only infusion 135min prior to conditioning resulted in potentiation of cocaine preference (one-way ANOVA, welchcorrected, $F_{4, 10.49} = 7.80$, $P = 0.004$; Dunnett's T3 post-hoc, $P = 0.001$) (Figure 3.4C). Separately, infusion of a 5-HT4 antagonist prior to cocaine conditioning was tested and failed to potentiate preference, implying that this potentiation is not a general consequence of 5-HTR inhibition (Figure 3.4C). GR 127935 failed to potentiate cocaine preference in the group that received a second infusion of antagonist 75min prior to cocaine conditioning, indicating that this potentiation of cocaine CPP is sensitive to 5HT1B receptor blockade during cocaine administration (Figure 3.4C). These results

demonstrate that a prior decrease in activation of NAc 5-HT1B receptors is sufficient to potentiate subsequent cocaine preference and mimic the effects of rFSS.

To assess whether this reward potentiation is specific to cocaine or reflective of a broader change in reward processing the effect of 5-HT1B antagonism on social preference was evaluated. Semi-chronic stressors have been shown to increase social preference [43], but a potential role for 5-HT1B receptors in this process has not been examined. Mice received infusions of GR 127935 or ACSF into the mNAc and 135min later were assayed for social preference, a behavior regulated NAc 5-HT1B receptors [23]. In this assay, mice could explore an apparatus with an empty, inverted pencil cup in one corner and a pencil cup containing a novel mouse in the opposite corner (Figure 4D, 4E). Social interaction scores were significantly greater in mice pretreated with GR 127935 than ACSF (t test, P= 0.028) (Figure 3.4F). These findings indicate that a prior blockade of 5-HT1B receptors, utilized here to reflect decreased serotonin tone in the mNAc, induces reward potentiation that generalizes beyond cocaine preference.

rFSS increases 5-HT1B transcript expression in Pdyn+ neurons in the NAc

Chronic exposure to stress increases 5-HT1B transcript in the NAc, which may represent a compensatory increase in reward sensitivity in response to stress [42,44,45]. However, regulation by sub-chronic stress exposure, such as the rFSS used in this study, has not been detected. This may be attributed to low sensitivity of prior techniques or difficulty assessing cell-type specific changes. We used RNAscope to evaluate expression of Htr1b in NAc subpopulations. In unstressed mice, Htr1b

colocalized with Pdyn, Adorsa2a, and Chat-expressing cells (Figure 5A, 5B, S5). To assess the effects of rFSS on Htr1b expression, brains were dissected 30min and 24hr after rFSS and stained tissue sections were compared to unstressed controls (Figure 5C). Total levels of Htr1b, Pdyn, and Adora2a transcript did not change after rFSS (two-way ANOVA, $P> 0.05$) (Figure 3.5D). In contrast, examining the levels of Htr1b in Pdyn and Adora2a subpopulations revealed a significant and selective increase in Htr1b expression in Pdyn+ cells 30min after stress (two-way ANOVA; $F_{2,36}= 3.53$, $P= 0.040$; Sidak post-hoc, $P= 0.046$) (Figure 3.5E). These results indicate that the sub-chronic stressor (rFSS) which potentiates cocaine CPP induces a transient and selective increase in 5-HT1B transcript in Pdyn+ cells of the mNAc.

Discussion

The principal findings of the present study provide insight into the mechanisms by which stress impinges on the serotonin system to sensitize animals to subsequent reward. KOR expression within serotonergic neurons and dynorphin expression within the mNAc were critical to rFSS potentiation of cocaine reward. Our results are schematically summarized (Figure 3.5F). Temporally precise manipulations of DRN circuitry showed that acute inhibition of DRN serotonin neurons drives negative affect and can potentiate subsequent cocaine preference. Additional experiments indicated that KOR-induced decreases in serotonin within the NAc regulate both behavioral coping and cocaine preference. We isolated the effect of decreased serotonin tone at the 5-HT1B receptor by transient blockade of 5-HT1B receptors, which was sufficient to recapitulate the potentiation of cocaine preference observed following KOR activation

(Figure 5F). Lastly, we show that rFSS selectively increases expression of 5-HT1B transcript in Pdyn+ neurons (Figure 3.5F). Together, this evidence details a potential Dyn-KOR-5-HT-5HT1B axis contained within the mNAc, in which rFSS provokes a transient decrease of serotonin tone that is central to passive coping, aversion, and increased cocaine preference.

Stressful events in humans and non-human primates are associated with increased drug preference and drug taking that may facilitate the transition to habitual use [46–49]. RFSS is a sub-chronic, inescapable stressor that induces robust physiological and behavioral responses, and we employed it in this study to model the effects of a stressful event on cocaine preference [1,50]. Similar effects have been observed following other stressors, including nicotine withdrawal and social defeat [9,17,51]. The discrete nature of stress exposure in rFSS allowed for precise control of the timing of stress relative to cocaine administration and facilitated interrogation of the effects of stress on subsequent cocaine preference.

Stress and KOR activation potentiate cocaine preference through interactions at serotonin terminals in the ventral striatum, but the circuitry involved has not been fully characterized [1,5,8,17]. We indicate that the KOR-expressing neurons in the lateral DRN that project to the mNAc and Pdyn-expressing neurons located within the mNAc likely regulate stress potentiation of cocaine preference. Retrograde tracing of dynorphin inputs to the mNAc revealed only inputs from the mNAc itself, implying that Pdyn+ neurons may provide the sole source of dynorphin to this region. This indicates

that in addition to a critical role in stress-potentiation of cocaine preference, Pdyn+ neurons in the NAc may also regulate other behaviors that are dependent on KOR activation in the NAc, including escalation of drug taking, learned helplessness, and pain-induced negative affect and anhedonia [6,20,52–55].

We observed robust aversion to SERTDRN neuronal inhibition in the present study. Although place preference is not a direct measure of affect, this finding supports theories of serotonin function that assert a central role of decreased serotonin tone in negative affect [10,26]. Together with data indicating the necessity of KORSERT in stress potentiation of cocaine CPP, these results suggest that a decrease in serotonin tone may mediate stress-induced dysphoria, thereby increasing subsequent preference for cocaine [9,49]. During stress potentiation of cocaine preference, stress likely decreases NAc serotonin prior to cocaine administration, but this effect is unlikely persistent, as cocaine inhibition of SERT function dramatically increases NAc serotonin tone [9,56]. Thus, temporally precise manipulation of DRN serotonin was crucial to evaluating our central hypothesis that a prior stress-induced decrease in serotonin tone drives subsequent increased sensitivity to drug reward. Our findings support this model and may support a general framework by which KOR and 5-HT-mediated dysphoria increases the relative impact of reward on affect.

Recently, an integral role of SERT-DRN neurons in regulating response to stress and reward has begun to come into focus, but how SERT-DRN neurons mediate the impact of stress on responses to natural and drug reward remains opaque [25,32,34,57]. We

isolated the potential role of decreased serotonin tone in stress potentiation of cocaine preference first by selective inhibition of SERT-DRN neurons prior to cocaine conditioning and demonstrated that a prior reduction in serotonin was sufficient to potentiate subsequent cocaine preference. Surprisingly, we found that inhibition of VGluT3DRN neurons, which overlap extensively with SERT-DRN, strongly attenuated subsequent cocaine preference. We note different baseline cocaine preferences in these genotypes, which may be attributed to strain differences and inter-wave assay variability. However, these differences are likely not responsible for the observed effects of neuronal inhibition, in part because the observed effects were large and controls and experimental mice were assayed concurrently. These findings further demonstrate that the DRN is a critical regulator of reward behavior, and we reason that these divergent effects may be mediated by the non-overlapping fraction of these DRN populations (i.e., SERT+/VGluT3- neurons drive reward potentiation) and their projections. The population of overlapping VGluT3+/SERT+ DRN neurons project to a myriad of target regions, including the lateral hypothalamus, ventral tegmental area and many aspects of the cortex [33]. Based on our DRN in-situ hybridization and projection tracing studies, we suggest the population responsible for stress potentiation of cocaine preference may comprise SERT+/VGluT3/KOR+ neurons of lateral DRN that project to the mNAc. This subregion is anatomically segregated, highly responsive to stress, and separate from parts of the DRN known to innervate other regions involved in reward processing [35,58].

Historically, the effect of stress on serotonin in the NAc has been controversial, with evidence for increases, decreases, and no effect on serotonin tone [9,59–62]. While we did not directly measure 5-HT tone, this study leveraged the neurochemically and anatomically precise nature of terminal optogenetic stimulation during stress to manipulate the SERTDRN-NAc projection and indicate that a decrease in 5-HT tone within the mNAc promotes stress-induced immobility. These findings contribute to recent findings of parallel DRN serotonin subsystems innervating distinct targets to regulate reward and response to stressors [32,34]. Thus, while serotonin tone within the mNAc is a critical regulator of passive coping behavior, serotonin tone in other regions may also regulate passive coping, possibly in coordination with the DRN-mNAc projection.

In this study, we examined potential contributions of the 5-HT1B receptor to stress potentiation of reward. 5-HT1B receptors are Gi-coupled GPCRs that inhibit neurotransmitter release and have been implicated in regulating the response to stressors and psychostimulants [40]. However, the direction of these effects is dependent on brain region, involvement of autoreceptors or heteroreceptors, and stage of addiction cycle [63– 66]. In the mNAc, transient overexpression of 5-HT1B heteroreceptors during mild stress enhances stress-induced potentiation of the psychomotor effects of amphetamine [40]. We observed that transient antagonism of 5-HT1B receptors in the NAc was sufficient to recapitulate potentiation of cocaine preference induced by stress or decreased serotonin tone. Transient antagonism of NAc 5-HT1B receptors also potentiated social preference, a behavior mediated by NAc

5-HT1B receptors, which also recapitulates reports of stressinduced increases in social preference [23,43]. At the behavioral level, these increases in drug and social reward seeking may represent an attempt to buffer the negative hedonic effects of stress [27,67]. At the receptor level, these data suggest that 5-HT1B in the NAc acts as a critical signal transducer, sensing a decrease in 5-HT tone and initiating postsynaptic consequences that result in potentiation of reward. Our findings also indicate that the mechanism by which decreased 5-HT1B activation results in potentiation of subsequent cocaine reward may generalize to processing of other rewarding stimuli, including natural rewards. Lastly, we showed that potentiation of cocaine preference induced by transient prior blockade of NAc 5-HT1B was attenuated by an additional antagonist infusion that blocked 5-HT1B receptors during cocaine conditioning. These findings indicate that the 5-HT1B receptor is not only involved in initiating reward potentiation but is involved in mediating the expression of increased reward as well.

5-HT1B transcript is highly expressed in the NAc, and prior work indicates that chronic exposure to stressors or psychostimulants may regulate its expression within the accumbens to increase reward sensitivity [42,44]. Colocalization of the 5-HT1B transcript (Htr1b) with markers of the direct pathway (Pdyn), indirect pathway (Adora2a), and cholinergic interneurons (Chat) showed uniform distribution across these cell types, indicating that serotonin actions through 5-HT1B receptors may regulate these populations in concert to modulate processing in the NAc. Following stress, 5-HT1B mRNA increased within Pdyn+, but not Adora2a+ neurons, suggesting that stress selectively increases the expression of 5-HT1B transcript in cells of the direct pathway.

Whether this increase in transcript is accompanied by an increase in functional receptors remains to be tested. Prior work has also shown that overexpression of 5-HT1B receptors in the NAc sensitizes rats to the hedonic properties of cocaine [39,68], which intimates that stress-induced increases of postsynaptic 5-HT1B receptors in direct pathway neurons may mediate stress potentiation of reward. The attenuation of potentiated cocaine preference by 5-HT1B receptor blockade during cocaine conditioning supports this conclusion.

Chronic stress induces hedonic and motivational deficits that contribute to depression-like behavior, but sub-chronic stress can provoke coping responses. This coping response may include a proadaptive hedonic allostasis that increases sensitivity to reward and is reflected by increases in mNAc 5-HT1B expression. We indicate this coping response is maladaptive in the context of drug exposure, resulting in increased drug preference and enhanced addiction risk. Broadly, we hypothesize that the proadaptive compensatory adaptations that underlie reward potentiation are exhausted following chronic stress exposure. Collapse of adaptations in this circuit and others may be expected to decrease reward sensitivity. While our data are consistent with this interpretation, future work is required to assess the behavioral and cellular tenets of this theory. In human studies, polymorphisms of the 5-HT1B receptor have been associated with major depression and substance use disorder [69–71], and receptor binding studies show altered 5-HT1B binding in the NAc of subjects with major depression and alcohol dependence [72,73]. Such findings suggest a central role of NAc 5-HT1B receptors in regulation of affect and substance use, but a potential connection to the

Dyn/KOR system and stress potentiation of addiction risk has not been previously evaluated. The insights gleaned from this study support a functional Dyn-KOR-5-HT-5-HT1B axis in which decreased 5-HT is a central regulator of drug preference, affect, and response to stressors. Future studies will be required to directly evaluate the consequences and kinetics of the stress and dynorphin-mediated effects on functional 5-HT1B receptors and evaluate the therapeutic potential of this dynamic circuit.

Author contributions: HMF, PS, CN, RT and AA conducted the experiments. HMF, PS, RT analyzed the results. All of the authors contributed to the design of the experiments. HMF and CC wrote the manuscript. JFN, PS, and BBL provided editorial comments.

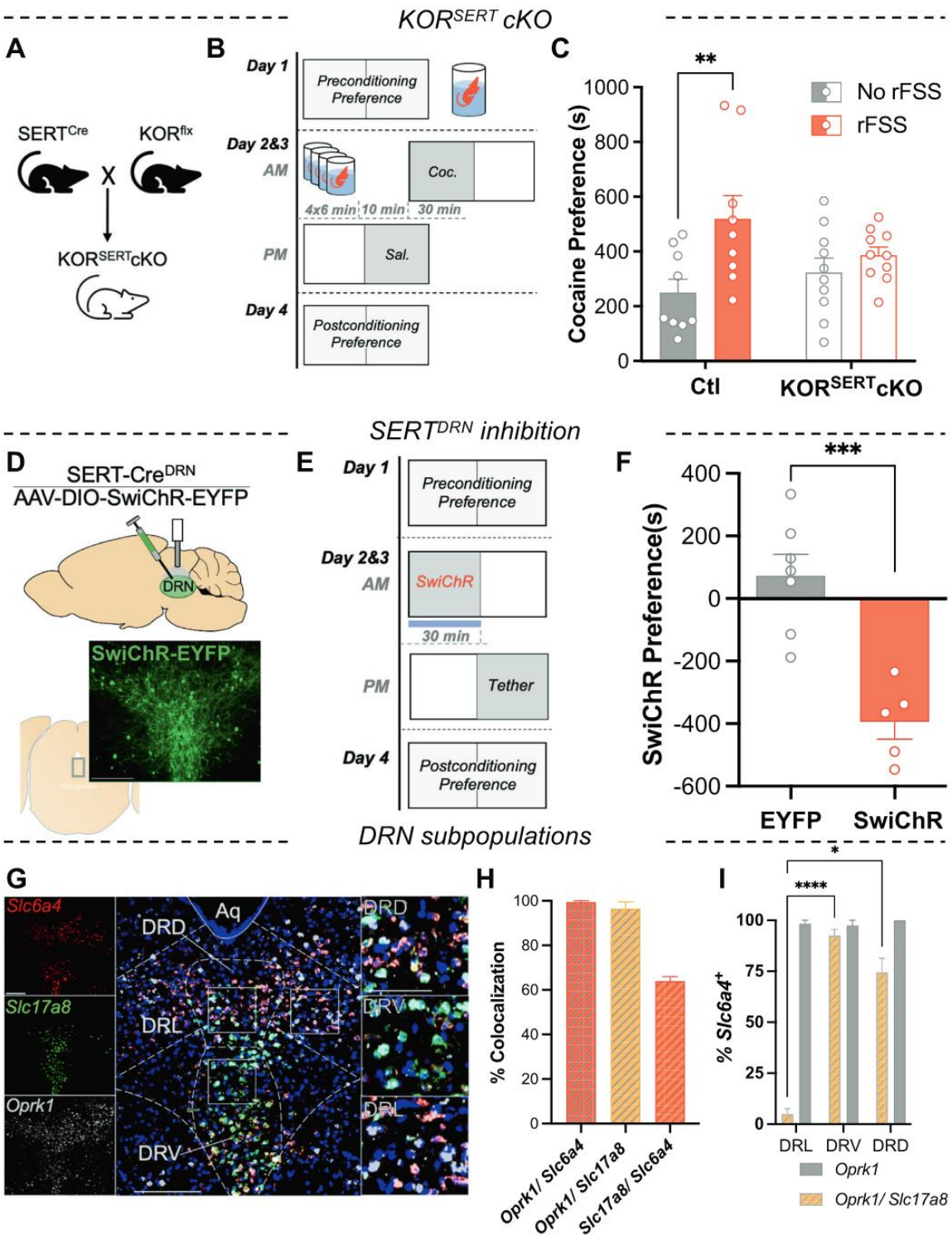
KOR^SERT cKO
A
SERT^Cre
KOR^flx
X
KOR^SERTcKO
B
Day 1
Preconditioning Preference
Day 2&3
AM
Coc.
4x6 min
10 min
30 min
PM
Sal.
Day 4
Postconditioning Preference
C
**
No rFSS
rFSS
Cocaine Preference (s)
1000
800
600
400
200
0
Ctl
KOR^SERTcKO
SERT^DRN inhibition
D
SERT-Cre^DRN
AAV-DIO-SwiChR-EYFP
DRN
SwiChR-EYFP
E
Day 1
Preconditioning Preference
Day 2&3
AM
SwiChR
30 min
PM
Tether
Day 4
Postconditioning Preference
F
***
SwiChR Preference(s)
400
200
0
-200
-400
-600
EYFP
SwiChR
DRN subpopulations
G
Slc6a4
Slc17a8
Oprk1
Aq
DRD
DRL
DRV
H
% Colocalization
100
80
60
40
20
0
Oprk1/ Slc6a4
Oprk1/ Slc17a8
Slc17a8/ Slc6a4
I
*
****
% Slc6a4+
100
75
50
25
0
DRL
DRV
DRD
Oprk1
Oprk1/ Slc17a8

Figure 3.1. Serotonin neuron kappa opioid receptors mediate stress potentiation of cocaine reward and can be mimicked by optogenetic inhibition. (A) Breeding scheme used to excise KOR gene from SERT expressing neurons. (B) Schematic of rFSS potentiation of cocaine CPP protocol. Mice were subjected to rFSS on day 1 and day 2 prior to cocaine conditioning. (C) Stress potentiation of cocaine preference scores for control and KORSERT cKO mice with or without prior stress (n=9-10). (D) Cartoon depicting DRN injection of inhibitory opsin (AAV5-DIO-SwiChR-EYFP) and cannula placement in a SERT-cre mouse. Below: image showing EYFP expression in the DRN. Scale bar= 50 µm. (E) Schematic of optogenetic CPA protocol. During optogenetic conditioning, the mouse was confined to one chamber where it received opto-inhibition of SERTDRN neurons. (F) Serotonin inhibition preference scores (postconditioning-preconditioning preference for opto-paired chamber) for control and SwiChR-inhibition conditioned groups (n=5-7). (G) Representative image showing expression of transcripts for SERT (Slc6a4), VGluT3 (Slc17a8), and KOR (Oprk1) in the medial DRN. Right insets: higher magnification of rectangular regions showing colocalization in cells of the dorsal, ventral, and lateral aspects of the DRN (DRD, DRV, DRL, respectively). Scale bar= 200µm, 200µm, 25 µm. (H) Quantitation of cells co-expressing two transcripts, expressed as percentage cells in the denominator indicated (n=3). (I) Quantitation of Slc6a4+ cells coexpressing Oprk1 or both Oprk1 and Slc17a8 in each subregion, expressed as percentage of Slc6a4+ cells per subregion.

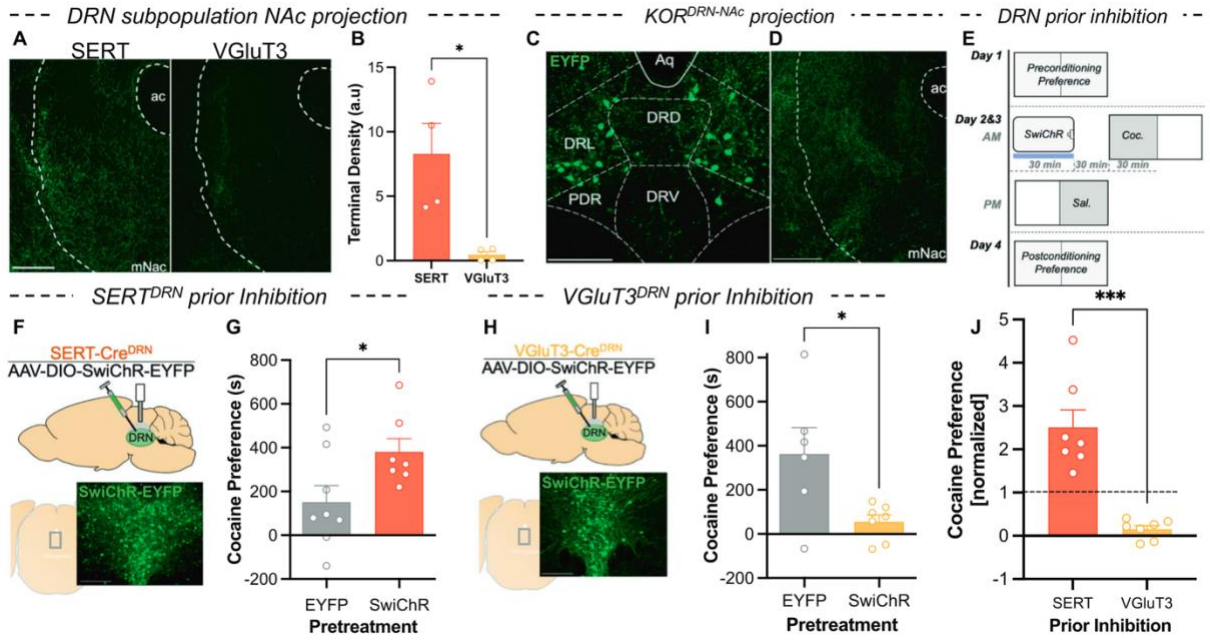

Figure 3.2. Prior inhibition of DRN serotonin subpopulations with distinct projection bias has divergent effects on cocaine preference. (A) NAc terminal expression of EYFP-tagged ChR2 in a SERT-Cre and VGluT3-Cre mouse. Scale bar=200µm. (B) Quantification of terminal density (arbitrary units) in the NAc of SERT-cre and VGluT3cre mice (n=4). (C) Expression of retrogradely-delivered EYFP in subregions of central DRN of KOR-Cre mouse. Scale bar=200µm. (D) Expression of EYFP+ terminals in the NAc of KOR-Cre mice. Scale bar=200µm (E) Schematic showing assay of optogenetic replication of KOR-mediated cocaine CPP potentiation. Mice received optogenetic inhibition of specified DRN subpopulations prior to cocaine conditioning. (F) Cartoon depicting injection of AAV5-DIO-SwiChR-eYFP into the DRN and placement of cannula above injection site. Below: expression of EYFP-tagged SwiChR in the DRN of a SERTCre mouse. Scale bar=50µm (G) Cocaine preference scores (postconditioning preference-preconditioning preference) for groups subject to control treatment and SERT+ neuron inhibition prior to conditioning (n=7-8). (H) Cartoon depicting injection of AAV5-DIO-SwiChR-EYFP into the DRN and placement of the cannula above the injection site. Below: expression of EYFP-tagged SwiChR in the DRN of a VGluT3-Cre mouse. Scale bar=50µm. (I) Cocaine preference scores for groups subjected to control treatment and VGluT3+ neuron inhibition prior to conditioning (n=6-7). (J) Comparison of cocaine preference scores (normalized to respective EYFP controls) following inhibition of SERTDRN or VGluT3DRN neurons (n=7).

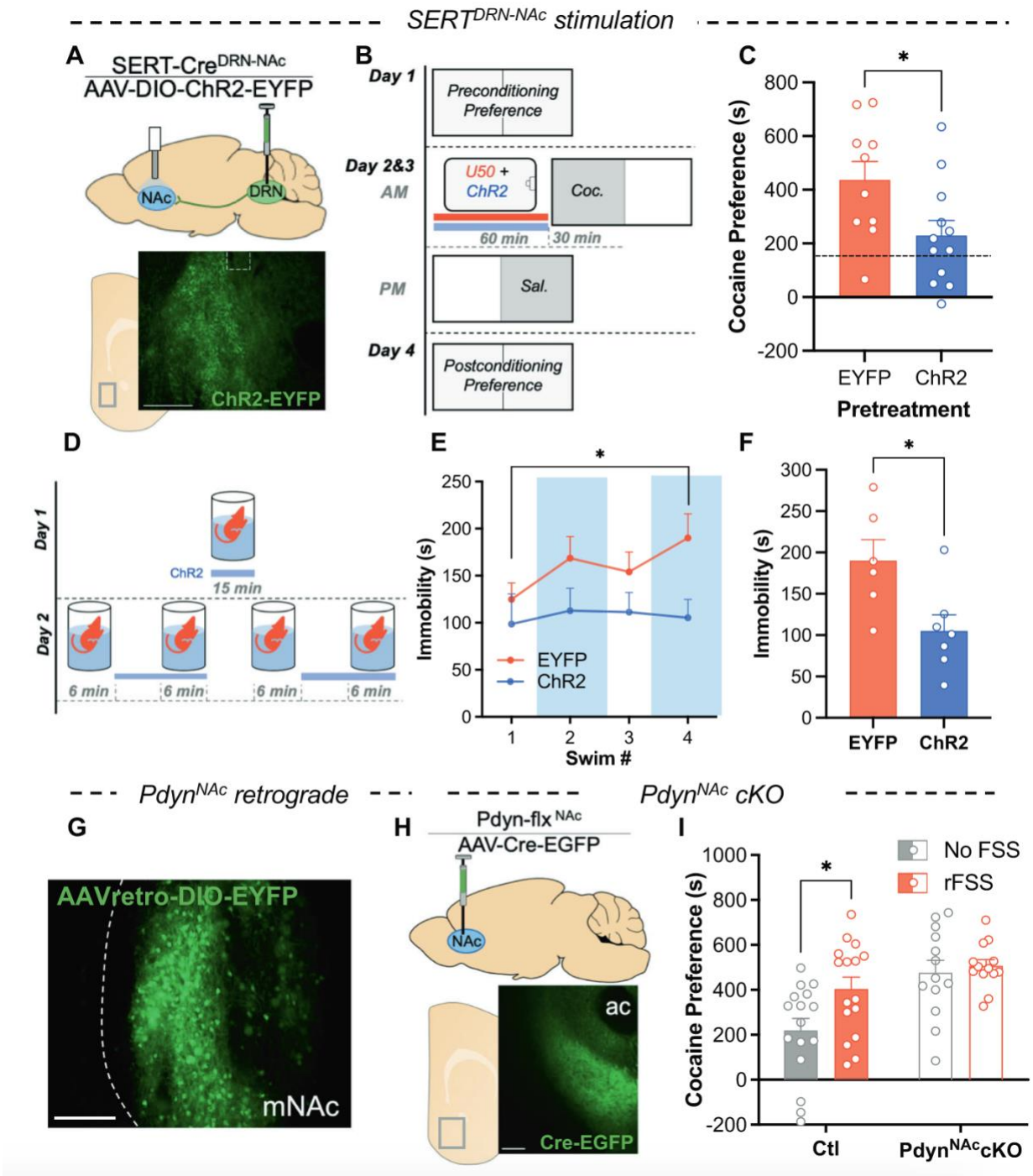
SERT^DRN-NAc stimulation
A
SERT-Cre DRN-NAc
AAV-DIO-ChR2-EYFP
NAc
DRN
ChR2-EYFP
B
Day 1
Preconditioning Preference
Day 2&3
AM
U50 + ChR2
Coc.
60 min
30 min
PM
Sal.
Day 4
Postconditioning Preference
C
Cocaine Preference (s)
EYFP
ChR2
Pretreatment
D
Day 1
ChR2
15 min
Day 2
6 min
6 min
6 min
6 min
E
Immobility (s)
EYFP
ChR2
Swim #
F
Immobility (s)
EYFP
ChR2
Pdyn^NAc retrograde
Pdyn^NAc cKO
G
AAVretro-DIO-EYFP
mNAc
H
Pdyn-flx NAc
AAV-Cre-EGFP
NAc
ac
Cre-EGFP
I
No FSS
rFSS
Cocaine Preference (s)
Ctl
Pdyn^NAc cKO

Figure 3.3. Stimulation of DRN-NAc serotonin terminals and PdynNAc cKO regulates cocaine preference. (A) Cartoon showing DRN injection of AAV5-DIO-ChR2-EYFP and placement of optical cannula above the NAc in a SERT-Cre mouse. Below: expression of EYFP+ terminals in NAc of SERT-Cre mouse. (B) Schematic of cocaine CPP with pretreatment of KOR agonist and stimulation of serotonin terminals prior to cocaine conditioning. Prior to each cocaine conditioning session, mice were pretreated with KOR agonist (U50488; 5mg/kg I.P.) and received concurrent optical stimulation of serotonin terminals in the NAc or control treatment. (C) Cocaine preference scores of mice receiving KOR agonist prior to cocaine conditioning with or without concurrent ChR2 stimulation of SERT+ terminals in the NAc (Dashed line shows typical unstressed cocaine preference) (n=10-12). (D) Schematic of optical stimulation of SERT+ terminals in the NAc during rFSS. (E) Time immobile during swim bouts on day 2 of rFSS for mice with stimulation of NAc SERT terminals and controls (n=6-7). (F) Time immobile during last swim bout of rFSS in panel E. (G) Representative images showing expression of retrogradely-delivered fluorophore (EYFP) in the NAc of a Pdyn-Cre mouse. Scale bar=200µm. (H) Cartoon showing injection of virus delivering Cre-recombinase (AAV-Cre-EGFP) to the NAc of Pdyn-flx mice. Below: representative image showing expression of AAV-Cre-EGFP in the NAc. (I) Raw cocaine preference scores for control and PdynNAc cKO mice with or without prior stress (n=13-16).

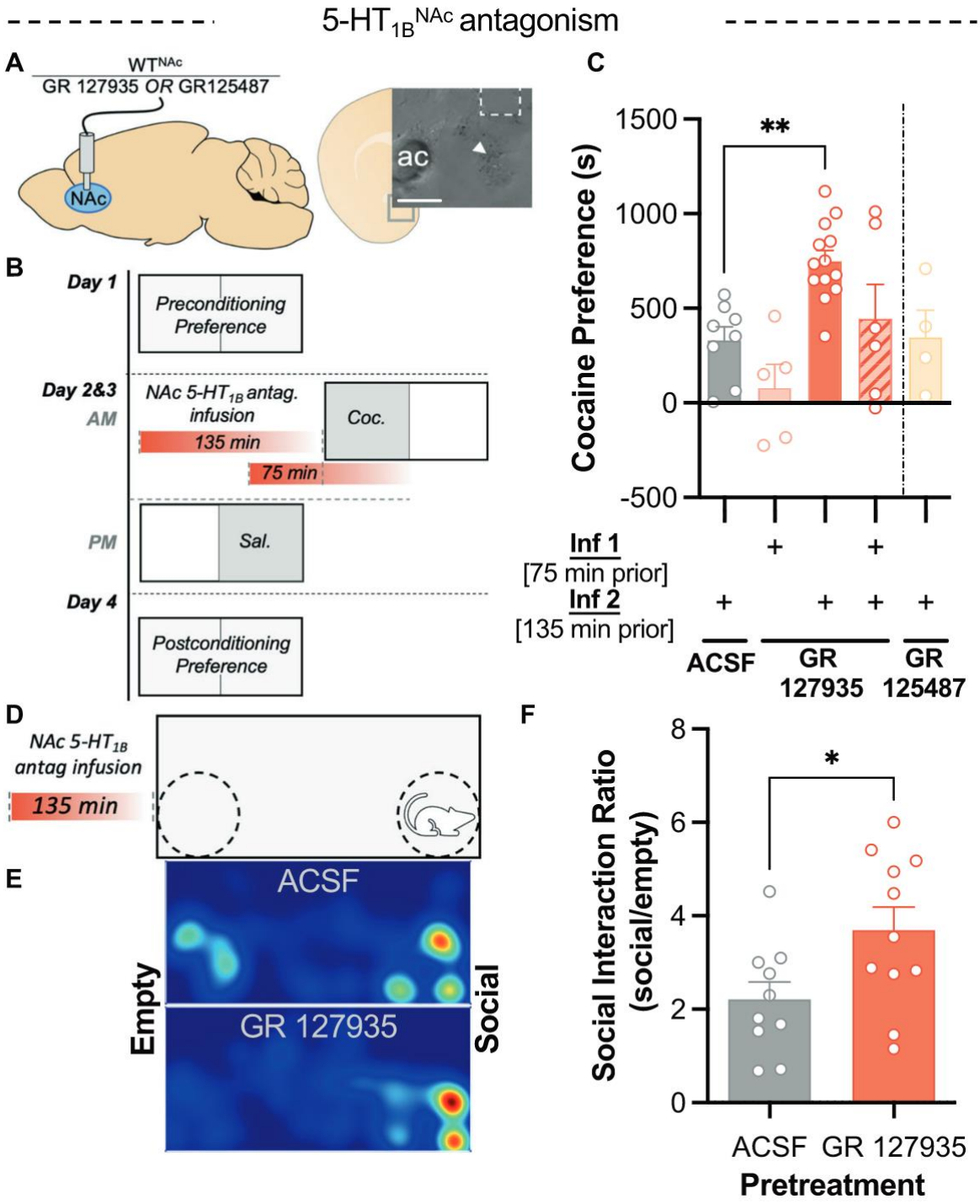
5-HT1BNAc antagonism
A
WTNAc
GR 127935 OR GR125487
NAc
ac
B
Day 1
Preconditioning Preference
Day 2&3
AM
NAc 5-HT1B antag. infusion
135 min
75 min
Coc.
PM
Sal.
Day 4
Postconditioning Preference
C
Cocaine Preference (s)
1500
1000
500
0
-500
**
Inf 1
[75 min prior]
Inf 2
[135 min prior]
ACSF
GR 127935
GR 125487
D
NAc 5-HT1B antag infusion
135 min
E
ACSF
GR 127935
Empty
Social
F
Social Interaction Ratio (social/empty)
8
6
4
2
0
*
ACSF
GR 127935
Pretreatment

Figure 3.4. Prior 5-HT1B receptor antagonism in NAc potentiates subsequent cocaine and social preference. (A) Cartoon showing implantation of fluid cannula for infusion of 5-HTR antagonists into the NAc of WT mice. (Inset) image showing dye injection (arrow) and damage from cannula confirming placement in medial NAc. Scale bar=200µm. (B) Schematic of cocaine CPP procedure showing pretreatment with NAc infusions of 5-HT1B antagonist (GR 127935) at time points 75min or 135min prior to cocaine conditioning. (C) Cocaine place preference scores (postconditioning-preconditioning preference) for mice following infusions of 5-HT1B antagonist GR 127935, 5-HT4 antagonist GR 125487, or ACSF in the NAc at time points 135min, 75min, or 135min+75min prior to cocaine conditioning (as depicted in panel B) (n=4-13) (D) Schematic showing pretreatment NAc infusion of 5-HT1B antagonist prior to three-chamber social interaction assay. (E) Representative heatmaps indicating the distribution of time spent in the social interaction apparatus after infusion of GR 127935 into the NAc 135min prior and ACSF infusion control. (F) Social interaction ratio (time spent in social zone/time spent in empty zone) following pretreatment with GR 127935 (n=10-11).

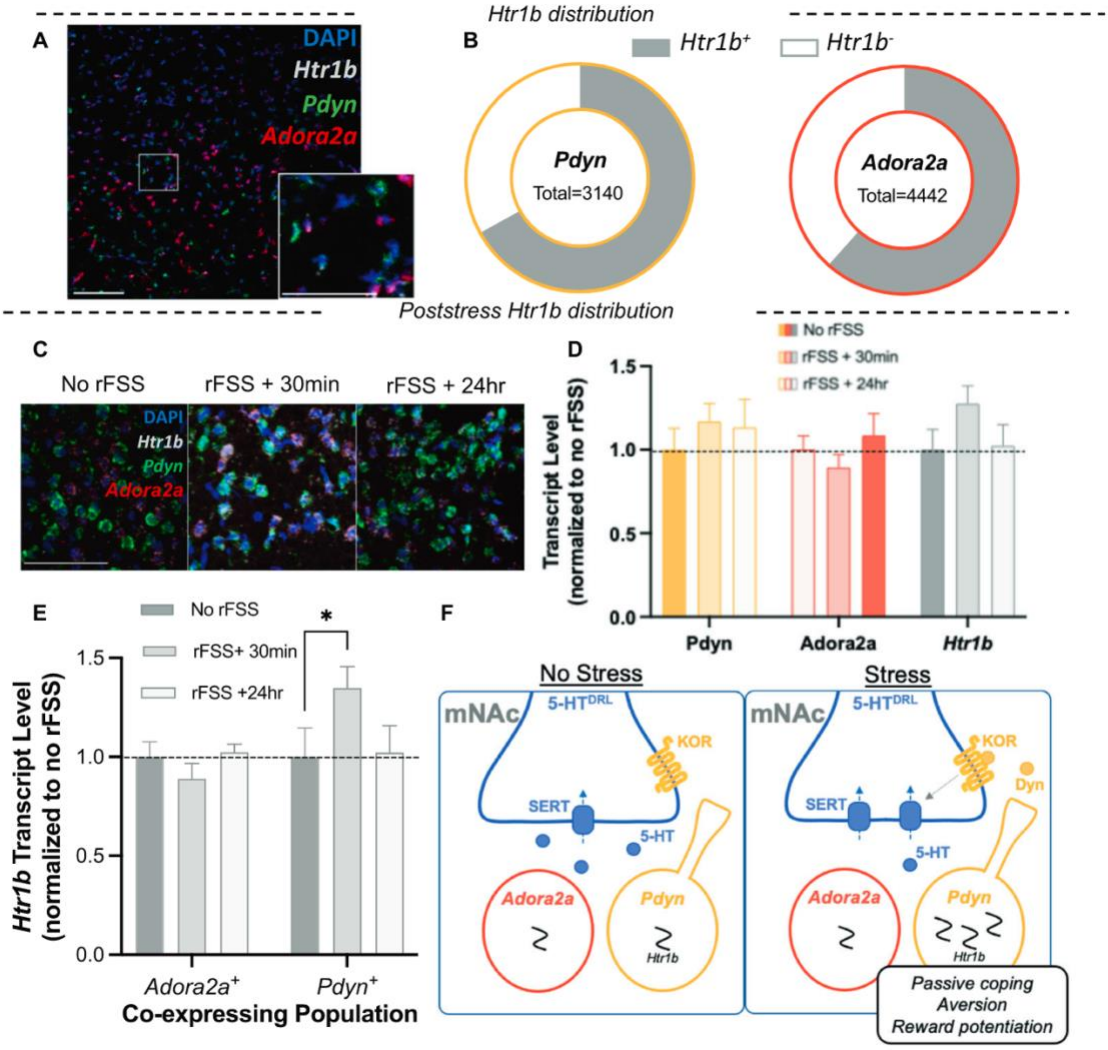
A
DAPI
Htr1b
Pdyn
Adora2a
B
Htr1b distribution
Htr1b+
Htr1b-
Pdyn
Total=3140
Adora2a
Total=4442
Poststress Htr1b distribution
C
No rFSS
rFSS + 30min
rFSS + 24hr
DAPI
Htr1b
Pdyn
Adora2a
D
No rFSS
rFSS + 30min
rFSS + 24hr
Transcript Level
(normalized to no rFSS)
1.5
1.0
0.5
0.0
Pdyn
Adora2a
Htr1b
E
No rFSS
rFSS+ 30min
rFSS +24hr
*
Htr1b Transcript Level
(normalized to no rFSS)
1.5
1.0
0.5
0.0
Adora2a+
Pdyn+
Co-expressing Population
F
No Stress
Stress
mNAc
5-HTDRL
KOR
SERT
5-HT
Dyn
Adora2a
Pdyn
Htr1b
Passive coping
Aversion
Reward potentiation

Figure 3.5. Stress induces a transient and cell-type specific increase in Htr1b expression in the NAc. (A) Representative image showing in-situ hybridization labeling Pdyn, Adora2a, and Htr1b transcripts in the medial NAc. Inset: higher magnification of rectangular region. Scale bar= 100µm, 25µm (inset). (B) Proportion of each subpopulation that expresses Htr1b. (C) Representative images showing colocalization and intensity of labelling of Pdyn, Adora2a, and Htr1b transcripts in the medial NAc after stress. Scale bar=25µm. (D) Quantified total levels of Pdyn, Adora2a, and Htr1b following stress, normalized to no rFSS controls (n=6-8). (E) Quantified levels of Htr1b transcripts expressed in Pdyn+ and Adora2a+ cells following stress, normalized to no rFSS controls. (F) Summary schematic of NAc circuit mediating response to stressors, aversion, and reward potentiation. With exception of SERT, the schematic is simplified to include only entities measured or manipulated in this study. Briefly: Stress activation of KOR by dynorphinergic neurons within the mNAc induces translocation of SERT, which decreases serotonin tone in the the mNAc. Decreased serotonin tone in the mNAc is aversive, drives passive stress response, and regulates subsequent cocaine preference. NAc 5-HT1B receptors are critical to the induction and expression of this stress potentiation of cocaine preference. RFSS induces a selective increase 5-HT1B transcript in the Pdyn+ neurons in the NAc, suggesting potential pathway specific regulation of reward processing following stress

REFERENCES

1. McLaughlin JP, Marton-Popovici M, Chavkin C. κ opioid receptor antagonism and prodynorphin gene disruption block stress-induced behavioral responses. J Neurosci. 2003;23:5674–5683.

2. Redila VA, Chavkin C. Stress-induced reinstatement of cocaine seeking is mediated by the kappa opioid system. Psychopharmacology (Berl). 2008;200:59–70.
3. Sinha R. Chronic Stress, Drug Use, and Vulnerability to Addiction. Ann N Y Acad Sci. 2008;1141:105–130.

4. Mantsch JR, Vranjkovic O, Twining RC, Gasser PJ, McReynolds JR, Blacktop JM. Neurobiological mechanisms that contribute to stress-related cocaine use. Neuropharmacology. 2014;76:383–394.

5. McLaughlin JP, Land BB, Li S, Pintar JE, Chavkin C. Prior Activation of Kappa Opioid Receptors by U50,488 Mimics Repeated Forced Swim Stress to Potentiate Cocaine Place Preference Conditioning. Neuropsychopharmacol Off Publ Am Coll Neuropsychopharmacol. 2006;31:787–794.

6. Whitfield TW, Schlosburg JE, Wee S, Gould A, George O, Grant Y, et al. Opioid Receptors in the Nucleus Accumbens Shell Mediate Escalation of Methamphetamine Intake. J Neurosci. 2015;35:4296–4305.

7. Smith JS, Lefkowitz RJ, Rajagopal S. Biased signalling: from simple switches to allosteric microprocessors. Nat Rev Drug Discov. 2018;17:243–260.

8. Land BB, Bruchas MR, Schattauer S, Giardino WJ, Aita M, Messinger D, et al. Activation of the kappa opioid receptor in the dorsal raphe nucleus mediates the aversive effects of stress and reinstates drug seeking. Proc Natl Acad Sci U S A. 2009;106:19168–19173.

9. Schindler AG, Messinger DI, Smith JS, Shankar H, Gustin RM, Schattauer SS, et al. Stress Produces Aversion and Potentiates Cocaine Reward by Releasing Endogenous Dynorphins in the Ventral Striatum to Locally Stimulate Serotonin Reuptake. J Neurosci. 2012;32:17582–17596.

10. Luo M, Zhou J, Liu Z. Reward processing by the dorsal raphe nucleus: 5-HT and beyond. Learn Mem. 2015;22:452–460.

11. Yuanyuan J, Rui S, hua T, Jingjing C, Cuola D, Yuhui S, et al. Genetic association analyses and meta-analysis of Dynorphin-Kappa Opioid system potential functional variants with heroin dependence. Neurosci Lett. 2018;685:75–82.

12. Gerra G, Leonardi C, Cortese E, D'Amore A, Lucchini A, Strepparola G, et al. Human Kappa opioid receptor gene (OPRK1) polymorphism is associated with opiate addiction. Am J Med Genet B Neuropsychiatr Genet. 2018;144B:771–775.

13. Yuferov V, Levran O, Proudnikov D, Nielsen DA, Kreek MJ. Search for Genetic Markers and Functional Variants Involved in the Development of Opiate and Cocaine Addiction, and Treatment. Ann N Y Acad Sci. 2010;1187:184–207.

14. Caspi A, Sugden K, Moffitt TE, Taylor A, Craig IW, Harrington H, et al. Influence of life stress on depression: moderation by a polymorphism in the 5-HTT gene. Science. 2003;301:386–389.

15. Land BB, Bruchas MR, Lemos JC, Xu M, Melief EJ, Chavkin C. The Dysphoric Component of Stress Is Encoded by Activation of the Dynorphin -Opioid System. J Neurosci. 2008;28:407–414.

16. Ehrich JM, Messinger DI, Knakal CR, Kuhar JR, Schattauer SS, Bruchas MR, et al. Kappa Opioid Receptor-Induced Aversion Requires p38 MAPK Activation in VTA Dopamine Neurons. J Neurosci. 2015;35:12917–12931.

17. Bruchas MR, Schindler AG, Shankar H, Messinger DI, Miyatake M, Land BB, et al. Selective p38α MAPK Deletion in Serotonergic Neurons Produces Stress Resilience in Models of Depression and Addiction. Neuron. 2011;71:498–511.

18. Lemos JC, Roth CA, Messinger DI, Gill HK, Phillips PEM, Chavkin C. Repeated Stress Dysregulates -Opioid Receptor Signaling in the Dorsal Raphe through a p38 MAPKDependent Mechanism. J Neurosci. 2012;32:12325–12336.

19. McDevitt RA, Tiran-Cappello A, Shen H, Balderas I, Britt JP, Marino RAM, et al. Serotonergic versus Nonserotonergic Dorsal Raphe Projection Neurons: Differential Participation in Reward Circuitry. Cell Rep. 2014;8:1857–1869.

20. Liu Z, Zhou J, Li Y, Hu F, Lu Y, Ma M, et al. Dorsal Raphe Neurons Signal Reward through 5-HT and Glutamate. Neuron. 2014;81:1360–1374.

21. Qi J, Zhang S, Wang H-L, Wang H, de Jesus Aceves Buendia J, Hoffman AF, et al. A glutamatergic reward input from the dorsal raphe to ventral tegmental area dopamine neurons. Nat Commun. 2014;5:5390.

22. Wang H-L, Zhang S, Qi J, Wang H, Cachope R, Mejias-Aponte CA, et al. Dorsal Raphe Dual Serotonin-Glutamate Neurons Drive Reward by Establishing Excitatory Synapses on VTA Mesoaccumbens Dopamine Neurons. Cell Rep. 2019;26:1128-1142.e7.

23. Walsh JJ, Christoffel DJ, Heifets BD, Ben-Dor GA, Selimbeyoglu A, Hung LW, et al. 5-HT release in nucleus accumbens rescues social deficits in mouse autism model. Nature. 2018;560:589.

24. Marcinkiewcz CA, Mazzone CM, D'Agostino G, Halladay LR, Hardaway JA, DiBerto JF, et al. Serotonin engages an anxiety and fear-promoting circuit in the extended amygdala., Serotonin engages an anxiety and fear-promoting circuit in the extended amygdala. Nat Nat. 2016;537, 537:97, 97–101.

25. Zhong W, Li Y, Feng Q, Luo M. Learning and Stress Shape the Reward Response Patterns of Serotonin Neurons. J Neurosci. 2017;37:8863–8875.

26. Cohen JY, Amoroso MW, Uchida N. Serotonergic neurons signal reward and punishment on multiple timescales. ELife. 2015;4.

27. Steger JS, Land BB, Lemos JC, Chavkin C, Phillips PEM. Insidious Transmission of a Stress-Related Neuroadaptation. Front Behav Neurosci. 2020;14.

28. Bruchas MR, Xu M, Chavkin C. Repeated Swim-Stress Induces Kappa Opioid-Mediated Activation of ERK1/2 MAPK. Neuroreport. 2008;19:1417–1422.

29. Lesiak AJ, Coffey K, Cohen JH, Liang KJ, Chavkin C, Neumaier JF. Sequencing the serotonergic neuron translatome reveals a new role for Fkbp5 in stress. Mol Psychiatry. 2020. 4 May 2020. https://doi.org/10.1038/s41380-020-0750-4.

30. Berndt A, Lee SY, Ramakrishnan C, Deisseroth K. Structure-Guided Transformation of Channelrhodopsin into a Light-Activated Chloride Channel. Science. 2014;344:420–424.

31. Chen C-C, Lu J, Yang R, Ding JB, Zuo Y. Selective activation of parvalbumin interneurons prevents stress-induced synapse loss and perceptual defects. Mol Psychiatry. 2018;23:1614.

32. Ren J, Friedmann D, Xiong J, Liu CD, Ferguson BR, Weerakkody T, et al. Anatomically Defined and Functionally Distinct Dorsal Raphe Serotonin Sub-systems. Cell. 2018. 23 August 2018. https://doi.org/10.1016/j.cell.2018.07.043.

33. Ren J, Isakova A, Friedmann D, Zeng J, Grutzner SM, Pun A, et al. Single-cell transcriptomes and whole-brain projections of serotonin neurons in the mouse dorsal and median raphe nuclei. ELife. 2019;8:e49424.

34. Teissier A, Chemiakine A, Inbar B, Bagchi S, Ray RS, Palmiter RD, et al. Activity of raphé serotonergic neurons controls emotional behaviors. Cell Rep. 2015;13:1965–1976.

35. Valentino RJ, Lucki I, Van Bockstaele E. Corticotropin-releasing Factor in the Dorsal Raphe Nucleus: Linking Stress Coping and Addiction. Brain Res. 2010;1314C:29.

36. Okaty BW, Sturrock N, Escobedo Lozoya Y, Chang Y, Senft RA, Lyon KA, et al. A singlecell transcriptomic and anatomic atlas of mouse dorsal raphe Pet1 neurons. ELife. 2020;9.

37. Brown P, Molliver ME. Dual Serotonin (5-HT) Projections to the Nucleus Accumbens Core and Shell: Relation of the 5-HT Transporter to Amphetamine-Induced Neurotoxicity. J Neurosci. 2000;20:1952–1963.

38. Tervo DGR, Hwang B-Y, Viswanathan S, Gaj T, Lavzin M, Ritola KD, et al. A Designer AAV Variant Permits Efficient Retrograde Access to Projection Neurons. Neuron. 2016;92:372–382.

39. Neumaier JF, Vincow ES, Arvanitogiannis A, Wise RA, Carlezon WA. Elevated Expression of 5-HT1B Receptors in Nucleus Accumbens Efferents Sensitizes Animals to Cocaine. J Neurosci. 2002;22:10856–10863.

40. Ferguson SM, Sandygren NA, Neumaier JF. Pairing mild stress with increased serotonin1B receptor expression in the nucleus accumbens increases susceptibility to amphetamine. Eur J Neurosci. 2009;30:1576–1584.

41. Carhart-Harris RL, Nutt DJ. Serotonin and brain function: a tale of two receptors. J Psychopharmacol (Oxf). 2017;31:1091–1120.

42. Furay AR, McDevitt RA, Miczek KA, Neumaier JF. 5-HT1B mRNA expression after chronic social stress. Behav Brain Res. 2011;224:350–357.

43. Taylor GT. Fear and affiliation in domesticated male rats. J Comp Physiol Psychol. 1981;95:685–693.

44. Hoplight BJ, Vincow ES, Neumaier JF. Cocaine increases 5-HT1B mRNA in rat nucleus accumbens shell neurons. Neuropharmacology. 2007;52:444–449.

45. Neumaier JF, McDevitt RA, Polis IY, Parsons LH. Acquisition of and withdrawal from cocaine self-administration regulates 5-HT mRNA expression in rat striatum. J Neurochem. 2009;111:217–227.

46. Morgan D, Grant KA, Gage HD, Mach RH, Kaplan JR, Prioleau O, et al. Social dominance in monkeys: dopamine D 2 receptors and cocaine self-administration. Nat Neurosci. 2002;5:169–174.

47. Hoyland MA, Latendresse SJ. Stressful life events influence transitions among latent classes of alcohol use. Psychol Addict Behav J Soc Psychol Addict Behav. 2018;32:727– 737.

48. Newcomb MD, Harlow LL. Life events and substance use among adolescents: mediating effects of perceived loss of control and meaninglessness in life. J Pers Soc Psychol. 1986;51:564–577.

49. Bruchas MR, Land BB, Chavkin C. The dynorphin/kappa opioid system as a modulator of stress-induced and pro-addictive behaviors. Brain Res. 2010;1314:44–55.

50. Porsolt RD, Le Pichon M, Jalfre M. Depression: a new animal model sensitive to antidepressant treatments. Nature. 1977;266:730–732.

51. McLaughlin JP, Li S, Valdez J, Chavkin TA, Chavkin C. Social defeat stress-induced behavioral responses are mediated by the endogenous kappa opioid system. Neuropsychopharmacol Off Publ Am Coll Neuropsychopharmacol. 2006;31:1241–1248.

52. Nealey KA, Smith AW, Davis SM, Smith DG, Walker BM. κ-opioid receptors are implicated in the increased potency of intra-accumbens nalmefene in ethanol-dependent rats. Neuropharmacology. 2011;61:35–42.

53. Shirayama Y, Ishida H, Iwata M, Hazama G, Kawahara R, Duman RS. Stress increases dynorphin immunoreactivity in limbic brain regions and dynorphin antagonism produces antidepressant-like effects. J Neurochem. 2004;90:1258–1268.

54. Newton SS, Thome J, Wallace TL, Shirayama Y, Schlesinger L, Sakai N, et al. Inhibition of cAMP Response Element-Binding Protein or Dynorphin in the Nucleus Accumbens Produces an Antidepressant-Like Effect. J Neurosci. 2002;22:10883–10890.

55. Massaly N, Copits BA, Wilson-Poe AR, Hipólito L, Markovic T, Yoon HJ, et al. PainInduced Negative Affect Is Mediated via Recruitment of The Nucleus Accumbens Kappa Opioid System. Neuron. 2019;102:564-573.e6.

56. Andrews CM, Lucki I. Effects of cocaine on extracellular dopamine and serotonin levels in the nucleus accumbens. Psychopharmacology (Berl). 2001;155:221–229.

57. Seo C, Guru A, Jin M, Ito B, Sleezer BJ, Ho Y-Y, et al. Intense threat switches dorsal raphe serotonin neurons to a paradoxical operational mode. Science. 2019;363:538–542.

58. Bang SJ, Commons KG. Forebrain GABAergic Projections From the Dorsal Raphe Nucleus Identified by Using GAD67–GFP Knock-In Mice. J Comp Neurol. 2012;520:4157–4167.

59. Kirby LG, Allen AR, Lucki I. Regional differences in the effects of forced swimming on extracellular levels of 5-hydroxytryptamine and 5-hydroxyindoleacetic acid. Brain Res. 1995;682:189–196.

60. Price ML, Kirby LG, Valentino RJ, Lucki I. Evidence for corticotropin-releasing factor regulation of serotonin in the lateral septum during acute swim stress: adaptation produced by repeated swimming. Psychopharmacology (Berl). 2002;162:406–414.

61. De La Garza R, Mahoney JJ. A distinct neurochemical profile in WKY rats at baseline and in response to acute stress: implications for animal models of anxiety and depression. Brain Res. 2004;1021:209–218.

62. Carlezon WA, Béguin C, DiNieri JA, Baumann MH, Richards MR, Todtenkopf MS, et al. Depressive-Like Effects of the κ-Opioid Receptor Agonist Salvinorin A on Behavior and Neurochemistry in Rats. J Pharmacol Exp Ther. 2006;316:440–447.

63. Filip M, Papla I, Nowak E, Jungersmith K, Przegaliński E. Effects of serotonin (5-HT) 1B receptor ligands, microinjected into accumbens subregions, on cocaine discrimination in rats. Naunyn Schmiedebergs Arch Pharmacol. 2002;366:226–234.

64. Fletcher PJ, Azampanah A, Korth KM. Activation of 5-HT1B receptors in the nucleus accumbens reduces self-administration of amphetamine on a progressive ratio schedule. Pharmacol Biochem Behav. 2002;71:717–725.

65. Pentkowski NS, Acosta JI, Browning JR, Hamilton EC, Neisewander JL. Stimulation of 5HT1B receptors enhances cocaine reinforcement yet reduces cocaine-seeking behavior. Addict Biol. 2009;14:419–430.

66. Pentkowski NS, Harder BG, Brunwasser SJ, Bastle RM, Peartree NA, Yanamandra K, et al. Pharmacological Evidence for an Abstinence-Induced Switch in 5-HT 1B Receptor Modulation of Cocaine Self-Administration and Cocaine-Seeking Behavior. ACS Chem Neurosci. 2014;5:168–176.

67. Ditzen B, Heinrichs M. Psychobiology of social support: The social dimension of stress buffering. Restor Neurol Neurosci. 2014;32:149–162.

68. Barot SK, Ferguson SM, Neumaier JF. 5-HT1B receptors in nucleus accumbens efferents enhance both rewarding and aversive effects of cocaine. Eur J Neurosci. 2007;25:3125– 3131.

69. Sun H-FS, Chang Y-T, Fann CS-J, Chang C-J, Chen Y-H, Hsu Y-P, et al. Association study of novel human serotonin 5-HT1B polymorphisms with alcohol dependence in taiwanese han. Biol Psychiatry. 2002;51:896–901.

70. Huang Y, Oquendo MA, Harkavy Friedman JM, Greenhill LL, Brodsky B, Malone KM, et al. Substance Abuse Disorder and Major Depression are Associated with the

Human 5-HT 1B Receptor Gene (HTR1B) G861C Polymorphism. Neuropsychopharmacology. 2003;28:163–169.

71. Cao J, LaRocque E, Li D. Associations of the 5-hydroxytryptamine (serotonin) Receptor 1B gene (HTR1B) with alcohol, cocaine, and heroin abuse. Am J Med Genet B Neuropsychiatr Genet. 2013;162:169–176.

72. Murrough JW, Neumeister A. The Serotonin 1B Receptor: A New Target for Depression Therapeutics? Biol Psychiatry. 2011;69:714–715.

73. Hu J, Henry S, Gallezot J-D, Ropchan J, Neumaier JF, Potenza MN, et al. Serotonin 1B Receptor Imaging in Alcohol Dependence. Biol Psychiatry. 2010;67:800–803.

Supplemental Results

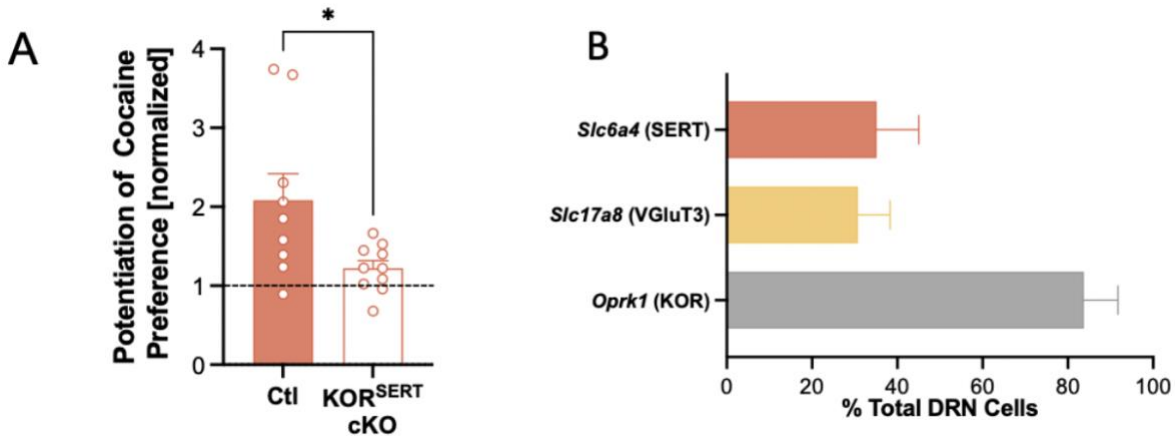

Supplemental Figure S1 (A) Cocaine preference scores with each genotype normalized to its unstressed control (n=9-10). (B) Quantitation of cells expressing transcripts for SERT, VGluT3, KOR, expressed as percentage of total DRN cells (n=3).

We found that KOR transcript was expressed in the majority of DRN cells (84±8.0%) (Figure S1B). Slc6a4 and Slc17a8 were present in a roughly equal percentage of DRN neurons (35±9.9% and 31±7.5%, respectively).

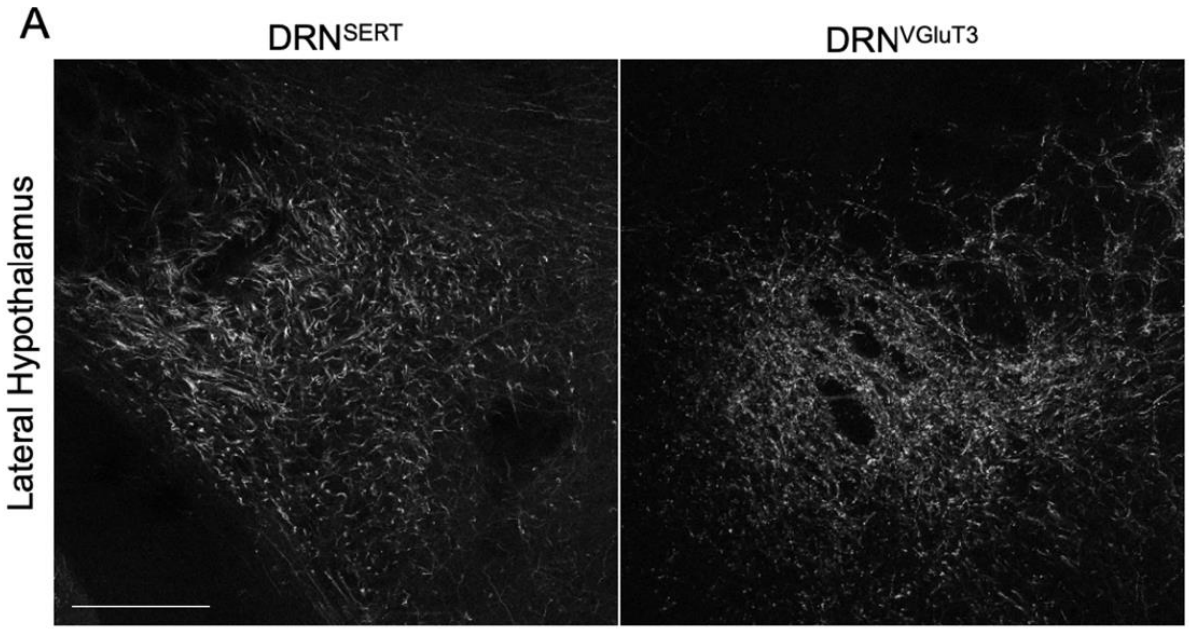

Supplemental Figure S2 (A) Expression of EYFP labeled terminals in lateral hypothalamus following injection of AAV5-DIO-ChR2-EYFP in VGluT3-Cre or SERT-Cre mouse. Scale bar= 200µm.

In contrast to differences observed in terminal density within the mNAc, we observed that the terminal density in the lateral hypothalamus was similar for SERT+ and VGluT3+ projections.

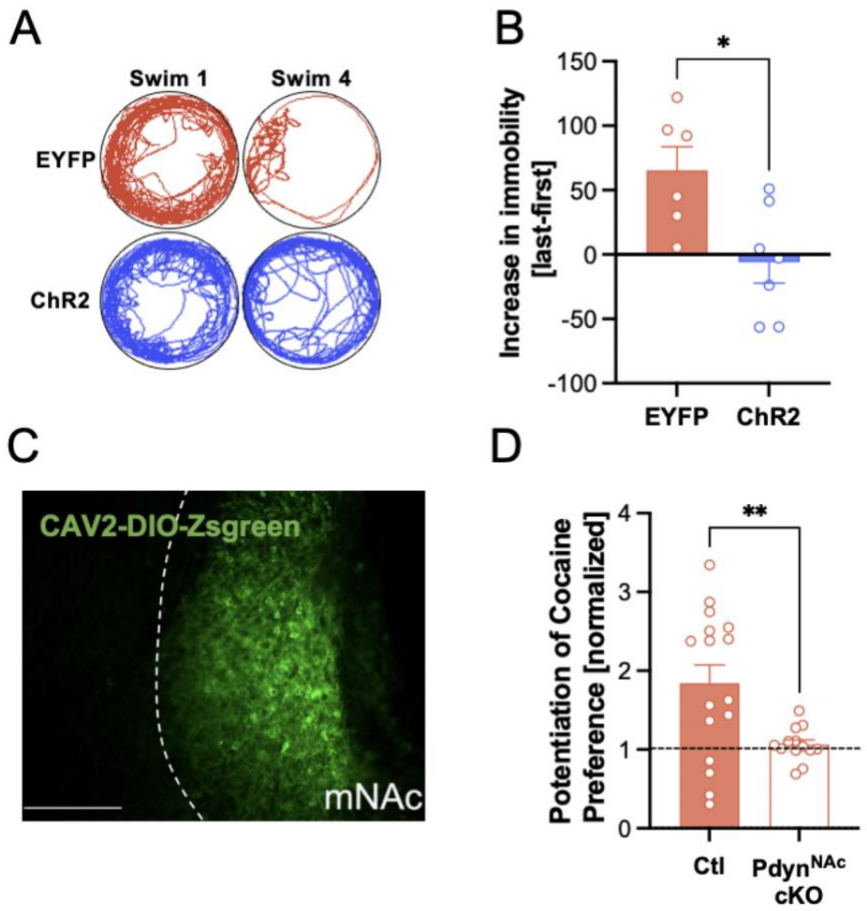

Supplemental Figure S3 (A) Representative track traces during first and last swims on day 2. (B) Change in immobility from first to last swim on day 2 (n=6-7). (C) Representative image of ZsGreen expression in NAc of a Pdyn-Cre mouse. (D) Cocaine preference scores with each group normalized to its unstressed controls (n=13-16).

Movement was tracked during swim sessions and indicated a decrease in movement in the EYFP group that was not apparent in SERTDRN-NAc ChR2 group (Figure S3A). To calculate the escalation of immobility in mice of each group, time immobile during first swim was subtracted from the last swim of day 2 (Figure S3B). The results indicate that

stimulation of serotonergic terminals in the NAc prevents escalation of immobility within subjects (t test, P= 0.014).

Retrograde tracing utilizing a second virus (CAV2-DIO-ZsGreen) injected into the mNAc of a Pdyn-cre mouse also found expression that was restricted to the mNAc. These findings are likely not due to technical limits of the virus or transgenic line, as a recent report using the same virus and transgenic line noted expression in several regions following viral injection into the VTA [11].

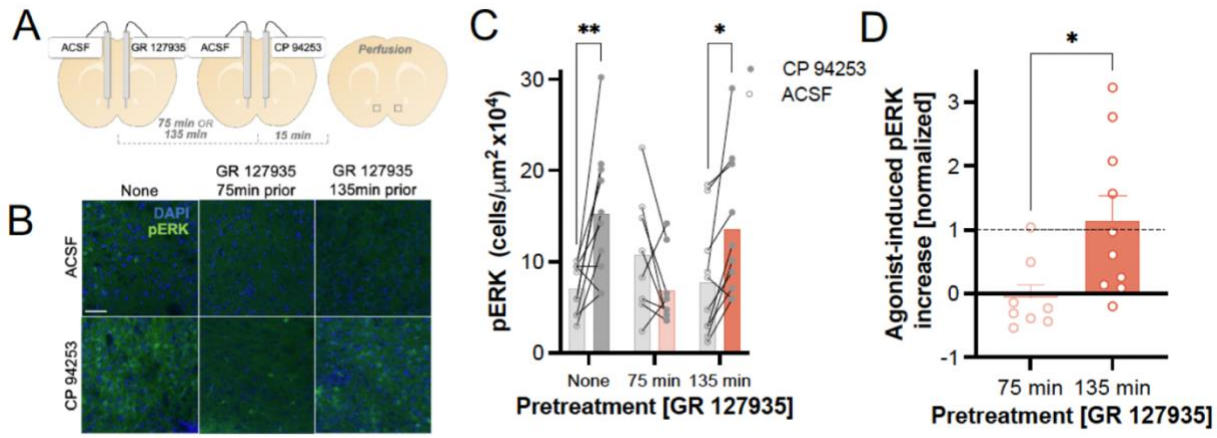

Supplemental Figure S4 (A) Schematic of unilateral NAc infusion of 5-HT1B antagonist GR 127935, followed 75 or 135min later by infusion of 5-HT1B agonist CP 94253 and perfusion. Rectangles show imaging field. (B) Representative images showing immunofluorescent lab phospho-ERK1/2 (pERK) in ACSF (control) hemisphere and hemisphere receiving 5-HT1B ligand infusions. Scale bar= 50μm. (C) Quantification of pERK+ cells in control hemisphere and agonist-infused hemispheres following NAc infusion of GR 127935 prior to CP 94253 (n=8-10). (D) Quantification of pERK+ cells following GR 127935 pretreatment, expressed as percentage of agonist-induced increase in pERK compared to ACSF and normalized to agonist-induced increase without pretreatment (n=8-10).

Two time points were selected to evaluate the duration of antagonist-mediated blockade of the receptor. Injection cannula were placed in the mNAc of WT mice and 5-HT1B antagonist GR 127935 was infused unilaterally (Figure S4A). This was followed either

75min or 135min later by unilateral infusion of 5-HT1B agonist CP 93129 and perfusion of the brain 15min later. ACSF was infused in the opposite hemisphere during each drug infusion to control for nonspecific effects of the infusion procedure on ERK phosphorylation. Coronal sections containing the mNAc were probed for pERK-immunoreactivity (IR), a consequence of 5-HT1B activation (Figure S4B) [12]. Comparison of treatments showed a significant main effect of agonist treatment on agonist stimulated pERK-IR and a significant interaction (two-way ANOVA, agonist main effect, $F_{1,25} = 7.12$, $P= 0.013$; pretreatment X agonist interaction, $F_{2,25}= 8.04$, $P= 0.002$). Post-hoc comparisons indicated that treatment with CP 93129 induced a significant increase in pERK-IR cells as compared to the ACSF control hemisphere in the absence of antagonist pretreatment (Sidak post-hoc, $P= 0.002$). This result confirmed that local infusion of the 5-HT1B agonist induces pERK-IR within mNAc cell bodies. Pretreatment with the antagonist GR 127935 75 min prior to CP 93129 infusion blocked the agonist-induced increase in pERK-IR (Sidak post-hoc, $P= 0.293$), whereas pretreatment 135min prior did not (Sidak post-hoc, $P= 0.033$) (Figure S4C). To further interrogate antagonist duration, the number of pERK+ cells were normalized to the ACSF hemisphere for each subject, and this value was expressed as a fraction of the effect from agonist treatment alone (Figure S4D). This direct comparison of antagonist pretreatment timing illustrates the transient block of pERK-IR caused by GR 127935 infused 75min before CP 93129, but not 135min before agonist (t test, $P= 0.014$).

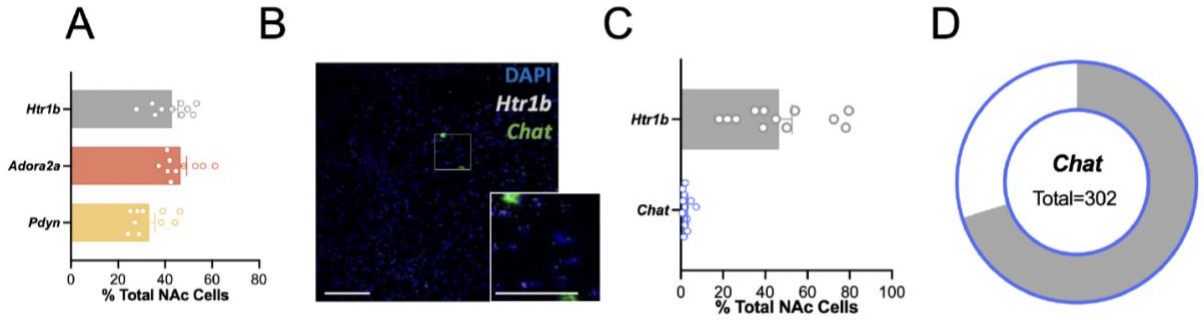

Supplemental Figure S5 (A) Quantification of percent of total cells in the medial NAc positive for Htr1b, Pdyn, and Adora2a (n=6). (B) Representative image showing in-situ hybridization labeling and Htr1b and Chat transcripts in the medial NAc. Inset: higher magnification of rectangular region. Scale bar=100µm, 25µm. (C) Quantification of percent of total cells in the medial NAc positive for Htr1b and Chat (n=6). (D) Fraction of Chat cells expressing Htr1b.

Staining and imaging were performed to assess the colocalization of Htr1b with Pdyn and Adora2a. Results indicate that nearly half (43±2.7%) of the neurons within the mNAc express Htr1b (Figure S5A). Staining for other markers show that Pdyn and Adora2a were detected in a sizeable fraction of neurons (33±2.5% and 45±2.5%, respectively). A second experiment was performed to establish Htr1b colocalization with Chat (Figure S5B, S5C). Chat was expressed sparsely (2.5±0.5%), in line with prior findings, and Htr1b was present in a majority of these neurons (Figure S5C, S5D)[13].

Supplemental References

1. Cai X, Huang H, Kuzirian MS, Snyder LM, Matsushita M, Lee MC, et al. Generation of a KOR-Cre knockin mouse strain to study cells involved in kappa opioid signaling. Genes N Y N 2000. 2016;54:29–37.

2. Ehrich JM, Messinger DI, Knakal CR, Kuhar JR, Schattauer SS, Bruchas MR, et al. Kappa Opioid Receptor-Induced Aversion Requires p38 MAPK Activation in VTA Dopamine Neurons. J Neurosci. 2015;35:12917–12931.

3. McLaughlin JP, Marton-Popovici M, Chavkin C. κ opioid receptor antagonism and prodynorphin gene disruption block stress-induced behavioral responses. J Neurosci. 2003;23:5674–5683.

4. Schindler AG, Messinger DI, Smith JS, Shankar H, Gustin RM, Schattauer SS, et al. Stress Produces Aversion and Potentiates Cocaine Reward by Releasing Endogenous Dynorphins in the Ventral Striatum to Locally Stimulate Serotonin Reuptake. J Neurosci. 2012;32:17582–17596.

5. Steger JS, Land BB, Lemos JC, Chavkin C, Phillips PEM. Insidious Transmission of a Stress-Related Neuroadaptation. Front Behav Neurosci. 2020;14.

6. Bruchas MR, Xu M, Chavkin C. Repeated Swim-Stress Induces Kappa Opioid-Mediated Activation of ERK1/2 MAPK. Neuroreport. 2008;19:1417–1422.

7. Lemos JC, Roth CA, Messinger DI, Gill HK, Phillips PEM, Chavkin C. Repeated Stress Dysregulates -Opioid Receptor Signaling in the Dorsal Raphe through a p38 MAPKDependent Mechanism. J Neurosci. 2012;32:12325–12336.

8. Lesiak AJ, Coffey K, Cohen JH, Liang KJ, Chavkin C, Neumaier JF. Sequencing the serotonergic neuron translatome reveals a new role for Fkbp5 in stress. Mol Psychiatry. 2020. 4 May 2020. https://doi.org/10.1038/s41380-020-0750-4.

9. Franklin KBJ. The mouse brain in stereotaxic coordinates. 3rd ed. New York: Academic Press; 2008.

10. Pinto DFC, Yang H, Dorocic IP, Jong JW de, Han VJ, Peck JR, et al. Characterization of transgenic mouse models targeting neuromodulatory systems reveals organizational principles of the dorsal raphe. Nat Commun. 2019;10:1–14.

11. Fellinger L, Jo YS, Hunker AC, Soden ME, Zweifel LS. A midbrain dynorphin circuit promotes threat generalization. BioRxiv. 2020:2020.04.21.053892.

12. Liu Y, Gibson AW, Levinstein MR, Lesiak AJ, Ong S-E, Neumaier JF. 5-HT 1B ReceptorMediated Activation of ERK1/2 Requires Both Gα i/o and β-Arrestin Proteins. ACS Chem Neurosci. 2019;10:3143–3153.

13. Virk MS, Sagi Y, Medrihan L, Leung J, Kaplitt MG, Greengard P. Opposing roles for serotonin in cholinergic neurons of the ventral and dorsal striatum. Proc Natl Acad Sci U S A. 2016;113:734–739.

Chapter 4

Structure-guided engineering of a fast genetically encoded sensor for real-time physiological and pathophysiological H_2O_2 monitoring

This chapter was formatted for this thesis from the following article in review. “Structure-guided engineering of a fast genetically encoded sensor for real-time physiological and pathophysiological H_2O_2 monitoring”. Lee JD, Won W, Kimball K, Neiswanger C, Wang Y, Schattauer S, Rappleye M, Yeboah F, Ruiz MV, Evitts KM, Bremner SB, Chun C, Smith N, Mack DL, Young JE, Lee CJ, Chavkin C, Berndt A. (2024) *In review.*

My contribution to this work is shown in Figure 6, including fiber photometry and 2-photon microscopy data collection and analysis.

This study highlights the oROS-Gr sensor, a reactive oxygen species (ROS) sensor modified from HyPerRed to have enhanced kinetics for more precise tracking of both transient and steady-state H_2O_2 levels. H_2O_2 dynamics were observed in human stem cell-derived neurons, primary neurons, astrocytes, and mouse brains, demonstrating a broad utility profile. With a growing amount of evidence of the importance of ROS in GPCR regulation, this detection method has been paramount in enhancing our ability to measure ROS generation both for in vivo photometry and ex vivo 2-photon imaging. We are able to achieve single cell resolution with the combination of these methods, allowing us to further interrogate the consequences of ROS signaling in KOR.

Introduction

Endogenous Reactive Oxygen Species (ROS) are indispensable components of aerobic metabolism, which hallmarks the rise of complex life(*1*, *2*). Due to their damaging impact on biological macromolecules at high concentrations, redox homeostasis is tightly regulated in most aerobic systems, and high-level accumulation of ROS is often viewed as a pathogenic marker in degenerative diseases (e.g. Alzheimer's disease, Duchenne Muscular Dystrophy), tumorigenesis, and inflammation (*3*–*6*). Furthermore, an increasing number of studies report the role of low-level ROS as a physiologic mediator in normal cellular signaling processes(*7*–*9*). Specifically, H_2O_2 is a key redox signaling molecule, owing to its relative stability and ability to modify cysteine residues in proteins, enabling selective downstream signaling(*10*). On the other hand, excessive H_2O_2 is a common pathological marker affecting phenotypic and disease progression in various cell types(*11*–*13*). Nevertheless, limited analytic tools to spatiotemporally monitor specific oxidants *in situ* with precision have been a bottleneck to deciphering their specific role in physiology and the cause and effect of their imbalance(*14*, *15*). Thus, methods to interrogate the role of H_2O_2 would be broadly applicable to the study of redox biology(*15*).

Most synthetic ROS-sensitive dyes are unsuited for these considerations because of their short working time window, low sensitivity, and low specificity(*16*). Alternatively, protein-based peroxide sensors have been engineered to overcome these shortcomings. For example, the roGFP sensor family fuses roGFP, a redox-sensitive

green fluorescent protein variant, to H_2O_2-specific enzymes like Orp1 (thiol peroxidase), or Tsa2 (typical 2-Cys peroxiredoxin) from yeast to achieve peroxide-specific roGFP fluorescence changes via redox relay(*17*, *18*). The HyPer sensor family is based on the direct fusion of circularly permuted fluorescent protein (cpFP) to the regulatory domain of bacterial peroxide sensor protein OxyR for conformational coupling that leads to H_2O_2-specific fluorescence change(*19–24*). HyPer sensors either use nmOxyR (*Neisseria meningitidis* OxyR) or ecOxyR (*Escherichia coli* OxyR), the most extensively studied OxyR variant, as their sensing domain. Remarkably existing ecOxyR-based peroxide sensors exhibit slow oxidation kinetics (seconds under saturation conditions)(*21*, *22*, *25*), while studies reported peroxide-dependent oxidation of ecOxyR at a sub-second scale(*26*). We hypothesized that the discrepancy stems from the disruption of structural flexibility in the sensors. Under this consideration, we developed oROS-G (optogenetic hydRogen perOxide Sensor, Green), an ecOxyR-based peroxide sensor with a green fluorescent reporter protein (GFP, excitation: 488 nm, emission: 515 nm). oROS-G exhibits faster kinetics, enabling the visualization of peroxide diffusion in cells and their environment. We also engineered oROS-Gr, a ratiometric variant of oROS-G by fusing it with mCherry, which improves monitoring precision by normalizing sensor fluorescence intensity to the H_2O_2 inert red fluorescence. Here, we present diverse use cases of oROS sensors to monitor steady-state and transient H_2O_2 levels in various model systems. Specifically, we showed how oROS can detect varying H_2O_2 levels in astrocytes in the context of Alzheimer's disease models and assessed the efficacy of a drug in reducing aberrant peroxide levels. Also, we investigated how different glucose levels can result in different intracellular oxidative environments in

conjunction with mitochondrial respiratory depression. Lastly, we monitored opioid-dependent acute H_2O_2 generation in mouse brains both *ex vivo* and *in vivo*, demonstrating the potential utility of oROS sensors as a functional downstream reporter for G-protein-biased opioid receptor activation.

Results

Structure-guided engineering to improve sensitivity and kinetics of ecOxyR-based H_2O_2 sensor.

Rational engineering strategies for oROS-G

ecOxyRs is an H_2O_2 sensor protein that regulates the transcription of antioxidative genes in response to low-level cellular H_2O_2 in *E.Coli*. The specificity of OxyR stems from its unique H_2O_2 binding pocket(*27*). Previous studies have shown that binding H_2O_2 leads to an intermediate state that facilitates the disulfide bridging of two conserved cysteine residues (C199-C208, based on exOxyR-RD numbering(*22*)) which triggers the transition into the oxidized conformational state of OxyR. Due to its characteristic as an H_2O_2 sensor with low scavenging capacity(*27*), OxyR is an ideal scaffold for building a protein-based H_2O_2 reporter. However, the slow kinetics of existing ecOxyR sensors(*19*, *21–23*, *25*) deviate from the reported ecOxyR properties. Hence, we revisited the sensor design **[Fig. 1A],** to create a green genetically encoded indicator for H_2O_2 with accelerated kinetics**.** OxyR-based peroxide sensors integrate circular permuted fluorescent proteins (cpFP) within the loop between residues C199 and C208. However, the crystal structure of oxidized ecOxyR [PDB:1I6A] predicted an evident peak of B-factor **[Fig. 1B]** indicating this loop region is more flexible than its

surroundings. We hypothesized that inserting the cpFP in the region (e.g. in HyPer sensors) may increase the conformational entropy of the intermediate state that brings C199 and C208 into proximity(*27*). We performed a pairwise residue distance analysis between oxidized and reduced ecOxyR structures and found that the region between residues 209-220 goes through noticeable peroxide-dependent conformational change. cpGFP insertion between residue 211 and 212 elicited a robust response (ΔF/Fo = 97.55%; confidence interval 95% (ci) = [96.6, 98.52]) to 300 µM extracellular peroxide in HEK293 cells, which fully oxidizes previous OxyR-based sensors(*22*). The 211-212 variant exhibited a faster change in fluorescence in response to H_2O_2 (time from 25% to 75% max. sensor response = 1.06s; ci = [1.05, 1.07]) compared to other ecOxyR-based sensors(*19*, *21*, *22*, *25*). Moreover, the variant showed improved response amplitudes (ΔF/Fo = 20.41%; ci = [19.62, 21.17]) to low peroxide levels (10µM) compared to HyperRed (ΔF/Fo = 2.8%; ci = [2.61, 3.0]), the previously most sensitive H_2O_2 sensor derived from ecOxyR(*22*). To further optimize the dynamic range of the 211-212 variant, we applied engineering principles from the calcium indicator GCaMP5(*28*), and introduced large and hydrophobic amino acid tyrosine at the residue sites proximal to the cpGFP opening to reduce solvent access. We found the E215Y mutation increased response amplitude (ΔF/Fo) by 2.1-fold at full oxidation (ci = [1.99, 2.26]) and named this variant oROS-G. Furthermore, the H_2O_2-induced fluorescence increase was effectively disrupted by the C199S mutation. This confirms the sensor function is dependent on interactions at the C199-C208 pair consistent with the OxyR conformational changes in response to peroxide. We also confirmed the sensor

activation is fully reversible following treatment with the reducing agent Dithiothreitol (10 mM, DTT).

Characterization of kinetics and sensitivity of oROS-G in mammalian host systems.

We first characterized oROS-G sensor following expression in mammalian HEK293 cell cultures. Direct application of exogenous H_2O_2 increases intracellular H_2O_2 by diffusion across the plasma membrane through aquaporins, which creates a gradient of H_2O_2(*29–31*) across cell membranes. Under these conditions, the intracellular concentration of H_2O_2 is reported to be about 2 or 3 magnitudes lower than that of extracellular H_2O_2(*22, 32*). HyPerRed is the most sensitive sensor designed based on ecOxyR(*22*). Thus, despite differences in spectral properties, we first sought to benchmark oROS-G against HyPerRed for their response to H_2O_2. The signal amplitude of oROS-G (ΔF/Fo = 192.34%; ci = [190.45, 194.23]) at saturation (300 µM H_2O_2) was ≈2-fold greater than that of HyPerRed (ΔF/Fo = 97.74%; ci = [96.52, 99.06]) **[Fig. 4.1C]** while oROS-G exhibited significant improvement in on-kinetics compared to HyPerRed with ≈23 times faster 25-75% ΔF/Fo kinetics *in situ* (oROS-G: 0.4 ; ci = [0.26, 0.51], HyPerRed: 9.19; ci = [8.92, 9.46]) **[Fig. 1D]**. In addition, we observed a >7 times larger response at low-level peroxide stimulation (oROS-G: ΔF/Fo = 116.22%; ci = [110.85, 121.73] vs HyPerRed: ΔF/Fo = 16.45%; ci = [15.98, 16.95]) **[Fig. 1E]**. Improved sensitivity profile of oROS-G also found to be at equivalent level (i.e. 10 µM/300 µM exogenous H_2O_2 response ratio) compared to HyPer7, the newest iteration of HyPer sensor family **[Fig. 4.1F]**. oROS-G and HyPer7 take a fundamentally different approach to gain sensitivity as HyPer7 was designed by swapping the sensing domain with a more sensitive OxyR

variant from *Neisseria meningitidis* (nmOxyR) with fluorescent reporter insertion contained to the C-C loop region **[Fig. 4.1F]**(*24*). Intriguingly, oROS-G exhibited much faster off-kinetics in HEK293 cells while they both exhibit near-immediate response to saturating level of bolus H_2O_2 **[Fig. 4.1G]**. When both oROS-G and HyPer7 were activated with 100 µM H_2O_2 followed by media wash to measure endogenous reduction kinetic in HEK293 cells, oROS-G reached ≈90% reduction from its maximum saturation in 4.17 minutes, whereas HyPer7 only achieved about ≈20% reduction from its full saturation in the same duration, consistent with previous studies. (HyPer7: 0.81; ci = [0.8, 0.82], oROS-G: 0.12; ci = [0.1, 0.15]) In contrast, oROS-G showed 2.63 times faster decay kinetics than HyPer7 based on the reduction time to 85% of the saturation level **[Fig. 4.1G, H]**. Lastly, we confirmed the robust expression and function of oROS-G in rat cortical neurons and human-induced pluripotent stem cell-derived cardiomyocytes (hiPSC-CMs) demonstrating a versatile application range **[Fig. 4.1I]**.

Visualizing extracellular and intracellular diffusion H_2O_2 using oROS-G.

We exploited oROS-G's fast kinetics by visualizing H_2O_2 diffusion in the extracellular environment and in intracellular space in HEK293 cells. Due to its slower kinetics, the HyPerRed exhibits spatially uniform sensor activation across the field of view (660 x 660 µM) in response to exogenous H_2O_2 stimulation **[Fig. 4.2A]**. In contrast, oROS-G's faster response allowed the spatial H_2O_2 propagation to be visualized in the image field of view **[Fig. 4.2B]**. To better estimate the diffusion kinetics of the H_2O_2 propagation in the field-of-view, we transformed the time-series fluorescence profile into a time-series pixel-wise activation map that depicts when pixel intensity reached 50% of the observed

maximum. Convolution of the activation map perpendicular to the direction of H_2O_2 propagation revealed the speed of the H_2O_2 diffusion across the field-of-view to be ≈ 0.8 mm/s **[Fig. 4.2C]**. Next, we created a pixel-wise chronological activation map that depicts H_2O_2 diffusion kinetics within cells. **[Fig. 4.2D]**. Intriguingly, patterns of intracellular H_2O_2 entry were diverse, potentially representing aquaporin-driven passive transmembrane diffusion(*30*, *33*). For example, we noticed cells exhibiting a radial entry pattern along their membranes **[Fig. 4.2Ei]**, while others displayed a more polarized entry pattern aligned with the direction of global H_2O_2 diffusion **[Fig. 4.2Eii]**. It was also revealed that neighboring cells were topologically distinguishable from each other, implying that H_2O_2 transport at the cell-to-cell junctions may also be limited by the abundance of the transporters present at the cell-cell interface **[Fig. 4.2Eiii]**. Taken together, visualization of bolus H_2O_2 exposure using oROS-G allowed real-time observation of extra and intracellular peroxide diffusion. The significance of the heterogeneous intracellular H_2O_2 diffusive pattern could hint to potential factors, like aquaporins, that regulate H_2O_2 diffusivity within spatial contexts. These insights could support studies on how extracellular H_2O_2 build-up effects intracellular H_2O_2 pools(*34*).

Ratiometric variant oROS-Gr improves temporal flexibility of H_2O_2 measurement.

Design of oROS-Gr: a ratiometric variant of oROS-G for improved precision of long-term H_2O_2 monitoring.

We created oROS-Gr, by fusing mCherry to oROS-G, creating an equimolar reference point inert to H_2O_2. Flow cytometry analysis confirmed a strong linear correlation between green (Em. 510 nm) and red (Em. 605 nm) emission intensity of oROS-Gr

expressed in HEK293 cells (n = 16,326) **[Fig. 4.3A]**. Thus, oROS-Gr can be used for long-term and non-continuous monitoring by calculating the green-to-red light emission ratio independent of sensor expression levels. Upon exogenous H_2O_2 stimulation, the oROS-Gr ratio (Em. 510/605) showed a dose-dependent response in HEK293 cells. (1 µM: 0.06 (n = 327); ci = [0.06, 0.06], 10 µM: 0.11 (n = 306); ci = [0.1, 0.11], 25 µM: 0.14 (n = 405); ci = [0.14, 0.14], 50 µM: 0.15 (n = 469); ci = [0.15, 0.15]) **[Fig. 4.3B]** In addition, the oROS-Gr green-to-red ratio predictably followed a sequence of exogenous H_2O_2 stimulation (100 uM) and DTT (10 mM) reduction **[Fig. 4.3C]**. Menadione treatment has been widely used to model oxidative stress in biological systems (*35*–*39*). Still, studies to monitor its intracellular effect have been mostly limited to short time windows or non-continuous snapshots at varying time points, which do not enable insights into the real-time impact on redox homeostasis and its impact over a longer period. In HEK293 cells, oROS-G acutely responded to 10 µM and 50 µM menadione in a dose-dependent manner ($\Delta F/Fo$, 10 µM: 89.56 %; ci = [81.79, 97.57], 50µM: 173.68%; ci = [166.81, 180.35]) in HEK293 cells. The trend was consistent in human primary astrocytes. Next, we continuously measured the effects of menadione on cellular H_2O_2 levels over a ten-hour time window in HEK293 cells. Initially, menadione at 0, 1, 10, and 50 uM induced acute dose-dependent elevation of H_2O_2. However, within 30 minutes, the H_2O_2 levels at 10 µM exposure were higher than those at 50 µM, which returned to a dose-dependent trend within four hours **[Fig. 4.3D]**. Further analysis of intracellular redox landscape analysis and the functional role of putative cellular antioxidative elements(*40*, *41*) is required to understand this phenomenon fully. Nevertheless, the impact of menadione on intracellular H_2O_2 levels

demonstrates the necessity to measure cellular oxidative stress at various time points. We also evaluated whether oROS-Gr improved the readout precision over oROS-G. We compared the coefficient of variation (CoV) of the ratiometric signal (Em. 510/605 ratio) against the single wavelength signal (Em. 510 nm) **[Fig. 4.3D, E].** The ratiometric readout showed about 2-fold lower CoV compared to the single wavelength mode, confirming improvements in precision [Ratiometric: 0.27 (n = 484), non-Ratiometric: 0.46 (n = 484)].

Glucose-dependent basal oxidation level in mammalian cells.

Superoxide and peroxide are continuously generated as byproducts of electron transfer during aerobic metabolism(*42-44*). In this context, glucose, as one of the primary substrates of aerobic metabolic pathways, plays a crucial role in modulating cellular metabolic activity(*45*). Intriguingly, low as well as high glucose levels were reported to result in depressed respiratory activity in cultured human podocytes(*46*). The study also showed that the reduction of metabolic rates in high-glucose conditions can be reversed by incubation with the antioxidant N-acetyl cysteine (NAC), indicating that respiratory suppression is correlated with oxidative stress. Thus, we hypothesized that high glucose (HG = 25 mM) and low glucose (LG = 1 mM) media would result in higher basal peroxide levels than medium glucose (MG = 10 mM). We incubated HEK293 cells for 48 hours in HG, NG, and LG media and compared the ratiometric oROS-Gr signals. Here, low and high glucose conditions caused greater peroxide levels than MG (MG: 0.38; ci = [0.378, 0.382], LG: 0.402; ci = [0.4, 0.404], HG: 0.392; ci = [0.389, 0.394]). **[Fig. 4.3F].** We directly measured metabolic activities and found that basal and maximum

respiratory rates were also the lowest under low and high glucose conditions, indicating an inverse correlation with increased peroxide levels. Indeed, cells pre-incubated with 1 mM of the antioxidant NAC under HG conditions brought the oROS-Gr level 84% closer to MG conditions, indicating modest suppression of oxidative stress.

oROS-Gr in human stem cell-derived cardiomyocytes and cortical neurons.

We confirmed the robust expression and functionality of oROS-Gr in various human stem cell-derived cells. For example, we measured peroxide levels in hiPSC-derived cortical neurons in response to 24-hour 10 µM and 50 µM Menadione incubation to be 1.77-fold and 2-fold of oROS-Gr ratio observed at vehicle negative control, respectively (Vehicle: 1.0; ci = [0.82, 1.21], 10 µM: 1.77; ci = [1.62, 1.88], 50 µM: 2.01; ci = [1.97, 2.03]) **[Fig. 4.3G]**. Next, we used the sarcoendoplasmic reticulum calcium ATPase (SERCA) blocker cyclopiazonic acid (CPA, 10 µM) to elevate Ca^{2+} in the cytosol of hiPSC-cardiomyocytes (CM)(*47*). When hiPSC-CMs expressed oROS-Gr, we measured increased cytosolic peroxide levels within 2 hours of CPA incubation. As previously reported, this portrays a tight coupling between intracellular Ca^{2+} and ROS levels(*48*–*51*).

Monitoring the effect of antioxidants on intracellular peroxide level in Alzheimer's model.

Next, we explored using oROS-G in the context of antioxidants that target intracellular peroxides. N-acetyl-cysteine (NAC) is a cysteine prodrug widely used as a classical "antioxidant". Although its detailed mechanism of action has not been established,

recent studies highlight its antioxidative role via the production of low-level sulfane sulfur species(*52*, *53*). Using oROS-G, we measured the effect of NAC-dependent catabolism on cellular H_2O_2 levels in real-time. With a 1-hour preincubation of 1 mM NAC, oROS-G expressed in HEK293 showed a 73% diminished response to exogenous 10 μM peroxide exposure. Similarly, we incubated oROS-G expressing HEK293 cells to either NAC (10 mM) or Vehicle (DMSO) for 20 minutes before 10 μM menadione exposure. NAC significantly attenuated the response by 72 percent. We next examined the ability of the oROS-G sensor in primary cultured astrocytes to detect intracellular H_2O_2 levels to assess the H_2O_2-scavenging effects of molecules. Initially, we expressed oROS-G in the astrocytes and tested H_2O_2 concentration-dependent functionality. We observed an increase of 21.3 ± 5.3% and 57.7 ± 9.4% in fluorescence with 10 and 100 μM H_2O_2, respectively, indicating a functional response of the oROS-G sensor in primary cultured astrocytes. Previously, we have shown that aberrant H_2O_2 production by reactive astrocytes, a pathological form of astrocytes, is a contributing factor to Alzheimer's disease (AD) pathology(*11*, *54*). In detail, upregulated monoamine oxidase B (MAOB) in reactive astrocytes produces H_2O_2 by breaking down oligomerized amyloid beta (oAβ)-metabolites, such as putrescine, leading to pathological H_2O_2 generation(*55*, *56*) **[Fig. 4.4A].** Therefore, we tested whether we could monitor aberrant endogenous H_2O_2 production in oROS-G transfected astrocytes treated with oAβ (5 μM) or putrescine (180 μM). Over a 40-hour continuous recording **[Fig. 4.4B]**, we observed a significant increase in oAβ-induced oROS-G fluorescence, indicating a notable rise in H_2O_2 **[Fig. 4.4C, D].** Conversely, the application of KDS2010 (1 μM), a selective MAOB inhibitor, and sodium pyruvate (1 mM), a potential H_2O_2 scavenger, showed a smaller increase in

H_2O_2 levels. Additionally, incubation with putrescine, a pre-substrate of MAOB, also significantly increased oROS-G sensor fluorescence **[Fig. 4.4E, F]**. However, this H_2O_2 elevation was significantly reduced by KDS2010 and partially reduced by sodium pyruvate. Taken together, these results suggest that the oROS-G sensor in primary cultured astrocytes is a reliable tool for monitoring endogenous H_2O_2 production under AD-like conditions and evaluating the efficacy of potential H_2O_2-scavenging compounds. Then, we asked whether we could measure the endogenous H_2O_2 levels in mouse brains. To test this idea, we bilaterally injected the AAV5-GFAP104-oROS-G virus into the CA1 hippocampus of APP/PS1 mice(*56*, *57*), a well-characterized Alzheimer's disease model, to express oROS-G sensor specifically in the astrocytes **[Fig. 4.4G].** Two weeks post-injection, we prepared brain slices and tested the H_2O_2 concentration-dependent functionality of the sensor. Again, to test the functionality of the sensor, we applied 10 and 100 μM H_2O_2 through bath application. We found an increase of 13.2 ± 1.2% and 39.5 ± 3.12% in fluorescence with 10 and 100 μM H_2O_2, respectively **[Fig. 4.4H, I].** Like *in vitro*, the oROS-G sensor functions effectively in astrocytes *ex vivo*. Next, we examined the capability to measure elevated H_2O_2 levels in astrocytes of APP/PS1 mice. We hypothesized that treatment with DTT would unmask the portion activated by astrocytic H_2O_2. Following DTT (10 mM) administration, we observed a reduction in fluorescence below the baseline levels. Notably, we demonstrated that APP/PS1 mice exhibited a greater reduction compared to wild-type, suggesting a potential method for measuring endogenous H_2O_2 levels **[Fig. 4.4J-L].** Taken together, these results demonstrate that the oROS-G sensor functions effectively *ex vivo*,

presenting a potential method for measuring endogenous H_2O_2 levels and investigating the antioxidant capacity of various molecules.

G-protein biased agonists elicit H_2O_2 generation in κ and μ opioid receptor-expressing neurons in the Ventral Tegmental Area *ex vivo* and *in vivo*.

We previously reported that peroxide generated by a NADPH oxidase (NOX) mechanism regulated opioid receptor signaling(*58*, *59*), which exemplifies intricate functional G-protein biased agonists' influence on arrestin-independent inactivation profile of μ and κ opioid receptors. Briefly, G-protein-biased opioid receptor activation triggers cJUN N-terminal kinase (JNK) phosphorylation. Phosphorylated JNK then activates peroxiredoxin 6 (PRDX6), producing superoxide (SO) from NOX. SO can quickly oxidize the Gαi protein complex to inactivate the opioid receptors. This event can be captured using H_2O_2 as a marker of opioid receptor activation because superoxide is readily transformed into H_2O_2 by superoxide dismutase(*60–63*) **[Fig. 4.5A]**. Given the robust responses of oROS-Gr, we sought to monitor transient H_2O_2 generation in the animal brain in response to G-protein-biased agonists.

As a proof of concept, we showed that morphine, a potent G-protein biased agonist of μ-opioid receptors (MOR), triggers transient peroxide generation in MOR-expressing neurons in the ventral tegmental area (VTA) of MOR-Cre transgenic mice, which is consistent with our previous findings. The oROS signals were measured using 2-photon microscopy on *ex vivo* live brain slices after viral delivery of the AAV1-DIO-oROS-Gr into the VTA of MOR-Cre transgenic mice. Expression of oROS-Gr in the VTA was verified with one-photon confocal microscopy of post-mortem fixed brain slices **[Fig.**

4.5B]. The VTA in *ex vivo* brain slices showed an acute increase in sensor fluorescence during bath application of 1 µM morphine over 30 minutes of monitoring. This increase was blocked by the opioid receptor antagonist 1 µM Naloxone (Normalized ∆F/Fo to first 5 baseline frames, MOR: 3.35; ci = [1.94, 4.82], MOR+NLX: 0.63; ci = [0.42, 0.85]) **[Fig. 4.5C]**.

κ-opioid receptor (KOR) has emerged as a promising drug target for pain management with fewer side effects(*64*). We previously showed behavioral and pharmacological evidence on how the oxidative pressure of JNK-PRDX6-PLA2-NOX cascade from KOR results in acute analgesic tolerance, as shown in the warm water tail withdrawal assay(*58*). Nalfurafine is a functionally selective G-protein biased κ-opioid agonist shown to have therapeutic potential as a non-dysphoric antipruritic analgesic(*65*). Here, we explored the use of the oROS sensor to directly monitor acute H_2O_2 response to Nalfurafine *in vivo*, confirming activation of JNK-PRDX6-PLA2-NOX in KOR-positive neurons in the VTA. KOR-Cre transgenic mice were injected with AAV1-DIO-oROS-Gr, and the sensor fluorescence (ex:488/em:510) was monitored by fiber photometry in the VTA **[Fig. 4.5D]**. Intraperitoneal administration of 100 µg/kg Nalfurafine led to a transient increase of H_2O_2. Mice pre-treated 30 min prior to a 100 µg/kg Nalfurafine injection with a high dose of naloxone (10 mg/kg), sufficient to block KOR(*66*), showed no significant increase in fluorescence compared to mice only treated with Nalfurafine **[Fig. 4.5E]**. This confirms that the Nalfurafine-induced H_2O_2 signal in KOR-expressing neurons of VTA is opioid receptor-specific.

Discussion

Our refinement of the oROS sensor framework resulted in significant improvements in the kinetics and sensitivity compared to previous ecOxyR-based peroxide sensors. This optimization can largely be attributed to the relocation of the cpGFP insertion site to maintain the flexibility of the C199-C208 loop in ecOxyR and the incorporation of bulky residues adjacent to the cpGFP barrel opening. Interestingly, the diversity of OxyR variants in nature, each characterized by a conserved peroxide oxidation mechanism, opens avenues for exploring a range of sensor functionalities. Notably, OxyRs from different bacterial strains exhibit distinct reduction mechanisms; ecOxyR predominantly follows a Grx (glutaredoxin)-dependent reduction pathway, where Grx proteins facilitate the reduction of oxidized proteins(*67*). In contrast, other variants like nmOxyR (*Neisseria meningitidis*), used by HyPer7(*68*), might employ a Trx (thioredoxin)-dependent reduction mechanism involving the Trx system known for mitigating cellular oxidative stress. This variation necessitates further exploration of these domains for sensors in mammalian systems, and they could serve as complementary tools for dissecting peroxide biology in various redox environments(*68*). In addition, our study demonstrated the versatility of oROS sensors in a range of experimental applications. We successfully monitored H_2O_2 levels in astrocytes, both *in vitro* and *ex vivo*, shedding light on elevated oxidative stress in Alzheimer's models. Moreover, the ratiometric oROS-Gr sensor enabled us to observe the effects of glucose on cytoplasmic peroxide levels, which correlated with known patterns of mitochondrial oxidative stress. Additionally, our work highlights the oROS sensor's efficacy in detecting opioid-induced peroxide increase *in vivo*, further emphasizing the role of ROS in signaling mechanisms. In conclusion, oROS sensors, exemplified by oROS-G and oROS-Gr, offer real-time

application across various model systems. They can monitor complex redox processes that are present in virtually all eukaryotic cells, with significant implications for unraveling the pathophysiology of oxidative stress in diseases.

Methods

Protein structure analysis

Protein structure analysis and plotting were performed using Chimera-X-1.2.1. Oxidized [PDB:1I6A] and reduced [PDB:1I69] crystal structures of ecOxyR were imported from the Protein Data Bank (PDB). Pairwise residue distance between reduced and oxidized ecOxyR structure was achieved by aligning both structures using a matchmaker algorithm that superimposes protein structures by creating a pairwise sequence alignment and then fitting the aligned residue pairs to derive pairwise residue distances.

Molecular Biology

oROS-G variants were cloned based on the pC1 plasmid backbone from pC1-HyPer-Red (Addgene ID: 48249). Primers for point mutations or fragment assembly required to generate the oROS-G screening variants were designed for In Vitro Assembly cloning (IVA) technique(*69*), Gibson Assembly (New England Biolabs; E2611L) or blunt-end amplification for KLD-based site-directed mutagenesis methods. Primers were ordered from Integrated DNA Technologies (IDT). All gene fragment amplifications were done using either Q5-polymerase (New England Biolabs; M0492L) or Superfi-II polymerase (Invitrogen; 12368010). Amplification of DNA fragments were verified with agarose gel electrophoresis. 30 minutes of DpnI enzyme treatment were done on every PCR

product to remove the plasmid template from PCR samples. For IVA cloning circularization or assembly of the PCR products was achieved by transforming linear DNA products into competent *E.Coli* cells (DH5α or TOP10) and grown on agar plates that contain either ampicillin or kanamycin selection antibiotic (50 µg/mL). For gibson assembly and KLD cloning, circularized DNA was transformed as above. Upon colony formation, single colonies were picked and grown in 5mL cultures containing LB Broth (Fisher BioReagents; BP9723-2) and selection antibiotic (ampicillin/kanamycin; 50 µg/mL) overnight (37°C, 230 RPM). DNA was isolated using Machery Nagel DNA prep kits (Machery Nagel; 740490.250). Sanger sequencing (Genewiz; Seattle, WA) or Whole plasmid nanopore sequencing (Plasmidsarus; Eugene, OR) of the isolated plasmid DNA was used to confirm the presence of the intended mutation. Genes encoding the final variants were cloned into a CAG-driven backbone, pCAG-Archon1-KGC-EGFP-ER2-WPRE (Addgene; #108423), using the methods above(New England Biolabs; E2621L). All subsequences were verified with Sanger sequencing (Genewiz; Seattle, WA) or Whole plasmid nanopore sequencing (Plasmidsarus; Eugene, OR)

Chemicals

H_2O_2 working solutions were freshly prepared before every experiment from H_2O_2 solution 30% (w/w) in H_2O (Sigma-Aldrich, H1009). Stock solution of Menadione (VENDOR, CAT) was prepared in 100% DMSO at 50mM. Stock solution of Cyclopiazonic Acid (Tocris, 1235) was prepared in 100% DMSO at 20mM. Chemicals specific to other method sections can be found in their respective sections.

Cell culture and transfection

Human Embryonic Kidney (HEK293; ATCC Ref: CRL-1573) cells were cultured in Dulbecco's Modified Eagle Medium + GlutaMAX (Gibco; 10569-010) supplemented with 10% fetal bovine serum (Biowest; S1620). When cultures reached 85% confluency, the cultures were seeded at 150,000/75,000 cells per well in 24/48-well plates, respectively. 24 hours after cell seeding, the cells were transfected using Lipofectamine3000 (Invitrogen; L3000015) at 1000/500 ng of DNA per well of a 24/48-well plate, according to the manufacturer's instructions.

Primary rat neuron isolation

Primary cortical neurons were prepared as previously described [47,48]. Briefly, 24-well tissue culture plates were coated with Matrigel (mixed 1:20 in cold-PBS, Corning; 356231) solution and incubated at 4°C overnight prior to use. Sterile dissection tools were used to isolate cortical brain tissue from P0 rat pups (male and female). Tissue was minced until 1 mm pieces remained, then lysed in equilibrated (37°C, 5% CO_2) enzyme (20 U/mL Papain (Worthington Biochemical Corp; LK003176) in 5mL of EBSS (Sigma; E3024)) solution for 30 minutes at 37°C, 5% CO_2 humidified incubator. Lysed cells were centrifuged at 200 xg for 5 minutes at room temperature, and the supernatant was removed before cells were resuspended in 3 mL of EBSS (Sigma; E3024). Cells were triturated 24x with a pulled Pasteur pipette in EBSS until homogenous. EBSS was added until the sample volume reached 10 mL prior to spinning at 0.7 rcf for 5 minutes at room temperature. Supernatant was removed, and enzymatic dissociation was stopped by resuspending cells in 5 mL EBSS (Sigma; E3024) + final concentration of 10 mM HEPES Buffer (Fisher; BP299-100) + trypsin inhibitor soybean (1 mg/mL in EBSS at a final concentration of 0.2%; Sigma, T9253) + 60 µl of fetal bovine serum (Biowest;

S1620) + 30 µl 100 U/mL DNase1 (Sigma;11284932001). Cells were washed 2x by spinning at 0.7 RCF for 5 minutes at room temperature and removing supernatant + resuspending in 10 mL of Neuronal Basal Media (Invitrogen; 10888022) supplemented with B27 (Invitrogen; 17504044) and glutamine (Invitrogen; 35050061) (NBA++). After final wash spin and supernatant removal, cells were resuspended in 10 mL of NBA++ prior to counting. Just before neurons were plated, matrigel was aspirated from the wells. Neurons were plated on the prepared culture plates at desired seeding density. Twenty-four hours after plating, 1 µM AraC (Sigma; C6645) was added to the NBA++ growth media to prevent the growth of glial cells. Plates were incubated at 37°C and 5% CO_2 and maintained by exchanging half of the media volume for each well with fresh, warmed Neuronal Basal Media (Invitrogen; 10888022) supplemented with B27 (Invitrogen; 17504044) and glutamine (Invitrogen; 35050061) every three days.

Human primary astrocytes, and stem cell derived cardiomyocytes and neurons

Astrocytes: Human primary cortical astrocytes were purchased from ScienCell Research Laboratories (Carlsbad, CA) and were stored, thawed and sub-cultured based on the manufacturer's protocol. Briefly, the astrocytes were cultured for 72 h in a base medium with an astrocyte growth supplement and fetal bovine serum provided by the same manufacturer. Cultures were maintained in a 37°C/5% CO_2 incubator throughout the culture period, and the astrocytes with low passage numbers (p0-p3) were used to guarantee consistent phenotype expression. When the culture became 70% confluent, the cells were dissociated with TrypLE (Thermo Fisher), followed by passaging on the PDL-coated 24 coverslips for oROS-G1 transfection. The transfected cells were then

cultured for an additional 96 h before H_2O_2 treatment (10 µM, 100 µM) for recording the fluorescence response upon H_2O_2 stimulation.

Cardiomyocytes: Undifferentiated IMR90 (WiCell) hiPSCs were maintained on Matrigel (Corning) coated tissue culture plates in mTeSR1 (Stemcell Technologies). Cardiomyocyte directed differentiation was performed using a modified small molecule Wnt-modulating protocol using Chiron 99021 and IWP-4 as previously described.(*70*, *71*). Lactate enrichment was performed following differentiation to purify hiPSC-CMs.(*72*)

Cortical neurons: Neurons were generated from the previously characterized wild type CV background human induced pluripotent stem cell line (Young et al. 2015). Neural progenitor cells (NPCs) from this cell line were differentiated from hiPSCs using dual-SMAD inhibition and NPCs were differentiated to neurons as previously described (Knupp et al., 2020; Shin et al., 2023). Briefly, for cortical neuron differentiation from NPCs, NPCs were expanded into 10 cm plates in Basal Neural Maintenance Media (BNMM) (1:1 DMEM/F12 (#11039047 Life Technologies) + glutamine media/neurobasal media (#21103049, GIBCO), 0.5% N2 supplement (# 17502-048; Thermo Fisher Scientific,) 1% B27 supplement (# 17504-044; Thermo Fisher Scientific), 0.5% GlutaMax (# 35050061; Thermo Fisher Scientific), 0.5% insulin-transferrin-selenium (#41400045; Thermo Fisher Scientific), 0.5% NEAA (# 11140050; Thermo Fisher Scientific), 0.2% β-mercaptoethanol (#21985023, Life Technologies) + 20 ng/mL Fibroblast Growth Factor (FGF) (R&D Systems, Minneapolis, MN). Once the NPCs reached 100% confluence, they were switched to Neural Differentiation Media (BNMM +0.2 mg/mL brain-derived neurotrophic factor (CC# 450–02; PeproTech) + 0.2 mg/mL

glial-cell-derived neurotrophic factor (CC# 450–10; PeproTech) + 0.5 M dbcAMP (CC# D0260; Sigma Aldrich). Neural Differentiation Media was changed twice a week for 21 days at which point the differentiation is considered finished. Neurons were replated at a density of 500,000 cells/cm^2.

Imaging and data collection

Imaging experiments described in this study were performed as follows unless specifically noted. Epifluorescence imaging experiments were performed on a Leica DMI8 microscope (Semrock bandpass filter: GFP ex/em: FF01-474-27/FF01-520-35, RFP ex/em:FF01-578-21/FF01-600-37) controlled by MetaMorph Imaging software, using a sCMOS camera (Photometrics Prime95B) and 20x magnification lens (Leica HCX PL FLUOTAR L 20x/0.40 NA CORR) or 10× objective (Leica HCX PL FLUOTAR L 10x/0.32 NA). Confocal imaging experiments were performed on a Leica SP8 confocal microscope from the Lynn and Mike Garvey Imaging Core at the Institute of Stem Cell and Regenerative Medicine. Cells were imaged in live cell imaging solution with 10 mM glucose (LCIS+, Gibco, A14291DJ) unless noted otherwise.

Analysis

Extraction and analysis of cellular fluorescence profiles

Extraction of cell fluorescence imaging data was done by FUSE, a custom cloud-based semi-automated time series fluorescence data analysis platform written in Python. First, the cell segmentation quality of the selected Cellpose(*73*) model was manually verified. For the segmentation of cells expressing cytosolic fluorescent indicators, model ‘cyto’ was selected as our base model. If the selected Cellpose model was low-performing, we further trained the Cellpose model using the Cellpose 2.0 human-in-the-loop

system(*74*). Using an “optimized” segmentation model, fluorescence time-series data is extracted for each region of interest. This allows for unbiased extraction of change in cellular fluorescence information for a complete set of experimental samples. When it is necessary, extracted fluorescence data is represented as ∆F/Fo(%) (eq. 1).

{\Delta} F/{F}_{0}=\frac{(F-{F}_{0})}{{F}_{0}}\times

100 (eq.1)

Spatiotemporal diffusion mapping

The spatiotemporal diffusion profile was analyzed using a custom-developed Python script. To construct a time-series pixel-wise activation map, the intensity of each pixel at each time point was normalized by dividing by the maximum observed intensity, followed by background subtraction. This resulted in a ratio value for each pixel, which was then used to create a boolean map where pixels with a ratio above 50% were assigned a value of 1, and those below 50% were assigned a value of 0. For global diffusion speed analysis, we assumed that the diffusion direction was parallel to the x-axis, as observed. We calculated the ratio of the number of activated pixels (value of 1) to the number of pixels activated at any time point throughout the experiment, and applied min-max normalization to express this as a percentage, creating a diffusion distance map. Diffusion speed was estimated from the time points at which the number of activated pixels reached 10% of the total, without interpolation. Finally, a chronological activation map was generated by determining the time at which 10% of pixels became activated in the previously mentioned activation map, which was smoothed using a Gaussian kernel (size 1.5) in FIJI software (version 2.14.0), to enhance spatial visualization.

Astrocyte study

Primary mouse astrocyte culture: Primary mouse cultured astrocytes were prepared from P1-P3 C57BL/6J mouse pups as previously described.(*75*) Briefly, 60-mm culture dishes were coated with 0.1 mg/ml poly-D-lysine (PDL, Sigma; P6407) solution prior to use. The hippocampal tissue was isolated and dissociated into single-cell suspension by trituration in Dulbecco's modified Eagle's medium supplemented with 4.5 g/L glucose, L-glutamine, sodium pyruvate (DMEM, Corning; 10-013-CV) + 10% heat-inactivated horse serum (Gibco; 26050-088) + 10% heat-inactivated fetal bovine serum (Dawin bio; A0100-010) + 1000 unit/ml penicillin-streptomycin (Gibco; 15140122). Dissociated cells were plated onto the PDL-coated dishes. Cultures were maintained at 37°C in an incubator with a humidified atmosphere containing 5% CO_2. On the third day, cells were vigorously washed with repeated pipetting using medium to remove debris and other floating cell types.

On the 10th day of culture, cultured primary astrocytes were electrophoretically transfected with oROS-G plasmid with a voltage protocol (1200 V, 20 pulse width, 2 pulses) using the Microporator (Invitrogen Neon Transfection System; MPK5000S) and replated onto coverslip coated with PDL (Sigma; P6407) or µ-Plate 96 Well Black (ibid; 89626).

Imaging of cultured primary mouse astrocytes: On the 14th day of culture, the oROS-G transfected cultured primary astrocytes were transferred to a recording chamber which were mounted on an inverted Nikon Ti2-U microscope and continuously perfused with an external solution contained (in mM): 150 NaCl, 10 HEPES, 5.5 glucose, 3 KCl, 2MgCl2, 2 CaCl2, and pH adjusted to pH 7.3. Intensity images of 525 nm wavelength

were taken at 485 nm excitation wavelengths using ORCA-Flash4.0 CMOS camera (Hamamatsu; C13440). Imaging workbench (INDEC Biosystem) and ImageJ (NIH) were utilized for image acquisition and ROI analysis of cultured astrocytes. To examine H_2O_2-dose dependent responses of oROS-G transfected cultured astrocytes, concentrations of either 10 or 100 μM of H_2O_2 (Sigma; 88597) were introduced by bath application. The peak response of the sensor was normalized to its baseline (ΔF/Fo), which was measured 90 seconds before introducing H_2O_2. For confocal live-cell imaging and monitoring antioxidant drugs, confocal imaging was performed by using a Nikon A1R confocal microscope mounted onto a Nikon Eclipse Ti body with 20x objective lens. A Live-cell imaging chamber and incubation system were used for maintaining environmental conditions at 10% CO_2 and 37°C during 40-hour continuous recording. Images were acquired by using NIS-element AR (Nikon). For image analysis, NIS-element (Nikon) and ImageJ (NIH) were used.

Animals: All APP/PS1 mice were group-housed in a temperature- and humidity-controlled environment with a 12 h light/dark cycle and had free access to food and water.

Virus injection: The AAV5-GFAP104-oROS-G viral vector was cloned and AAV containing GFAP-104-oROS-G was packaged by the IBS virus facility (Daejeon, Korea). Mice were deeply anesthetized via vaporized 1% isoflurane and immobilized in a stereotaxic (RWD Life Science). Following an incision on the midline of the scalp, bilateral craniotomies were performed above the hippocampus CA1 (anterior/posterior, -2 mm; medial/lateral, ±1.6 mm; dorsal/ventral, -1.45 mm from the bregma) using a

microdrill. The virus was bilaterally microinjected (0.1 µl/min for 10 min; total 0.8 µl) using a syringe pump (KD Scientific).

oROS-G imaging of GFAP-positive astrocytes in the brain slices: 2 weeks after viral injection into the hippocampus, animals were anesthetized with 1% isoflurane and then decapitated. The brains were submerged in chilled cutting solution that contained (in mM): 250 Sucrose, 26 NaHCO3, 10 D(+)-glucose, 4 $MgCl_2$, 0.1 $CaCl_2$, 2.5 KCl, 2 Sodium Pyruvate, 1.25 NaH_2PO_4, 0.5 ascorbic acid, and pH adjusted to pH 7.4. Coronal slices (300 µm thick) were prepared with a vibrating-knife microtome D.S.K LinearSlicer pro 7 (Dosaka EM Co. Ltd). For stabilization, brain slices were incubated at room temperature for at least 1 h before imaging. For imaging, the slices were transferred to a recording chamber which were mounted on an upright Zeiss Examiner D1 microscope and continuously perfused with an artificial cerebrospinal fluid (aCSF) solution that contained (in mM): 130 NaCl, 24 $NaHCO_3$, 1.25 NaH_2PO_4, 3.5 KCl, 1.5 $MgCl_2$, 1.5 $CaCl_2$, D(+)-glucose, and pH adjusted to pH 7.4. All solutions were equilibrated with 95% O_2 and 5% CO_2. Imaging was acquired at 0.25 frame per second with 60X water-immersion objective lens, a ORCA-Flash4.0 CMOS camera (Hamamatsu; C13440), and a LED (CoolLED) filtered with 485-nm fluorescence was applied. Imaging workbench (INDEC Biosystem) and ImageJ (NIH) were utilized for image acquisition and ROI analysis. To examine H_2O_2-dose dependent responses of sensor-expressing astrocytes, concentrations of either 10 or 100 µM of H_2O_2 were introduced by bath application. The peak response of the sensor was normalized to its baseline (ΔF/Fo), wich was measured 90 seconds before introducing H_2O_2. To measure endogenous H_2O_2 in astrocytes of APP/PS1 mice and their littermates, we used 10 mM DTT (Thermo;

R0861). This method reduced the oROS-G sensor bound to H_2O_2, resulting in fluorescence below the baseline levels. These reduced fluorescence responses were normalized to its baseline (ΔF/Fo), suggesting the basal endogenous H_2O_2 levels.

Generation of stable oROS-Gr expressing HEK293 cells.

HEK293 cells in a T75 flask were transfected (using lipofection, as described above) with oROS-Gr-P2A-Puromycin plasmid. 3 Days after the transfection, cells were passaged to 2 T75 flasks. 2 Days after, puromycin-based selection was performed for a week using complete DMEM media (as previously described) supplemented with puromycin (1 µg/mL). Cells after selection were expanded for 3 passages. Enrichment of cell populations with robust oROS-Gr expression was achieved with BD FACSAria II Cell Sorter at Flow and Imaging Core Lab of University of Washington South Lake Union Campus.

Glucose experiment and Seahorse Assay

oROS-Gr stable cells cultured in complete DMEM with 10 mM glucose were plated at 75,000/well in 24-well plates. oROS-Gr stable cells were plated at 75,000/well in 24-well plates. 1 day post seeding, FBS in the DMEM media was brought down to 2% from 10%. 2 day post seeding cells were in serum-free DMEM with various levels of glucose. Mannose was supplemented as needed to keep osmotic pressure of each media consistent (final total sugar content: 25 mM). oROS-Gr ratio (GFP/RFP) were imaged in LCIS media with varying glucose and mannose level. For Seahorse assay, oROS-Gr stable cells mentioned above were plated in a Matrigel-coated 96 well Seahorse plate at a density of 2×10^5 cells/well for an equivalent procedure as above. The MitoStress protocol in the Seahorse XF96 Flux Analyzer (Agilent Technologies, Santa Clara, CA,

USA) was performed two weeks later. An hour before the assay, the culture media was replaced with media (Agilent Seahorse XF base medium, 103334-100 Agilent Technologies, Santa Clara, CA, USA) supplemented with 25 mM glucose and 1 mM Sodium pyruvate (11360070 Gibco/Thermo Scientific, Waltham, MA, USA). Substrates and select inhibitors of the different complexes were added during the measurement to achieve final concentrations of oligomycin (2.5 μM), FCCP (1 μM), rotenone (2.5 μM) and antimycin (2.5 μM). The oxygen consumption rate (OCR) values were then normalized with readings from Hoechst staining (HO33342 Sigma-Aldrich, St. Louis, MO, USA), which corresponded to the number of cells in the well.

Opioid receptor study

AAV: An adenovirus associated double floxed inverted (AAV1-DIO) virus was generated containing the oROS-Gr by cloning oROS-Gr into pAAV1-Ef1a-DIO using Nhe1 and Asc1 restriction sites. AAV1 were prepared by the NAPE Molecular Genetics Resources Core as described previously (Gore, et al, 2013). HEK293T cells were transfected with 25 μg AAV1 vector plasmid and 50 μg packaging vector (pDG1) per 15 cm plate. Two days after transfection, cells were harvested and subjected to three freeze–thaw cycles. The supernatant was transferred to a Beckman tube containing a 40% sucrose cushion and spun at 27,000 rpm overnight at 4°C. Pellets were resuspended in CsCl at a density of 1.37 g/ml and spun at 65000 rpm 4 hours at 4°C. 1 ml CsCl fractions were run on an agarose gel, and genome-containing fractions were selected and spun at 50000 rpm overnight at 4°C. The 1 ml fractions were collected again, and genome containing fractions were dialyzed overnight. The filtered solution was transferred to a Beckman tube containing a 40% sucrose cushion and spun at 27,000 rpm overnight at 4°C. The

pellet (containing purified AAV) was resuspended in 150 µl 1× HBSS. Virus was aliquoted and stored at -80°C until use.

Animals and surgeries: Test naive C57BL/6 male mice were ear punched at least 21 days after birth and genotyped using Transnetyx genotyping services. PCR screening was performed for the presence of Cre recombinase. For brain slice studies, mice between 5-7 weeks of age were injected with 0.5 µL AAV1-Efla-FLEX-oROS-mCherry (CITE) construct containing oROS-Gr into a *Oprm1*-CRE positive mouse bilaterally into the VTA using coordinates: ML: +/- 0.5, AP: -3.28, DN: -4.5 zeroed at bregma. Isoflurane was used for anesthesia and carprofen for pain relief. Mice were mounted on a stereotaxic alignment system and injections were made using a Hamilton 2.0 µL model 7002 KH syringe. Similarly, for fiber photometry experiments, mice were injected with 0.5 µL AAV1-Efla-FLEX-oROS-mCherry unilaterally at a 15-degree angle, using the coordinates ML: -1.71, AP: -3.28, DN: -4.67 then implanted with a 400/430 µm diameter Mono fiberoptic cannula from Doric Lenses.

2-photon imaging of µ-opioid receptor expressing neurons in VTA: Two-four weeks after viral injection, the brain was dissected and 200 µm horizontal slices were prepared using a vibratome. Slices were incubated in NMDG (92 mM NMDG, 2.5 mM KCl, 1.25 mM NaH_2PO_4, 30 mM $NaHCO_3$, 20mM HEPES, 25 mM Glucose, 2 mM Thiourea, 5 mM Na-ascorbate, 3 mM Na-pyruvate, pH to 7.4, 0.5 mM $CaCl•4H_2O$, 10 mM $MgSO_4•7H_2O$). Recordings were made in a HEPES solution (92 mM NaCl, 2.5 mM KCl, 1.25 mM NaH_2PO_4, 30 mM $NaHCO_3$, 20 mM HEPES, 25 mM Glucose, 2 mM Thiourea, 5 mM Na-Ascorbate, 3 mM Na-Pyruvate). Image collection was done using a Bruker Investigator 2-photon microscope, software Prairie View 5.5, simultaneously collecting

both the mCherry (1040 nm fixed) and GFP (920 nm tunable) signals with a Nikon 16X water immersion objective, as well as a z-stack spanning 60 µm across an hour time course. Baseline recordings were made in ACSF (124 mM NaCl, 3 mM KCl, 2 mM $MgSO_4$, 1.25 mM NaH_2PO_4, 2.5 mM $CaCl_2$, 26 mM $NaHCO_3$, 10 mM Glucose) at 32ºC, before treatment. For confocal images, animals were perfused intracardially with phosphate-buffered saline (PBS) and 10% formalin. Brains were stored in 10% formalin for up to 24 hours then switched to a 20% sucrose solution at 4ºC until sectioning. Coronal slices of the VTA were collected at 40 µm each and mounted using VECTASHIELD HardSet mounting Medium with DAPI. Confocal images were taken with the Leica SP8x Confocal microscope located in the Keck Center at UW.

Fiber photometry of kappa-opioid expressing neurons in the VTA: A real-time signal processor (RZ5P; Tucker-Davis Technologies) connected to Synapse Software (Fiber Photometry) to set frequency of light stimulation and to record input from photodetectors. The RZ5P was connected to a light emitting diode (LED) driver (Doric Lenses) that controlled the power of a 465 nm and 560 nm Doric LED. A low autofluorescence patch cord (400/430) was attached to the LED, to a fluorescent MiniCube (Doric Lenses) with dichroic mirrors. Connected optical patch cords to the MiniCube with pigtailed rotary joining (FRJ; Doric Lenses) allowed free animal movement during data collection. Patch Cords were bleached with light prior to photometry sessions to minimize autofluorescence. Power of the LED at the fiber tip was set to ~30 µW and was tested prior to the start of each session. Signals were collected at a sampling frequency of 1017 Hz. Each of the sessions was downsampled by a factor of 100 and normalized to a 15-minute baseline period in the beginning of the

recording. Data were then smoothed using a moving average filter (100 sec window) to remove high frequency noise and detrended to remove linear drift. The isosbestic channel (405 nm) was fitted to the 470 nm channel using a least-squares method and subtracted to remove motion artifacts. Each session started with a 15 min baseline recording period prior to pharmacological experiments to calculate fluorescent change from baseline (ΔF/Fo; Change in fluorescence from baseline fluorescence/baseline fluorescence).

Figure 4.1 Structure-guided engineering to improve sensitivity and kinetics of ecOxyR-based H_2O_2

sensor.

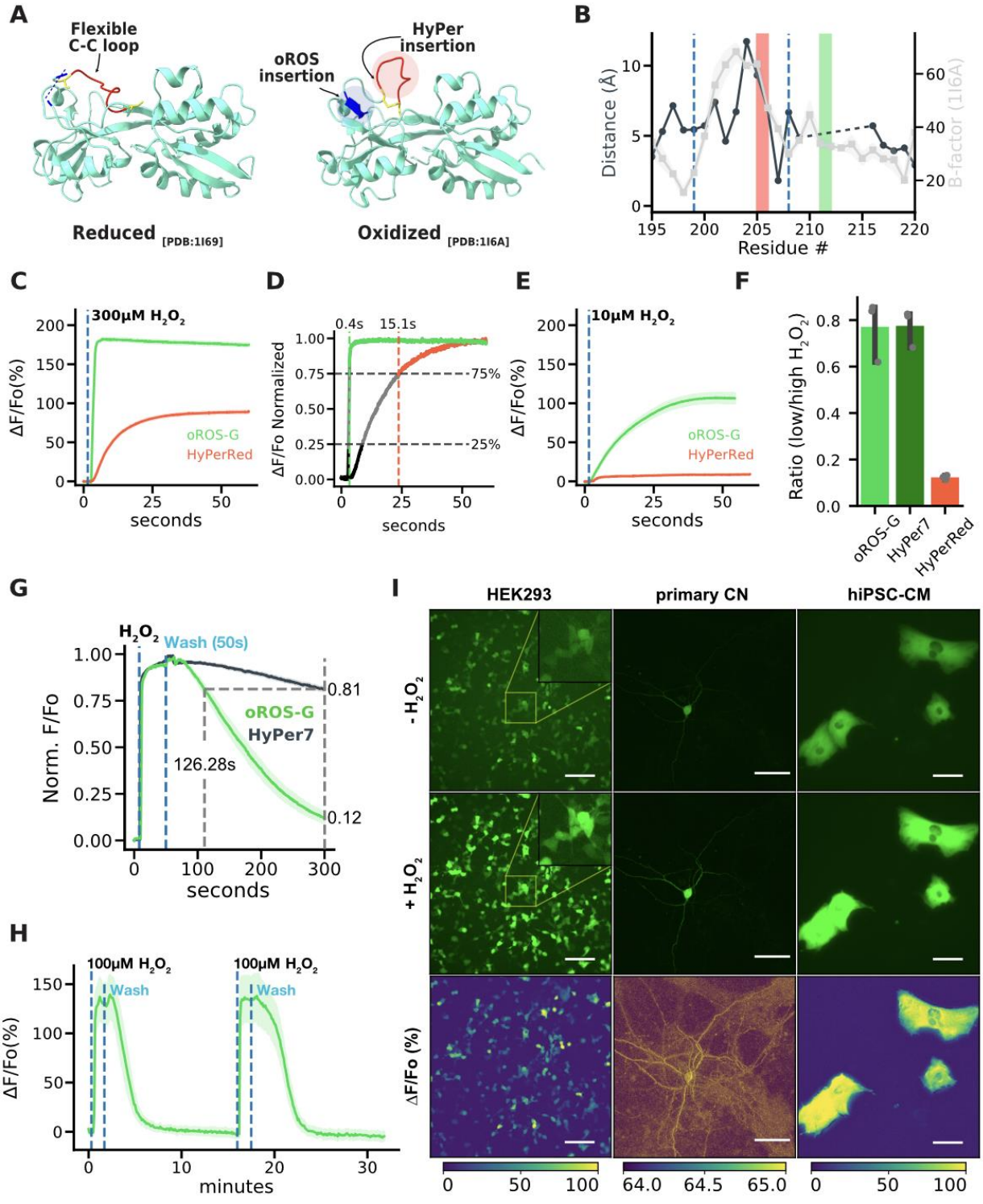

A-B Structure-guided design of an oROS sensor. **A** Crystal structure of reduced and oxidized forms of Regulatory Domain (RD) of *Escherichia coli* OxyR. C-C pair labeled in

yellow. Red indicates the fluorescent protein insertion loop for HyPer sensors, and Blue indicates the newly identified fluorescent protein insertion site for oROS sensors. **B** Overlay of B-factor of oxidized OxyR structure and residue-to-residue distance plots for a zoomed-in view of the putative region with high conformational change between oxidized and reduced form of ecOxyR. The red and green boxes indicate the insertion sites of HyPerRed and oROS-G, respectively. The insertion site proposed for oROS-G is outside of the loop between C199 and C208 (blue dashed line) to maximize the flexibility of the loop. **C** Fluorescence responses of oROS-G and HyPerRed to 300 μM exogenous H_2O_2. The barplot represents the mean of the maximum fluorescent response of cells in ΔF/Fo (change of fluorescence over baseline). **D** On-kinetic analysis of oROS-G and HyPerRed. Representative trace of 300μM peroxide-induced saturation of both sensors with normalized ΔF/Fo. Vertical dotted lines represent 75% and 25% sensor activation, labeled with 25-75% activation completion time. 100% indicates full sensor saturation. **E** Fluorescence responses of oROS-G and HyPerRed to 10 μM exogenous H_2O_2. **F** Benchmark test of oROS-G, HyPerRed, and HyPer7 for their H_2O_2 sensitivity. Each sensor was expressed in HEK293 cells, and their ΔF/Fo were calculated for their responses to exogenous administration of either 300 μM (high) or 10 μM (low) H_2O_2. Bar plot represents the low/high response (10 μM/300 μM) ratio of each sensor. **G** Representative reduction kinetics of oROS-G and HyPer7 after 100 μM H_2O_2 stimulation followed by media wash (n>100 cells per sensor). **H** HEK293 expressing oROS-G were stimulated with 100 μM H_2O_2 followed by media wash. The sequence was repeated twice. **I** Expression of oROS-G in HEK293 (Scale bar: 100 μM), primary rat cortical neuron (Scale bar: 50 μM), and hiPSC-derived cardiomyocyte (Scale bar:

100µM), and their responses to 300µM H_2O_2 stimulation. **Descriptive statistics:** Error bars and bands represent the bootstrap confidence interval (95%) of the central tendency of values using the Seaborn (0.11.2) statistical plotting package. Cell-of-interests were collected from 3 biological replicates unless noted otherwise.

Figure 2 Visualizing extracellular and intracellular diffusion H_2O_2 using oROS-G. **A-B** Normalized (min-max scaled) fluorescence response of oROS-G **(A)** and HyPerRed **(B)** to 300µM H_2O_2 stimulation captured at 10Hz. Region-of-interests (ROI) were color-coded for their respective X-axis location. Scale bar = 150µm.Traces show oROS-G responses at varying locations along the X-axes. **C** Diffusion map derived from Fig. 2A. The image was transformed into an activation map that depicts the ratio of responding (i.e. activated) pixels along the x-axis over time. The map reveals the speed of the H_2O_2 diffusion to be ≈800µm/s. **D** Chronological pixel activation map of oROS-G expressing HEK293 cells. Colormap represents the time each pixel passes the 10% of the maximum threshold. Scale bar = 50µm. White dashed line: segmented cell outline. **E** Representative images of intracellular H_2O_2 diffusion. **(i)** radial diffusion **(ii)** polarized diffusion **(iii), (iv)** neighboring cell cluster. Scale bar = 25 µm. White dashed line: segmented cell

outline.

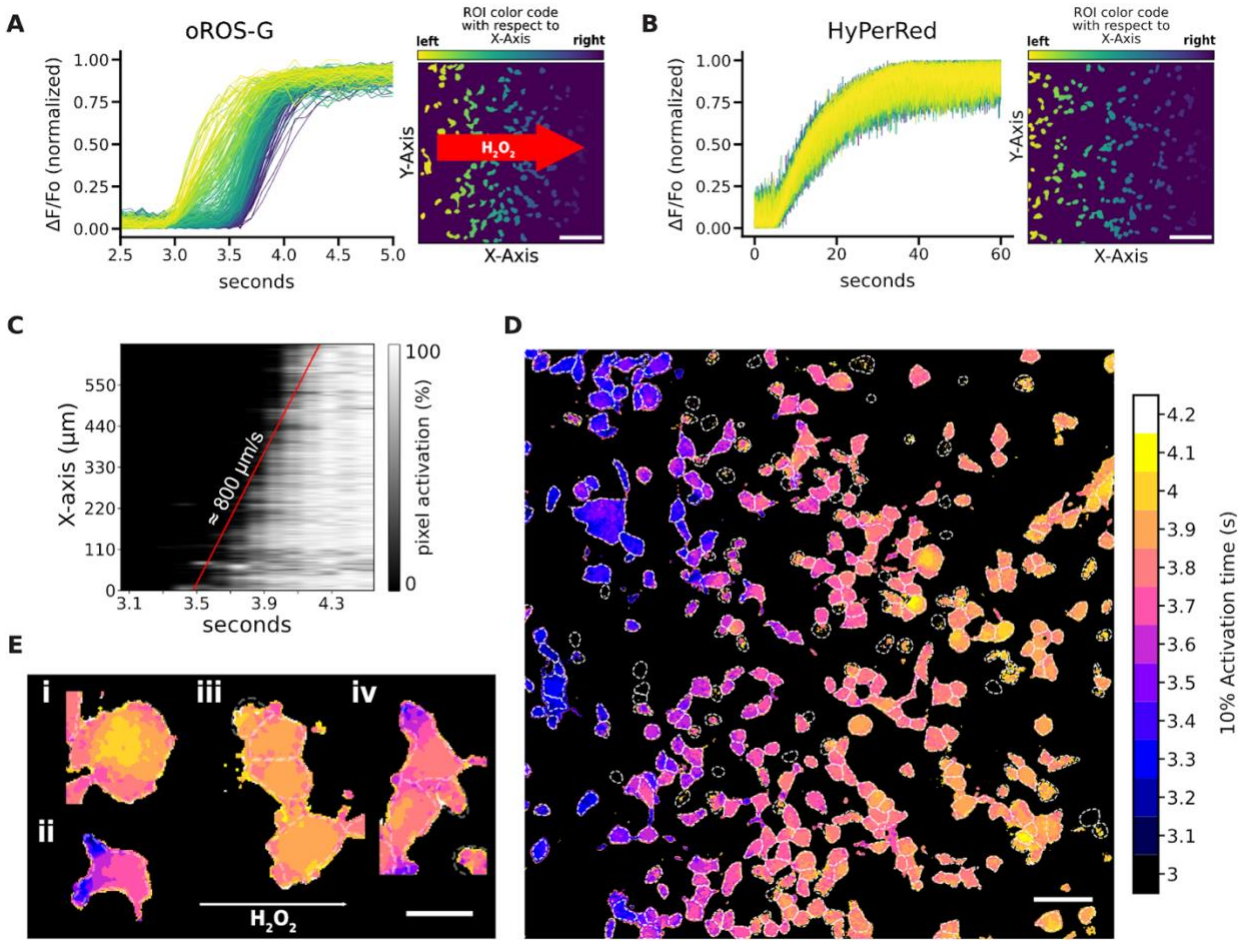

Figure 4.3 Ratiometric variant oROS-Gr improves temporal resolution of H_2O_2 measurement.

A ***left*** Schematic illustration of the oROS-Gr sensor design. oROS-Gr is an oROS-G variant with a C-terminus fusion of mCherry red fluorescent protein. ***right*** Flow cytometry result showed the linear relationship of green and red fluorescence levels of the oROS-G1r sensor expressed in HEK293 cells. **B** 510/605 nm emission ratio of oROS-Gr expressed in HEK293s stimulated with various concentrations of H_2O_2. Fluorescence emission ratios were captured a minute after the exposure. (n>100 cells

per condition) **C** 510/605 nm emission ratio change of oROS-Gr during activation and reversal upon stimulation with 100 µM H_2O_2 and 10 mM DTT in HEK293 WT cells (n=82 cells). **D** Continuous (10 hours) monitoring of oROS-Gr stable cells in response to various concentrations of menadione (n>100 cells per condition). ***Top*** Ratio: 510/605 nm emission ratio of oROS-Gr ***Bottom*** Non-ratio: unnormalized 510 nm emission intensity profile. **E** Aggregated Coefficient of Variation (CoV) of 510/605 nm emission ratio and 510 nm emission intensity from Figure 4D. **F** Observation of glucose-level dependent basal oxidation level of oROS-Gr (510/605 ratio) in oROS-Gr stable cells. The cells were incubated in LG (low glucose, 1 mM), NG, and HG incubation for 48 hours after they were serum-deprived overnight. The sensors were least oxidized in NG, exhibiting a U-shape dose-dependent response (n>100 cells per condition). **G** Resting oROS-Gr ratio expressed in hiPSC-derived cortical neurons incubated in various levels of menadione for 24 hours. (n=3-4 wells per condition) **Descriptive statistics:** Error bars and bands represent the bootstrap confidence interval (95%) of the central tendency of values using the Seaborn (0.11.2) statistical plotting package. Cell-of-interests were collected from 3 biological replicates unless noted otherwise. **Inferential statistics:** F - t-test independent samples. *P < 0.05, **P < 0.01,

***P<0.001.

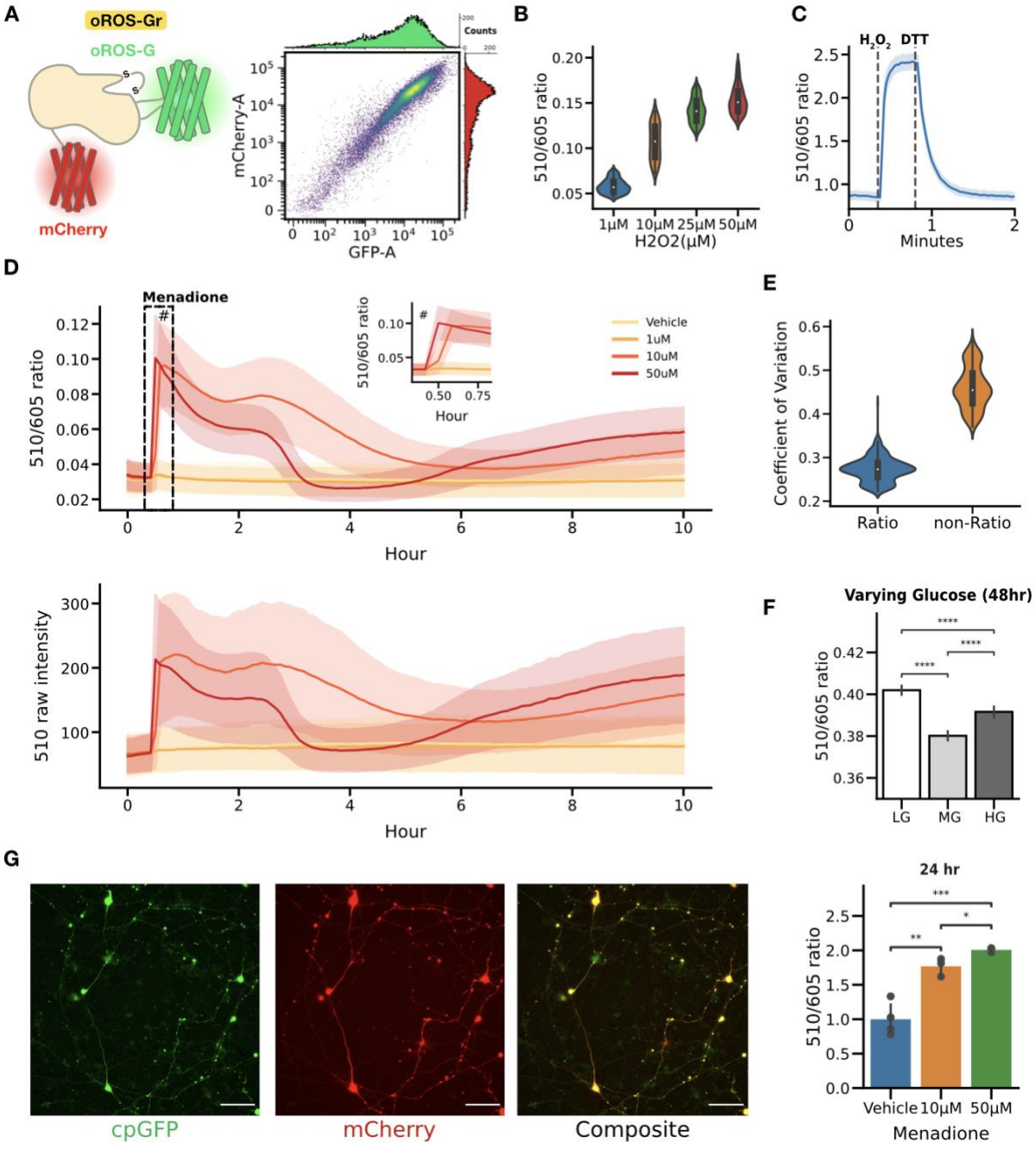

Figure 4.4 Monitoring the effects of antioxidants on intracellular peroxide levels in an Alzheimer's model.

A Schematic illustration of the experimental timeline showing oROS-G transfected primary astrocytes seeded in a 96-well plate, administered with 5 μM oligomerized

Amyloid beta (oAβ), 180 µM putrescine, 1 µM KDS2010 (selective and reversible MAOB inhibitor), and 1 mM sodium pyruvate (H_2O_2 scavenger) followed by 40-hour of confocal live imaging to monitor intracellular H_2O_2 and antioxidant effects. **B** Schematic diagram of the oAβ and putrescine induced H_2O_2 production. **C** 40-hour monitoring of oAβ-induced H_2O_2 production and antioxidant effects with KDS2010 and sodium pyruvate (Vehicle: n=22, oAβ: n=22, oAβ+Sodium Pyruvate: n=23, oAβ+KDS2010: n=13). **D** Summary bar graph representing fluorescence values normalized to the baseline, measured during the first hour. **E** Monitoring of putrescine-induced H_2O_2 production and antioxidant effects with KDS2010 and sodium pyruvate (Vehicle: n=24, Put.: n=25, Put.+Sodium Pyruvate: n=22, Put.+KDS2010: n=14). **F** Summary bar graph representing fluorescence values normalized to the baseline. **G** Schematic illustration of the bilateral virus injection of experimental design. **H** Fluorescence response of oROS-G to 10 µM (n=13) or 100 µM H_2O_2 (n=14) in astrocytes of hippocampal tissue. **I** H_2O_2 dose-dependent summary bar graph. **J** Representative images captured with a CMOS camera illustrating the expression of oROS-G in astrocytes located in the stratum radiatum (SR) of the hippocampal CA1 region, in coronal brain slices ex vivo. oROS-G virus, driven by the GFAP promoter, is selectively expressed in astrocytes, with no expression in pyramidal neurons (PYR). **K** Fluorescence response of oROS-G to 10 mM (DTT) in astrocytes of hippocampal tissue (WT: n=22, APP/PS1 n=14). **L** Summary bar graph representing the difference between baseline fluorescence and saturation values after DTT administration. **Descriptive statistics:** Data are presented as mean ± SEM. **Inferential statistics:** D, F - One-way ANOVA with Tukey's multiple comparison test, I, J - Unpaired t-test, two-tailed *P < 0.05, **P < 0.01, ***P <

0.001.

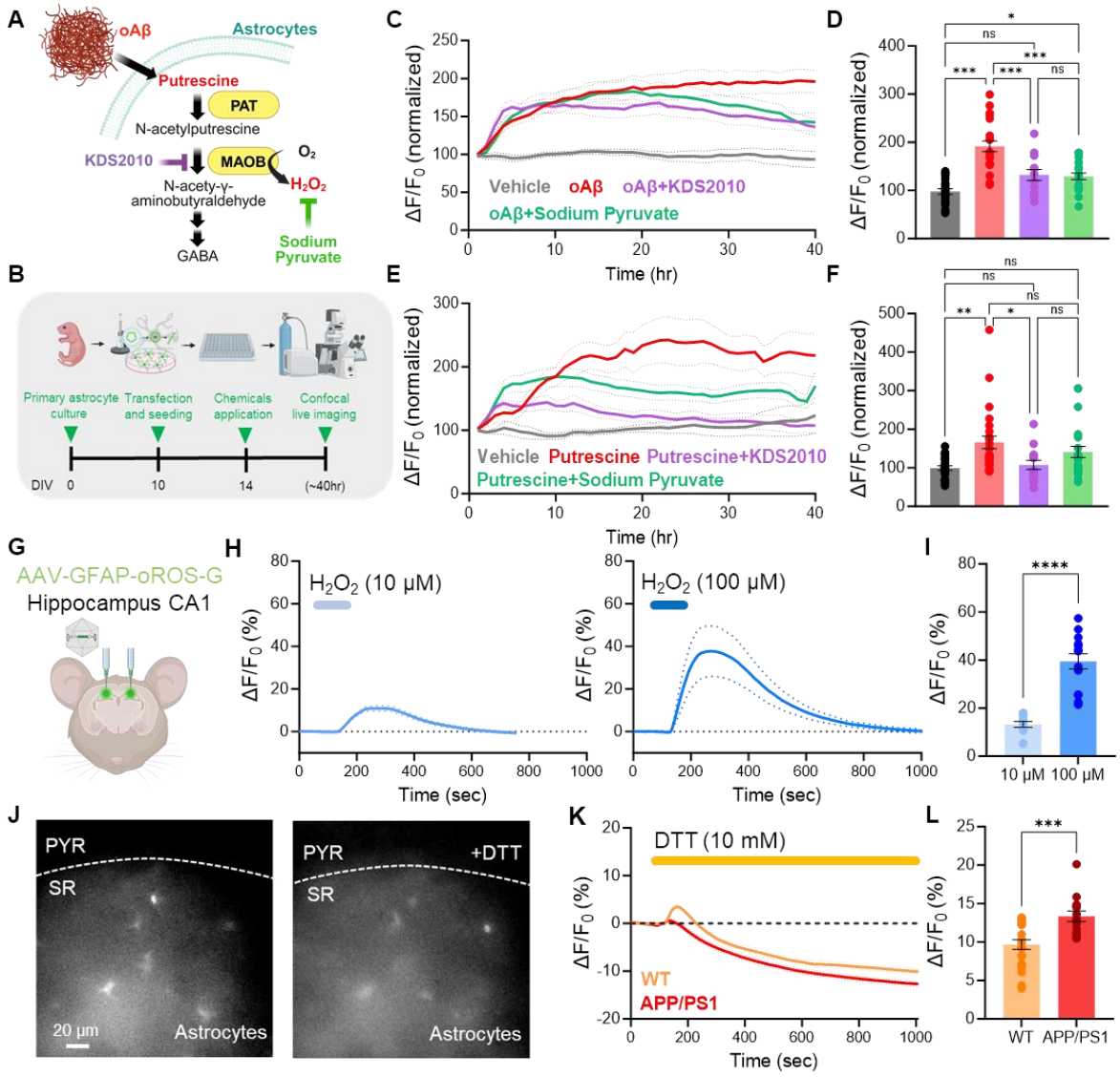

Figure 4.5 G-protein biased agonists elicit H_2O_2 generation in κ and μ opioid receptor-expressing neurons in the Ventral Tegmental Area *ex vivo* and *in vivo*.

A Schematic illustration of the JNK/PRDX6/NOX pathway for opioid receptor-dependent generation of H_2O_2. **B** Targeted expression of oROS-Gr in μ opioid receptor (MOR) positive neurons of Ventral tegmental Area (VTA) was achieved by AAV1-DIO-oROSGr injection in VTA of *Oprm1*-Cre animals. Fluorescent images show histological validation

of post-mortem slices via confocal microscopy. Scale bar = 100 µm **C** *Ex vivo* brain slice showing morphine-dependent H_2O_2 increase in MOR-positive neurons. (Morph: 1 µM Morphine, n=10 slices. Morph + NLX: 1µM Morphine co-administered with 1 µM Naloxone, n=9 slices) ***left*** real-time trace of morphine-induced oROS-Gr signals detected in µOR positive neurons of VTA. Naloxone, a competitive mu-opioid receptor antagonist, effectively diminishes Morphine-induced oROS-Gr signals. ***right*** maximal fluorescence response for each condition. **D** Schematic description of fiber photometry experimental set-up with *Oprk1*-Cre transgenic mouse injected with AAV1-DIO-oROSGr in VTA. Bottom-right fluorescent image shows histological validation of post-mortem slices via confocal microscopy. Scale bar = 100 µm **E** *in vivo* fiber photometry of oROS-Gr (only ex:488/em:510) showed significant fluorescence increase in response to Nalfurafine (100 µg/kg), which is readily blocked by pre-treatment of Naloxone (10 mg/kg). (Nalfurafine: n=14, Nalfurafine + NLX: n=7 mice) ***left*** real-time trace of fiber signal from oROS-Gr detected in KOR (trans positive neurons of VTA. ***right*** Area under curve (AUC) integrated for each animal in each condition using the composite trapezoidal rule (trapz function in NumPy python package: version 1.26). **Descriptive statistics:** C, E - Error bars and bands represent the bootstrap confidence interval (95%) of the central tendency of values using the Seaborn (0.11.2) statistical plotting package. **Inferential statistics:** C,E - t-test independent samples. *P < 0.05, **P <

0.01, ***P < 0.001.

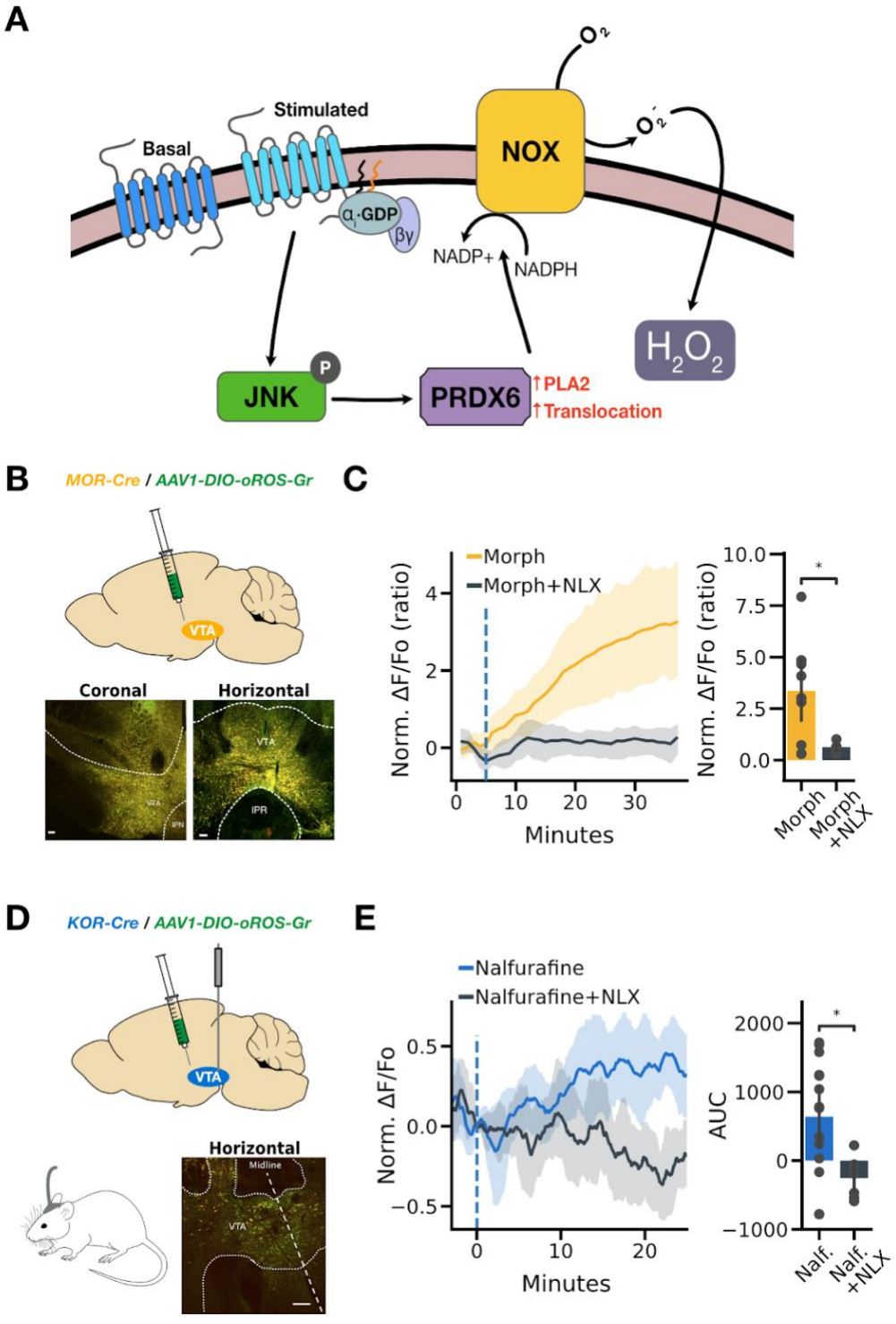
A
Stimulated
Basal
NOX
O_2
O_2^-
α_i·GDP
$\beta\gamma$
NADP+
NADPH
H_2O_2
JNK
P
PRDX6
↑PLA2
↑Translocation
B
MOR-Cre / AAV1-DIO-oROS-Gr
VTA
Coronal
Horizontal
C
Morph
Morph+NLX
Norm. ΔF/Fo (ratio)
Minutes
Morph
Morph +NLX
D
KOR-Cre / AAV1-DIO-oROS-Gr
Horizontal
Midline
E
Nalfurafine
Nalfurafine+NLX
Norm. ΔF/Fo
AUC
Nalf.
Nalf. +NLX

REFERENCES

1. P. G. Falkowski, M. E. Katz, A. J. Milligan, K. Fennel, B. S. Cramer, M. P. Aubry, R. A. Berner, M. J. Novacek, W. M. Zapol, The rise of oxygen over the past 205 million years and the evolution of large placental mammals. *Science* **309**, 2202–2204 (2005).

2. L. G. Koch, S. L. Britton, Aerobic metabolism underlies complexity and capacity. *J. Physiol.* **586**, 83–95 (2008).

3. H. Westerblad, D. G. Allen, Emerging roles of ROS/RNS in muscle function and fatigue. *Antioxid. Redox Signal.* **15**, 2487–2499 (2011).

4. K. J. Barnham, C. L. Masters, A. I. Bush, Neurodegenerative diseases and oxidative stress. *Nat. Rev. Drug Discov.* **3**, 205–214 (2004).

5. Y. M. Lee, W. He, Y.-C. Liou, The redox language in neurodegenerative diseases: oxidative post-translational modifications by hydrogen peroxide. *Cell Death Dis.* **12**, 58 (2021).

6. S. J. Forrester, D. S. Kikuchi, M. S. Hernandes, Q. Xu, K. K. Griendling, Reactive Oxygen Species in Metabolic and Inflammatory Signaling. *Circ. Res.* **122**, 877–902 (2018).

7. B. D'Autréaux, M. B. Toledano, ROS as signalling molecules: mechanisms that generate specificity in ROS homeostasis. *Nat. Rev. Mol. Cell Biol.* **8**, 813–824 (2007).

8. M. Schieber, N. S. Chandel, ROS function in redox signaling and oxidative stress. *Curr. Biol.* **24**, R453–62 (2014).

9. T. Finkel, Signal transduction by reactive oxygen species. *J. Cell Biol.* **194**, 7–15 (2011).

10. H. Sies, Hydrogen peroxide as a central redox signaling molecule in physiological oxidative stress: Oxidative eustress. *Redox Biol* **11**, 613–619 (2017).

11. H. Chun, H. Im, Y. J. Kang, Y. Kim, J. H. Shin, W. Won, J. Lim, Y. Ju, Y. M. Park, S. Kim, S. E. Lee, J. Lee, J. Woo, Y. Hwang, H. Cho, S. Jo, J.-H. Park, D. Kim, D. Y. Kim, J.-S. Seo, B. J. Gwag, Y. S. Kim, K. D. Park, B.-K. Kaang, H. Cho, H. Ryu, C. J. Lee, Severe reactive astrocytes precipitate pathological hallmarks of Alzheimer's disease via H2O2- production. *Nat. Neurosci.* **23**, 1555–1566 (2020).

12. Q. M. Chen, V. C. Tu, Y. Wu, J. J. Bahl, Hydrogen peroxide dose dependent induction of cell death or hypertrophy in cardiomyocytes. *Arch. Biochem. Biophys.* **373**, 242–248 (2000).

13. I. Afanas'ev, New nucleophilic mechanisms of ros-dependent epigenetic modifications: comparison of aging and cancer. *Aging Dis.* **5**, 52–62 (2014).

14. H. Sies, D. P. Jones, Reactive oxygen species (ROS) as pleiotropic physiological signalling agents. *Nat. Rev. Mol. Cell Biol.* **21**, 363–383 (2020).

15. H. Sies, V. V. Belousov, N. S. Chandel, M. J. Davies, D. P. Jones, G. E. Mann, M. P. Murphy, M. Yamamoto, C. Winterbourn, Defining roles of specific reactive oxygen species (ROS) in cell biology and physiology. *Nat. Rev. Mol. Cell Biol.* **23**, 499–515 (2022).

16. M. P. Murphy, H. Bayir, V. Belousov, C. J. Chang, K. J. A. Davies, M. J. Davies, T. P. Dick, T. Finkel, H. J. Forman, Y. Janssen-Heininger, D. Gems, V. E. Kagan, B. Kalyanaraman, N.-G. Larsson, G. L. Milne, T. Nyström, H. E. Poulsen, R. Radi, H. Van Remmen, P. T. Schumacker, P. J. Thornalley, S. Toyokuni, C. C. Winterbourn, H. Yin, B. Halliwell, Guidelines for measuring reactive oxygen species and oxidative damage in cells and in vivo. *Nat Metab* **4**, 651–662 (2022).

17. M. Gutscher, M. C. Sobotta, G. H. Wabnitz, S. Ballikaya, A. J. Meyer, Y. Samstag, T. P. Dick, Proximity-based protein thiol oxidation by H2O2-scavenging peroxidases. *J. Biol. Chem.* **284**, 31532–31540 (2009).

18. B. Morgan, K. Van Laer, T. N. E. Owusu, D. Ezeriņa, D. Pastor-Flores, P. S. Amponsah, A. Tursch, T. P. Dick, Real-time monitoring of basal H2O2 levels with peroxiredoxin-based probes. *Nat. Chem. Biol.* **12**, 437–443 (2016).

19. V. V. Belousov, A. F. Fradkov, K. A. Lukyanov, D. B. Staroverov, K. S. Shakhbazov, A. V. Terskikh, S. Lukyanov, Genetically encoded fluorescent indicator for intracellular hydrogen peroxide. *Nat. Methods* **3**, 281–286 (2006).

20. K. N. Markvicheva, D. S. Bilan, N. M. Mishina, A. Y. Gorokhovatsky, L. M. Vinokurov, S. Lukyanov, V. V. Belousov, A genetically encoded sensor for H2O2 with expanded dynamic range. *Bioorg. Med. Chem.* **19**, 1079–1084 (2011).

21. D. S. Bilan, L. Pase, L. Joosen, A. Y. Gorokhovatsky, Y. G. Ermakova, T. W. J. Gadella, C. Grabher, C. Schultz, S. Lukyanov, V. V. Belousov, HyPer-3: a genetically encoded H(2)O(2) probe with improved performance for ratiometric and fluorescence lifetime imaging. *ACS Chem. Biol.* **8**, 535–542 (2013).

22. Y. G. Ermakova, D. S. Bilan, M. E. Matlashov, N. M. Mishina, K. N. Markvicheva, O. M. Subach, F. V. Subach, I. Bogeski, M. Hoth, G. Enikolopov, V. V. Belousov, Red fluorescent genetically encoded indicator for intracellular hydrogen peroxide. *Nat. Commun.* **5**, 5222 (2014).

23. O. M. Subach, T. A. Kunitsyna, O. A. Mineyeva, A. A. Lazutkin, D. V. Bezryadnov, N. V. Barykina, K. D. Piatkevich, Y. G. Ermakova, D. S. Bilan, V. V. Belousov, K. V. Anokhin, G. N. Enikolopov, F. V. Subach, Slowly Reducible Genetically Encoded Green Fluorescent Indicator for In Vivo and Ex Vivo Visualization of Hydrogen Peroxide. *Int. J. Mol. Sci.* **20** (2019).

24. V. V. Pak, D. Ezeriņa, O. G. Lyublinskaya, B. Pedre, P. A. Tyurin-Kuzmin, N. M. Mishina, M. Thauvin, D. Young, K. Wahni, S. A. Martínez Gache, A. D. Demidovich, Y. G. Ermakova, Y. D. Maslova, A. G. Shokhina, E. Eroglu, D. S. Bilan, I. Bogeski, T. Michel, S. Vriz, J. Messens, V. V. Belousov, Ultrasensitive Genetically Encoded Indicator for Hydrogen Peroxide Identifies Roles for the Oxidant in Cell Migration and Mitochondrial Function. *Cell Metab.* **31**, 642–653.e6 (2020).

25. Y. Pang, Y. Zhang, J. Zhang, Z. Li, Y. He, Y. Wang, J. Oberholzer, H.-W. Ai, SHRIMP: Genetically Encoded mScarlet-derived Red Fluorescent Hydrogen Peroxide Sensor with High Brightness and Minimal Photoactivation, *bioRxiv* (2023)p. 2023.08.09.552302.

26. C. Lee, S. M. Lee, P. Mukhopadhyay, S. J. Kim, S. C. Lee, W.-S. Ahn, M.-H. Yu, G. Storz, S. E. Ryu, Redox regulation of OxyR requires specific disulfide bond formation involving a rapid kinetic reaction path. *Nat. Struct. Mol. Biol.* **11**, 1179–1185 (2004).

27. I. Jo, I.-Y. Chung, H.-W. Bae, J.-S. Kim, S. Song, Y.-H. Cho, N.-C. Ha, Structural details of the OxyR peroxide-sensing mechanism. *Proc. Natl. Acad. Sci. U. S. A.* **112**, 6443–6448 (2015).

28. J. Akerboom, T.-W. Chen, T. J. Wardill, L. Tian, J. S. Marvin, S. Mutlu, N. C. Calderón, F. Esposti, B. G. Borghuis, X. R. Sun, A. Gordus, M. B. Orger, R. Portugues, F. Engert, J. J. Macklin, A. Filosa, A. Aggarwal, R. A. Kerr, R. Takagi, S. Kracun, E. Shigetomi, B. S. Khakh, H. Baier, L. Lagnado, S. S.-H. Wang, C. I. Bargmann, B. E. Kimmel, V. Jayaraman, K. Svoboda, D. S. Kim, E. R. Schreiter, L. L. Looger, Optimization of a GCaMP calcium indicator for neural activity imaging. *J. Neurosci.* **32**, 13819–13840 (2012).

29. G. P. Bienert, F. Chaumont, Aquaporin-facilitated transmembrane diffusion of hydrogen peroxide. *Biochim. Biophys. Acta* **1840**, 1596–1604 (2014).

30. V. Montiel, R. Bella, L. Y. M. Michel, H. Esfahani, D. De Mulder, E. L. Robinson, J.-P. Deglasse, M. Tiburcy, P. H. Chow, J.-C. Jonas, P. Gilon, B. Steinhorn, T. Michel, C. Beauloye, L. Bertrand, C. Farah, F. Dei Zotti, H. Debaix, C. Bouzin, D. Brusa, S. Horman, J.-L. Vanoverschelde, O. Bergmann, D. Gilis, M. Rooman, A. Ghigo, S. Geninatti-Crich, A. Yool, W. H. Zimmermann, H. L. Roderick, O. Devuyst, J.-L. Balligand, Inhibition of aquaporin-1 prevents myocardial remodeling by blocking the transmembrane transport of hydrogen peroxide. *Sci. Transl. Med.* **12** (2020).

31. D. Wragg, S. Leoni, A. Casini, Aquaporin-driven hydrogen peroxide transport: a case of molecular mimicry? *RSC Chem Biol* **1**, 390–394 (2020).

32. J. B. Lim, T. F. Langford, B. K. Huang, W. M. Deen, H. D. Sikes, A reaction-diffusion model of cytosolic hydrogen peroxide. *Free Radic. Biol. Med.* **90**, 85–90 (2016).

33. G. P. Bienert, A. L. B. Møller, K. A. Kristiansen, A. Schulz, I. M. Møller, J. K. Schjoerring, T. P. Jahn, Specific aquaporins facilitate the diffusion of hydrogen peroxide across membranes. *J. Biol. Chem.* **282**, 1183–1192 (2007).

34. A. Ledo, E. Fernandes, A. Salvador, J. Laranjinha, R. M. Barbosa, In vivo hydrogen peroxide diffusivity in brain tissue supports volume signaling activity. *Redox Biol* **50**, 102250 (2022).

35. J. H. Birnbaum, D. Wanner, A. F. Gietl, A. Saake, T. M. Kündig, C. Hock, R. M. Nitsch, C. Tackenberg, Oxidative stress and altered mitochondrial protein expression in the absence of amyloid-β and tau pathology in iPSC-derived neurons from sporadic Alzheimer's disease patients. *Stem Cell Res.* **27**, 121–130 (2018).

36. G. Loor, J. Kondapalli, J. M. Schriewer, N. S. Chandel, T. L. Vanden Hoek, P. T. Schumacker, Menadione triggers cell death through ROS-dependent mechanisms involving PARP activation without requiring apoptosis. *Free Radic. Biol. Med.* **49**, 1925–1936 (2010).

37. D. N. Criddle, S. Gillies, H. K. Baumgartner-Wilson, M. Jaffar, E. C. Chinje, S. Passmore, M. Chvanov, S. Barrow, O. V. Gerasimenko, A. V. Tepikin, R. Sutton, O. H. Petersen, Menadione-induced reactive oxygen species generation via redox cycling promotes apoptosis of murine pancreatic acinar cells. *J. Biol. Chem.* **281**, 40485–40492 (2006).

38. V. Shneyvays, D. Leshem, Y. Shmist, T. Zinman, A. Shainberg, Effects of menadione and its derivative on cultured cardiomyocytes with mitochondrial disorders. *J. Mol. Cell. Cardiol.* **39**, 149–158 (2005).

39. Y.-H. Jan, J. R. Richardson, A. A. Baker, V. Mishin, D. E. Heck, D. L. Laskin, J. D. Laskin, Vitamin K3 (menadione) redox cycling inhibits cytochrome P450-mediated metabolism and inhibits parathion intoxication. *Toxicol. Appl. Pharmacol.* **288**, 114–120 (2015).

40. T. Ishii, E. Warabi, G. E. Mann, Mechanisms underlying Nrf2 nuclear translocation by non-lethal levels of hydrogen peroxide: p38 MAPK-dependent neutral sphingomyelinase2 membrane trafficking and ceramide/PKCζ/CK2 signaling. *Free Radic. Biol. Med.* **191**, 191–202 (2022).

41. C. Espinosa-Diez, V. Miguel, D. Mennerich, T. Kietzmann, P. Sánchez-Pérez, S. Cadenas, S. Lamas, Antioxidant responses and cellular adjustments to oxidative stress. *Redox Biol* **6**, 183–197 (2015).

42. H.-S. Wong, P. A. Dighe, V. Mezera, P.-A. Monternier, M. D. Brand, Production of superoxide and hydrogen peroxide from specific mitochondrial sites under different bioenergetic conditions. *J. Biol. Chem.* **292**, 16804–16809 (2017).

43. J.-H. Huang, H. K. Co, Y.-C. Lee, C.-C. Wu, S.-H. Chen, Multistability maintains redox homeostasis in human cells. *Mol. Syst. Biol.* **17**, e10480 (2021).

44. H. J. Forman, H. Zhang, Targeting oxidative stress in disease: promise and limitations of antioxidant therapy. *Nat. Rev. Drug Discov.* **20**, 689–709 (2021).

45. Y. Zhang, C. Qin, L. Yang, R. Lu, X. Zhao, G. Nie, A comparative genomics study of carbohydrate/glucose metabolic genes: from fish to mammals. *BMC Genomics* **19**, 246 (2018).

46. I. Audzeyenka, P. Rachubik, M. Typiak, T. Kulesza, A. Topolewska, D. Rogacka, S. Angielski, M. A. Saleem, A. Piwkowska, Hyperglycemia alters mitochondrial respiration efficiency and mitophagy in human podocytes. *Exp. Cell Res.* **407**, 112758 (2021).

47. J. C. Klima, L. A. Doyle, J. D. Lee, M. Rappleye, L. A. Gagnon, M. Y. Lee, E. P. Barros, A. A. Vorobieva, J. Dou, S. Bremner, J. S. Quon, C. M. Chow, L. Carter, D. L. Mack, R. E. Amaro, J. C. Vaughan, A. Berndt, B. L. Stoddard, D. Baker, Incorporation of sensing modalities into de novo designed fluorescence-activating proteins. *Nat. Commun.* **12**, 856 (2021).

48. J. B. Goodman, F. Qin, R. J. Morgan, J. M. Chambers, D. Croteau, D. A. Siwik, I. Hobai, M. Panagia, I. Luptak, M. Bachschmid, X. Tong, D. R. Pimentel, R. A. Cohen, W. S. Colucci, Redox-Resistant SERCA [Sarco(endo)plasmic Reticulum Calcium ATPase] Attenuates Oxidant-Stimulated Mitochondrial Calcium and Apoptosis in Cardiac Myocytes and Pressure Overload-Induced Myocardial Failure in Mice. *Circulation* **142**, 2459–2469 (2020).

49. F. Qin, D. A. Siwik, D. R. Pimentel, R. J. Morgan, A. Biolo, V. H. Tu, Y. J. Kang, R. A. Cohen, W. S. Colucci, Cytosolic H2O2 mediates hypertrophy, apoptosis, and decreased SERCA activity in mice with chronic hemodynamic overload. *Am. J. Physiol. Heart Circ. Physiol.* **306**, H1453–63 (2014).

50. F. Gonnot, L. Boulogne, C. Brun, M. Dia, Y. Gouriou, G. Bidaux, C. Chouabe, C. Crola Da Silva, S. Ducreux, B. Pillot, A. Kaczmarczyk, C. Leon, S. Chanon, C. Perret, F. Sciandra, T. Dargar, V. Gache, F. Farhat, L. Sebbag, T. Bochaton, H. Thibault, M. Ovize, M. Paillard, L. Gomez, SERCA2 phosphorylation at serine 663 is a key regulator of Ca2+ homeostasis in heart diseases. *Nat. Commun.* **14**, 3346 (2023).

51. T. Akaike, N. Du, G. Lu, S. Minamisawa, Y. Wang, H. Ruan, A Sarcoplasmic Reticulum Localized Protein Phosphatase Regulates Phospholamban Phosphorylation and Promotes Ischemia Reperfusion Injury in the Heart. *JACC: Basic to Translational Science* **2**, 160–180 (2017).

52. B. Pedre, U. Barayeu, D. Ezeriņa, T. P. Dick, The mechanism of action of N-acetylcysteine (NAC): The emerging role of H2S and sulfane sulfur species. *Pharmacol. Ther.* **228**, 107916 (2021).

53. D. Ezeriņa, Y. Takano, K. Hanaoka, Y. Urano, T. P. Dick, N-Acetyl Cysteine Functions as a Fast-Acting Antioxidant by Triggering Intracellular H2S and Sulfane Sulfur Production. *Cell Chem Biol* **25**, 447–459.e4 (2018).

54. H. Chun, J. Lim, K. D. Park, C. J. Lee, Inhibition of monoamine oxidase B prevents reactive astrogliosis and scar formation in stab wound injury model. *Glia* **70**, 354–367 (2022).

55. S. Lee, B.-E. Yoon, K. Berglund, S.-J. Oh, H. Park, H.-S. Shin, G. J. Augustine, C. J. Lee, Channel-mediated tonic GABA release from glia. *Science* **330**, 790–796 (2010).

56. S. Jo, O. Yarishkin, Y. J. Hwang, Y. E. Chun, M. Park, D. H. Woo, J. Y. Bae, T. Kim, J. Lee, H. Chun, H. J. Park, D. Y. Lee, J. Hong, H. Y. Kim, S.-J. Oh, S. J. Park, H. Lee, B.-E. Yoon, Y. Kim, Y. Jeong, I. Shim, Y. C. Bae, J. Cho, N. W. Kowall, H. Ryu, E. Hwang, D. Kim, C. J. Lee, GABA from reactive astrocytes impairs memory in mouse models of Alzheimer's disease. *Nat. Med.* **20**, 886–896 (2014).

57. J. L. Jankowsky, D. J. Fadale, J. Anderson, G. M. Xu, V. Gonzales, N. A. Jenkins, N. G. Copeland, M. K. Lee, L. H. Younkin, S. L. Wagner, S. G. Younkin, D. R. Borchelt, Mutant presenilins specifically elevate the levels of the 42 residue beta-amyloid peptide in vivo: evidence for augmentation of a 42-specific gamma secretase. *Hum. Mol. Genet.* **13**, 159–170 (2004).

58. S. S. Schattauer, B. B. Land, K. L. Reichard, A. D. Abraham, L. M. Burgeno, J. R. Kuhar, P. E. M. Phillips, S. E. Ong, C. Chavkin, Peroxiredoxin 6 mediates Gαi protein-coupled receptor inactivation by cJun kinase. *Nat. Commun.* **8**, 743 (2017).

59. S. S. Schattauer, A. Bedini, F. Summers, A. Reilly-Treat, M. M. Andrews, B. B. Land, C. Chavkin, Reactive oxygen species (ROS) generation is stimulated by κ opioid receptor activation through phosphorylated c-Jun N-terminal kinase and inhibited by p38 mitogen-activated protein kinase (MAPK) activation. *J. Biol. Chem.* **294**, 16884–16896 (2019).

60. J. Stanicka, E. G. Russell, J. F. Woolley, T. G. Cotter, NADPH oxidase-generated hydrogen peroxide induces DNA damage in mutant FLT3-expressing leukemia cells. *J. Biol. Chem.* **290**, 9348–9361 (2015).

61. T. F. Brewer, F. J. Garcia, C. S. Onak, K. S. Carroll, C. J. Chang, Chemical approaches to discovery and study of sources and targets of hydrogen peroxide redox signaling through NADPH oxidase proteins. *Annu. Rev. Biochem.* **84**, 765–790 (2015).

62. M. Muñoz, M. P. Martínez, M. E. López-Oliva, C. Rodríguez, C. Corbacho, J. Carballido, A. García-Sacristán, M. Hernández, L. Rivera, J. Sáenz-Medina, D. Prieto, Hydrogen peroxide derived from NADPH oxidase 4- and 2 contributes to the endothelium-dependent vasodilatation of intrarenal arteries. *Redox Biol* **19**, 92–104 (2018).

63. F. Johnson, C. Giulivi, Superoxide dismutases and their impact upon human health. *Mol. Aspects Med.* **26**, 340–352 (2005).

64. A. El Daibani, J. M. Paggi, K. Kim, Y. D. Laloudakis, P. Popov, S. M. Bernhard, B. E. Krumm, R. H. J. Olsen, J. Diberto, F. I. Carroll, V. Katritch, B. Wünsch, R. O. Dror, T. Che, Molecular mechanism of biased signaling at the kappa opioid receptor. *Nat. Commun.* **14**, 1338 (2023).

65. S. S. Schattauer, J. R. Kuhar, A. Song, C. Chavkin, Nalfurafine is a G-protein biased agonist having significantly greater bias at the human than rodent form of the kappa opioid receptor. *Cell. Signal.* **32**, 59–65 (2017).

66. A. J. Douglas, G. Clarke, S. J. MacMillan, P. M. Bull, I. Neumann, S. A. Way, D. M. Wright, B. G. McGrory, J. A. Russell, Effects of the kappa-opioid agonist U50,488 on parturition in rats. *Br. J. Pharmacol.* **109**, 251–258 (1993).

67. F. Aslund, M. Zheng, J. Beckwith, G. Storz, Regulation of the OxyR transcription factor by hydrogen peroxide and the cellular thiol-disulfide status. *Proc. Natl. Acad. Sci. U. S. A.* **96**, 6161–6165 (1999).

68. P. Kritsiligkou, T. K. Shen, T. P. Dick, A comparison of Prx- and OxyR-based H2O2 probes expressed in S. cerevisiae. *J. Biol. Chem.* **297**, 100866 (2021).

69. J. García-Nafría, J. F. Watson, I. H. Greger, IVA cloning: A single-tube universal cloning system exploiting bacterial In Vivo Assembly. *Sci. Rep.* **6**, 27459 (2016).

70. X. Lian, J. Zhang, S. M. Azarin, K. Zhu, L. B. Hazeltine, X. Bao, C. Hsiao, T. J. Kamp, S. P. Palecek, Directed cardiomyocyte differentiation from human pluripotent stem cells by modulating Wnt/β-catenin signaling under fully defined conditions. *Nat. Protoc.* **8**, 162–175 (2013).

71. S. B. Bremner, C. J. Mandrycky, A. Leonard, R. M. Padgett, A. R. Levinson, E. S. Rehn, J. M. Pioner, N. J. Sniadecki, D. L. Mack, Full-length dystrophin deficiency leads to contractile and calcium transient defects in human engineered heart tissues. *J. Tissue Eng.* **13**, 20417314221119628 (2022).

72. S. Tohyama, F. Hattori, M. Sano, T. Hishiki, Y. Nagahata, T. Matsuura, H. Hashimoto, T. Suzuki, H. Yamashita, Y. Satoh, T. Egashira, T. Seki, N. Muraoka, H. Yamakawa, Y. Ohgino, T. Tanaka, M. Yoichi, S. Yuasa, M. Murata, M. Suematsu, K. Fukuda, Distinct metabolic flow enables large-scale purification of mouse and human pluripotent stem cell-derived cardiomyocytes. *Cell Stem Cell* **12**, 127–137 (2013).

73. C. Stringer, T. Wang, M. Michaelos, M. Pachitariu, Cellpose: a generalist algorithm for cellular segmentation. *Nat. Methods* **18**, 100–106 (2021).

74. M. Pachitariu, C. Stringer, Cellpose 2.0: how to train your own model. *Nat. Methods* **19**, 1634–1641 (2022).

75. D. H. Woo, K.-S. Han, J. W. Shim, B.-E. Yoon, E. Kim, J. Y. Bae, S.-J. Oh, E. M. Hwang, A. D. Marmorstein, Y. C. Bae, J.-Y. Park, C. J. Lee, TREK-1 and Best1 channels mediate fast and slow glutamate release in astrocytes upon GPCR activation. *Cell* **151**, 25–40 (2012).

Chapter 5

The Therapeutic Potential of KOR antagonists – what are the advantages and disadvantages of receptor inactivators compared to simple competitive antagonists? Concluding comments and implications for the treatment of drug addiction and mood disorders in humans

Preclinical studies have established that the Dynorphin opioids have an important role in the stress response and KOR antagonists may potentially be useful in promoting stress resilience in vulnerable individuals (Chavkin, 2011; Lalanne et al., 2014). There is much still to learn about how this dyn/KOR system functions in humans because we have lacked selective tools, but hyperresponsivity to stressors exacerbates a wide range of human pathologies including anxiety disorders, clinical depression, cognitive disturbances during psychosis, and the risk of drug addiction (Bondi et al., 2008; Jawahar et al., 2015; Mizrahi, 2010). Dynorphin also contributes to the regulation of neuronal excitability and KOR antagonism could affect seizure risk, learning deficits, migraine, and chronic pain disorders (Baird et al., 2021; Dai et al., 2019; Gruol et al., 1983; Ito et al., 2023; Lee et al., 2014). Having safe and effective KOR antagonists for use in humans would enable studies to address these important questions about dynorphins' roles in human physiology and pathophysiology. However, studies described in this thesis highlight the complexity of KOR antagonism. Previously, we thought that selective high-affinity competitive KOR antagonists would be the drugs of choice. We now realize that KOR-inactivating medications are a possible alternative with potential advantages. Which therapeutic strategy will be preferable will be empirically determined, but we can speculate based on what we know now.

Dynorphin is thought to be released by chronic stress to activate the kappa opioid receptors (Knoll & Carlezon, 2010). In many neuronal systems, KOR is highly expressed and there are ‘spare’ receptors (Cox & Chavkin, 1983). This is physiologically important because dynorphin is released from distal sites and diffuses many 10s of microns from sites of release to sites of action. High levels of KOR expression enhance the sensitivity of the post-synaptic neuron to the neuropeptide diluted during diffusion. The presence of spare receptors makes the practical utility of competitive antagonists somewhat challenging. The antagonist medication would need to supersaturate the receptor to prevent dynorphin binding. Frequent dosing may be required and patient compliance would be a concern. A risk of off-target effects of high drug doses is also problematic. Receptor inactivation by low doses of KOR inactivating medications reduces the probability of off-target effects. The slow reversal of inactivation reduces the risk of treatment failure caused by missed dosing. The tissue selectivity of KOR inactivation demonstrated in this thesis is a unique advantage of the receptor inactivation approach. However, the slow reversal of inactivation may be concerning if adverse effects do develop.

The goal of the work presented here is to use what we have learned to continue to a) develop tools useful for determining molecular mechanisms of opioid signaling, b) use behavioral approaches in combination with those tools to deepen our understanding of biological outcomes of opioid signaling and, c) leverage our understanding of signaling and behavior within the dyn/KOR system to create novel, effective therapeutics for

treatment of the anhedonic component of drug addiction and mood disorders. This conclusion chapter will highlight how we came to our current understanding of how dyn/KOR is proposed to regulate drug addiction-, anxiety-, and depression-like behaviors, as well as implications for the treatment of these disorders in humans.

Koob and colleagues have developed an exceptionally relevant explanation of how the cycle of addiction occurs concerning changes in homeostasis or “baseline” emotional state. The cycle starts with binge/intoxication, in which the person uses a substance and enjoys the effects, leading to repeated use. This repeated use shifts the cycle into the withdrawal/negative affect stage in which the person starts to experience emotional dysregulation and as well as physical discomfort without the substance. This ultimately drives increased use. In the preoccupation/anticipation stage, the person’s focus becomes dominated by thoughts of obtaining and using the substance. This often occurs at the expense of relationships and responsibilities. This cycle is believed to be mediated by change and dysfunction of the reward and stress systems of the brain, especially PFC, NAc, VTA, and amygdala. Koob notes that this combination of behavior and brain chemistry cause addiction to be a chronic, relapsing disorder that often requires intervention to overcome (Koob et al., 2014).

As mentioned in the first chapter, the therapeutic potential for KOR was originally centered around activation causing analgesia without the euphoric effects of MOR agonists like morphine, suggesting they would have little to no abuse potential. However, studies were starting to determine the involvement of KOR in the stress

response as well as its role in drug reward and addiction behaviors (Carlezon et al., 1998; Kreek & Koob, 1998). While it had been suggested that KOR activation opposed drug-rewarding effects (Schenk et al., 1999), it was shown that the rFSS paradigm could enhance preference for cocaine. This enhancement, or potentiation, could be effectively blocked by pretreatment with norBNI or genetic deletion of the prodynorphin gene, suggesting that the effect was KOR-mediated (McLaughlin et al., 2003). This represented a turning point for norBNI, and KOR antagonism in general, turning it from a tool for the study of the dyn/KOR system, to a mechanism with therapeutic potential. Indeed, innumerable studies went on to show a host of different stress-related behaviors that could be blocked by KOR/dyn deletion or inhibition (Lalanne et al., 2014).

Key studies from this time period showed stress activation and subsequent KOR-mediated effects in drug-seeking and drug-taking behaviors (Beardsley et al., 2005; McLaughlin, Marton-Popovici, et al., 2003), depression- and anxiety-like behaviors (Bruchas et al., 2009, 2011), and social-interaction behaviors (McLaughlin et al., 2006). As previously stated, it has been demonstrated that downstream activation p38 MAPK is responsible for these KOR-mediated negative behaviors in both the dopamine and 5-HT systems. For this reason, we focused on the VTA in Chapter 1 for its previous implication in KOR-mediated aversion and reward control along with its high overlap of KOR and DA expression. Primarily implicated brain regions for KOR-mediated DA effects include the VTA, PFC, and NAc (Abraham et al., 2018; Chefer et al., 2013; Ehrich et al., 2014, 2015; Margolis et al., 2003; Tejeda et al., 2013; Yarur et al., 2023). Chapter 3 highlights the involvement of KOR signaling in decreased 5-HT tone in the

mNAc (Fontaine et al., 2021) and adds to the body of evidence suggesting excessive or repeated (but not acute) KOR activation causes a hyposerotonergic state via activation of p38 MAPK and increased translocation of SERT, leading to stress-vulnerability. Implicated brain areas for this KOR-mediated 5-HT effect include the NAc, DRN, and SNr (Land et al., 2009; Lemos et al., 2012; Schindler et al., 2012; Sundaramurthy et al., 2017; West et al., 2023).

Despite this ever-growing set of preclinical studies into KOR antagonism, it has been historically difficult to demonstrate safety and efficacy in clinical trials. For example, early oral dose testing of JDTic was quickly ended due to cardiac effects (Buda et al., 2015). It has even been suggested that there is simply too much of a mismatch between the human condition and our preclinical models, especially in regard to addiction (Banks, 2020). However, there has been recent success of KOR antagonists in clinical trials, in spite of the previously failed attempts. Navacaprant (BTRX-335140, NMRA-140) and Aticaprant (JNJ-67953964, CERC-501, and LY-2456302) are short-acting KOR antagonists in development for treatment of mood disorders (specifically, Major Depressive Disorder (MDD)). Both compounds have made their way to Phase III clinical trials after a host of preclinical and clinical work. While these treatments offer the first true clinical tests of KOR antagonism, short acting drugs present unique challenges including requiring high doses which present a higher likelihood of off-target side effects.

The treatments I have proposed (Chapter 2) offer a different mechanism entirely more akin to those originally tested using JDTic. The microdosing regimen introduces an added layer of safety to combat the toxicity issues seen with JDTic, essentially keeping the ability to “inactivate” as opposed to antagonizing KOR along with the use of drugs that have already been shown to be safe in humans. What we end up with is a slow, titratable accumulation of effect in which KOR can be inactivated in as little as 7 days, as long as 30 days, and possibly even longer than that. Continuing treatment of nalfurafine or nalmefene would maintain this effect, ideally without unwanted side effects. New tools like oROS-Gr (Chapter 4) have expanded our ability to assess downstream effectors, in this case ROS, with more spatial and temporal resolution than ever before both in vivo and in single-cell imaging. The findings reviewed here also present the opprotunity for new directed development of treatments that are similarly G-baised or low efficacy at KOR.

There has been some disagreement in the literature about aspects of nalfurafine action. Both behavioral consequences and signaling pathway activation range from being similar to U50,488 in aversion and activation of the GRK/arrestin pathway to being showing no aversion and being G-protein pathway biased. We believe that these discrepancies are due in part to improper dosing and misinterpretation of in vitro data. In previous work, Schattauer, et al. showed that nalfurafine is indeed G-biased based by comparing ERK phosphorylation at 5 min post-treatment (early phase pERK indicates activation of the G-protein dependent pathway, see Chapter 1) and p38 MAPK phosphorylation 30 min post-treatment (late phase, pp38 indicates activation of the

GRK3/arrestin pathway). This was done in cells expressing either the rat KOR (rKOR) or the human KOR (hKOR). rKOR showed a 10-20 fold bias for pERK in rKOR and a 100-fold bias for pERK in hKOR (Schattauer et al., 2017). It is important to note that nalfurafine shows a left shifted dose response curve for pERK compared to pp38. However, its efficacy in activating p38 is not reduced compared to U50,488, but simply requires a higher concentration than activation of ERK. The consequence of this is, given a high enough concentration of nalfurafine, the GRK3/arrestin pathway will be activated. In Dunn, et al., 2019, it is claimed that nalfurafine is biased for the GRK3/arrestin pathway. The evidence they use for this claim starts with a comparison of a radioligand binding for measurement of the G-protein pathway activation and a cell based assay for beta-arrestin2 recruitment, which are not biologically equivalent. They also correlate those measures with the rotor rod performance of mice after administration of nalfurafine and show that nalfurafine causes as much reduction in performance as U50,488 (Dunn et al., 2019). The disconnect here is that their dosing of 3 mg/kg is far too high. Based on previous studies, the anti-itch and analgesic doses of nalfurafine are in the range of 5-50 µg/kg. Indeed, it has been shown that in mice, anti-itch effects of nalfurafine are significant starting at 5 µg/kg and analgesic effects starting at 2.5 µg/kg. 20 µg/kg nalfurafine has a small but significant effect on rotor rod performance, but not conditioned place aversion or locomotor inhibition (Liu et al., 2019). In humans, doses of about 80 ng/kg/day are effective for uremic pruritis (Inui, 2015). In our hands (shown in Chapter 2), we can see KOR inactivation with 7 daily treatments of 100 ng/kg (700 ng/kg, cumulatively). From our dose-response curves of KOR-mediated prolactin increase, it is clear that in vivo, nalfurafine is exceptionally

more potent than U50,488 (EC50 = 2.91 µg/kg vs EC50 = 5.18 mg/kg). These data together suggest that nalfurafine is a G-biased KOR ligands at clinically relevant doses. Combined with its demonstrated safety in humans, nalfurafine is a plausible candidate for repeated dosing in clinical trials to inactivate KOR.

Nalmefene on the other hand, does not effectively cause activation of the GRK3/arrestin pathway, regardless of dose. This is due to its partial agonism at KOR (Mann et al., 2016). In the previously shown prolactin dose-response curves, the Emax of U50,488 is about 2.5-fold higher than nalmefene. Like with G-biased agonists, this lack of efficacy in downstream activation of p38 MAPK results in KOR activation without the dysphoric properties. As mentioned above, nalmefene has also been shown to be safe in humans. It has been used in Europe for the treatment of alcohol use disorder (Chick et al., 2021) and was previously used in the US for its MOR antagonist properties in the treatment of emergent opioid over dose (https://www.federalregister.gov/documents/2017/11/03/2017-23952/determination-that-revex-nalmefene-hydrochloride-injection-01-milligram-basemilliliter-and-10). We were able to show that as low as 100 µg/kg nalmefene given daily for 7 days was sufficient to inactivate KOR (Chapter 2). The limitation of nalmefene in the treatment of substance use disorder is that higher doses could cause precipitated withdrawal in opioid-dependent persons. It would need to be titrated in doses low enough to not acutely antagonize MOR. Similar to G-based KOR agonists, partial KOR agonists hold promise for treatment of the anhedonic component of addiction relapse and mood disorders.

The first step towards developing KOR-inactivating drugs for use by humans would be a Phase 1 human trial in healthy volunteers. My study predicts that both men and women on progesterone birth control would respond to daily dosing with either nalfurafine or nalmefene. The dose required would depend on the duration of the trial: 1 week of nalfurafine would likely require 100-500 ng/day; a 30-day trial would likely require 10-fold lower doses, 10-50 ng/day. At those low doses, it seems unlikely that the subjects would experience any noticeable adverse effects different from placebo. Inactivation of KOR could be determined by administering a challenge dose of KOR agonist. There are several to choose from, but I suggest 30-60 mg of pentazocine with 10 mg of naltrexone to block the mu-opioid agonist effects of pentazocine. KOR activation could be assessed by measuring stimulated prolactin and standard mood assessment scales to measure dysphoria. The powerful combination of an objective endocrine response and a clinically meaningful subjective mood response would provide a strong foundation for the subsequent Phase 2 clinical trial.

There are several clinical indications that could be assessed in the Phase 2 study. The most straightforward would be to study heavy smokers (>3 packs/day) in persons wishing to quit but unable to overcome the strong feelings of anhedonia during abstinence. Nicotine is a short-acting drug, and nicotine-dependent persons could be assessed after 12 hr of abstinence. Standard questionnaires have been developed that quantify nicotine abstinence and the anhedonic component during withdrawal is likely to be significantly reduced by KOR inactivation. An effect on craving during abstinence would be an interesting symptom to assess since the neurochemical basis of craving is poorly

understood. A role for dynorphin is expected, but not yet established. Craving during alcohol abstinence, cocaine, methamphetamine, and opioid abstinence could each be individually studied.

The competitive KOR antagonists Aticaprant and Navacaprant have been found in Phase 2 trials to significantly reduce the anhedonia experienced by persons with treatment-resistant clinical depression. By following the same protocol and study design, it will be very interesting to determine whether microdosing KOR inactivating medications is equally or more effective than the competitive antagonists.

The role of dynorphin during psychosis is very intriguing. Dynorphin is highly expressed in the cortical regions important for cognition. Preclinical studies have demonstrated that KOR inactivation prevents stress-induced cognitive disruption (Abraham et al., 2021). Human studies have documented that dynorphin peptides are elevated in the Cerebrospinal fluid of persons with schizophrenia, and high doses of non-selective opioid antagonists were found to block auditory hallucinations in a small double blind crossover study (Terenius & Wahlström, 1978).

A key feature of KOR antagonist therapy is that the drugs will only act when dynorphin tone is evident. Drugs that block mu opioid receptors cannot be distinguished from placebo unless the human subject is in pain. We presume that means that basal tone of endogenous opioids is low. We don’t yet know the circumstances under which dynorphin tone is elevated, but we can speculate that binge cocaine, ethanol, methamphetamine or

opioids is likely to produce sustained elevations of dynorphin. This prediction can be experimentally assessed.

In conclusion, my thesis has provided evidence that KOR inactivating medications are nearly in-hand. We look forward to the next era of study when we can better understand how the dynorphin/KOR system functions in humans. Preclinical studies using animal models of human disorders are powerful, but inherently unsatisfying because of the well-documented limitations of animal models of human disease. Advancing to human studies generates tremendous excitement and we look forward to this next step in KOR therapeutics.

REFERENCES

1. Abraham, A. D., Casello, S. M., Schattauer, S. S., Wong, B. A., Mizuno, G. O., Mahe, K., Tian, L., Land, B. B., & Chavkin, C. (2021). Release of endogenous dynorphin opioids in the prefrontal cortex disrupts cognition. *Neuropsychopharmacology*, *46*(13), 2330–2339. https://doi.org/10.1038/s41386-021-01168-2

2. Abraham, A. D., Fontaine, H. M., Song, A. J., Andrews, M. M., Baird, M. A., Kieffer, B. L., Land, B. B., & Chavkin, C. (2018). κ-Opioid Receptor Activation in Dopamine Neurons Disrupts Behavioral Inhibition. Neuropsychopharmacology, 43(2), 362–372. https://doi.org/10.1038/npp.2017.133

3. Abraham, A. D., Schattauer, S. S., Reichard, K. L., Cohen, J. H., Fontaine, H. M., Song, A. J., Johnson, S. D., Land, B. B., & Chavkin, C. (2018). Estrogen Regulation of GRK2 Inactivates Kappa Opioid Receptor Signaling Mediating Analgesia, But Not Aversion. Journal of Neuroscience, 38(37), 8031–8043. https://doi.org/10.1523/JNEUROSCI.0653-18.2018

4. Baird, M. A., Hsu, T. Y., Wang, R., Juarez, B., & Zweifel, L. S. (2021). κ Opioid Receptor-Dynorphin Signaling in the Central Amygdala Regulates Conditioned Threat Discrimination and Anxiety. *eNeuro*, *8*(1). https://doi.org/10.1523/ENEURO.0370-20.2020

5. Banks, M. L. (2020). The Rise and Fall of Kappa-Opioid Receptors in Drug Abuse Research. In M. A. Nader & Y. L. Hurd (Eds.), Substance Use Disorders: From Etiology to Treatment (pp. 147–165). Springer International Publishing. https://doi.org/10.1007/164_2019_268

6. Beardsley, P. M., Howard, J. L., Shelton, K. L., & Carroll, F. I. (2005). Differential effects of the novel kappa opioid receptor antagonist, JDTic, on reinstatement of cocaine-seeking induced by footshock stressors vs cocaine primes and its antidepressant-like effects in rats. Psychopharmacology, 183(1), 118–126. https://doi.org/10.1007/s00213-005-0167-4

7. Birch, P. J., Hayes, A. G., Sheehan, M. J., & Tyers, M. B. (1987). Norbinaltorphimine: Antagonist profile at kappa opioid receptors. European Journal of Pharmacology, 144(3), 405–408. https://doi.org/10.1016/0014-2999(87)90397-9

8. Bondi, C. O., Rodriguez, G., Gould, G. G., Frazer, A., & Morilak, D. A. (2008). Chronic Unpredictable Stress Induces a Cognitive Deficit and Anxiety-Like Behavior in Rats that is Prevented by Chronic Antidepressant Drug Treatment. *Neuropsychopharmacology*, *33*(2), 320–331. https://doi.org/10.1038/sj.npp.1301410

9. Browne, C. A., Smith, T., & Lucki, I. (2020). Behavioral effects of the kappa opioid receptor partial agonist nalmefene in tests relevant to depression. *European Journal of Pharmacology*, *872*, 172948. https://doi.org/10.1016/j.ejphar.2020.172948

10. Bruchas, M. R., & Chavkin, C. (2010). Kinase cascades and ligand-directed signaling at the kappa opioid receptor. Psychopharmacology, 210(2), 137–147. https://doi.org/10.1007/s00213-010-1806-y

11. Bruchas, M. R., Land, B. B., Aita, M., Xu, M., Barot, S. K., Li, S., & Chavkin, C. (2007). Stress-Induced p38 Mitogen-Activated Protein Kinase Activation Mediates κ-Opioid-Dependent Dysphoria. Journal of Neuroscience, 27(43), 11614–11623. https://doi.org/10.1523/JNEUROSCI.3769-07.2007

12. Bruchas, M. R., Land, B. B., Lemos, J. C., & Chavkin, C. (2009). CRF1-R Activation of the Dynorphin/Kappa Opioid System in the Mouse Basolateral Amygdala Mediates Anxiety-Like Behavior. *PLOS ONE*, *4*(12), e8528. https://doi.org/10.1371/journal.pone.0008528

13. Bruchas, M. R., Macey, T. A., Lowe, J. D., & Chavkin, C. (2006). Kappa Opioid Receptor Activation of p38 MAPK Is GRK3- and Arrestin-dependent in Neurons and Astrocytes *. Journal of Biological Chemistry, 281(26), 18081–18089. https://doi.org/10.1074/jbc.M513640200

14. Bruchas, M. R., Schindler, A. G., Shankar, H., Messinger, D. I., Miyatake, M., Land, B. B., Lemos, J. C., Hagan, C. E., Neumaier, J. F., Quintana, A., Palmiter, R. D., & Chavkin, C. (2011). Selective p38α MAPK Deletion in Serotonergic Neurons Produces Stress Resilience in Models of Depression and Addiction. *Neuron*, *71*(3), 498–511. https://doi.org/10.1016/j.neuron.2011.06.011

15. Bruchas, M. R., Yang, T., Schreiber, S., DeFino, M., Kwan, S. C., Li, S., & Chavkin, C. (2007). Long-Acting κ Opioid Antagonists Disrupt Receptor Signaling And Produce Noncompetitive Effects By Activating C-Jun N-Terminal Kinase*. Journal of Biological Chemistry, 282(41), 29803–29811. https://doi.org/10.1074/jbc.M705540200

16. Buda, J. J., Carroll, F. I., Kosten, T. R., Swearingen, D., & Walters, B. B. (2015). A Double-Blind, Placebo-Controlled Trial to Evaluate the Safety, Tolerability, and Pharmacokinetics of Single, Escalating Oral Doses of JDTic. Neuropsychopharmacology: Official Publication of the American College of Neuropsychopharmacology, 40(9), 2059–2065. https://doi.org/10.1038/npp.2015.27

17. Calabrese, F., Molteni, R., Racagni, G., & Riva, M. A. (2009). Neuronal plasticity: A link between stress and mood disorders. Psychoneuroendocrinology, 34, S208–S216. https://doi.org/10.1016/j.psyneuen.2009.05.014

18. Carlezon, W. A., Thome, J., Olson, V. G., Lane-Ladd, S. B., Brodkin, E. S., Hiroi, N., Duman, R. S., Neve, R. L., & Nestler, E. J. (1998). Regulation of cocaine reward by CREB. Science (New York, N.Y.), 282(5397), 2272–2275. https://doi.org/10.1126/science.282.5397.2272

19. Carr, G. V., Bangasser, D. A., Bethea, T., Young, M., Valentino, R. J., & Lucki, I. (2010). Antidepressant-Like Effects of κ-Opioid Receptor Antagonists in Wistar Kyoto Rats. Neuropsychopharmacology, 35(3), 752–763. https://doi.org/10.1038/npp.2009.183

20. Chartoff, E., Sawyer, A., Rachlin, A., Potter, D., Pliakas, A., & Carlezon, W. A. (2012). Blockade of kappa-opioid receptors attenuates the development of depressive-like behaviors induced by cocaine withdrawal in rats. Neuropharmacology, 62(1), 167–176. https://doi.org/10.1016/j.neuropharm.2011.06.014

21. Chatterjee, S., Feinstein, S. I., Dodia, C., Sorokina, E., Lien, Y.-C., Nguyen, S., Debolt, K., Speicher, D., & Fisher, A. B. (2011). Peroxiredoxin 6 Phosphorylation and Subsequent Phospholipase A2 Activity Are Required for Agonist-mediated Activation of NADPH Oxidase in Mouse Pulmonary Microvascular Endothelium and Alveolar Macrophages. The Journal of Biological Chemistry, 286(13), 11696–11706. https://doi.org/10.1074/jbc.M110.206623

22. Chavkin, C. (2011). The Therapeutic Potential of κ -Opioids for Treatment of Pain and Addiction. Neuropsychopharmacology, 36(1), Article 1. https://doi.org/10.1038/npp.2010.137

23. Chavkin, C. (2013). Dynorphin–Still an Extraordinarily Potent Opioid Peptide. Molecular Pharmacology, 83(4), 729–736. https://doi.org/10.1124/mol.112.083337

24. Chavkin, C. (2018). Kappa-opioid antagonists as stress resilience medications for the treatment of alcohol use disorders. Neuropsychopharmacology, 43(9), 1803–1804. https://doi.org/10.1038/s41386-018-0046-4

25. Chavkin, C., Cohen, J. H., & Land, B. B. (2019). Repeated Administration of Norbinaltorphimine Produces Cumulative Kappa Opioid Receptor Inactivation. Frontiers in Pharmacology, 10, 88. https://doi.org/10.3389/fphar.2019.00088

26. Chavkin, C., James, I. F., & Goldstein, A. (1982). Dynorphin Is a Specific Endogenous Ligand of the κ Opioid Receptor. Science, 215(4531), 413–415. https://doi.org/10.1126/science.6120570

27. Chefer, V. I., Bäckman, C. M., Gigante, E. D., & Shippenberg, T. S. (2013). Kappa Opioid Receptors on Dopaminergic Neurons Are Necessary for Kappa-Mediated Place Aversion. Neuropsychopharmacology, 38(13), 2623–2631. https://doi.org/10.1038/npp.2013.171

28. Chick, J., Andersohn, F., Guillo, S., Borchert, K., Toussi, M., Braun, S., Haas, J. S., Kuppan, K., Lemming, O. M., Reines, E. H., & Tubach, F. (2021). Safety and Persistence of Nalmefene Treatment for Alcohol Dependence. Results from Two

Post-authorisation Safety Studies. Alcohol and Alcoholism (Oxford, Oxfordshire), 56(5), 556–564. https://doi.org/10.1093/alcalc/agab045

29. Cox, B. M., & Chavkin, C. (1983). Comparison of dynorphin-selective Kappa receptors in mouse vas deferens and guinea pig ileum. Spare receptor fraction as a determinant of potency. *Molecular Pharmacology*, *23*(1), 36–43.

30. Craft, R. M. (2008). Sex differences in analgesic, reinforcing, discriminative, and motoric effects of opioids. Experimental and Clinical Psychopharmacology, 16(5), 376–385. https://doi.org/10.1037/a0012931

31. Dai, H., Wang, P., Mao, H., Mao, X., Tan, S., & Chen, Z. (2019). Dynorphin activation of kappa opioid receptor protects against epilepsy and seizure-induced brain injury via PI3K/Akt/Nrf2/HO-1 pathway. *Cell Cycle*, *18*(2), 226–237. https://doi.org/10.1080/15384101.2018.1562286

32. Dalefield, M. L., Scouller, B., Bibi, R., & Kivell, B. M. (2022). The Kappa Opioid Receptor: A Promising Therapeutic Target for Multiple Pathologies. *Frontiers in Pharmacology*, *13*. https://doi.org/10.3389/fphar.2022.837671

33. Determination That REVEX (Nalmefene Hydrochloride Injection), 0.1 Milligram Base/Milliliter and 1.0 Milligram Base/Milliliter, Was Not Withdrawn From Sale for Reasons of Safety or Effectiveness. (2017, November 3). Federal Register. https://www.federalregister.gov/documents/2017/11/03/2017-23952/determination-that-revex-nalmefene-hydrochloride-injection-01-milligram-basemilliliter-and-10

34. Dunn, A. D., Reed, B., Erazo, J., Ben-Ezra, A., & Kreek, M. J. (2019). Signaling Properties of Structurally Diverse Kappa Opioid Receptor Ligands: Toward in Vitro Models of in Vivo Responses. ACS Chemical Neuroscience, 10(8), 3590–3600. https://doi.org/10.1021/acschemneuro.9b00195

35. Ehrich, J. M., Messinger, D. I., Knakal, C. R., Kuhar, J. R., Schattauer, S. S., Bruchas, M. R., Zweifel, L. S., Kieffer, B. L., Phillips, P. E. M., & Chavkin, C. (2015). Kappa Opioid Receptor-Induced Aversion Requires p38 MAPK Activation in VTA Dopamine Neurons. Journal of Neuroscience, 35(37), 12917–12931. https://doi.org/10.1523/JNEUROSCI.2444-15.2015

36. Ehrich, J. M., Phillips, P. E. M., & Chavkin, C. (2014). Kappa Opioid Receptor Activation Potentiates the Cocaine-Induced Increase in Evoked Dopamine Release Recorded In Vivo in the Mouse Nucleus Accumbens. Neuropsychopharmacology, 39(13), Article 13. https://doi.org/10.1038/npp.2014.157

37. Endoh, T., Matsuura, H., Tanaka, C., & Nagase, H. (1992). Nor-binaltorphimine: A potent and selective kappa-opioid receptor antagonist with long-lasting activity in vivo. *Archives Internationales De Pharmacodynamie Et De Therapie*, *316*, 30–42.

38. Er, B., & Mj, K. (2001). Kappa-Opioid receptor agonist-induced prolactin release in primates is blocked by dopamine D(2)-like receptor agonists. European Journal of Pharmacology, 423(2–3). https://doi.org/10.1016/s0014-2999(01)01121-9

39. Ermakova, Y. G., Bilan, D. S., Matlashov, M. E., Mishina, N. M., Markvicheva, K. N., Subach, O. M., Subach, F. V., Bogeski, I., Hoth, M., Enikolopov, G., & Belousov, V. V. (2014). Red fluorescent genetically encoded indicator for intracellular hydrogen peroxide. Nature Communications, 5(1), 5222. https://doi.org/10.1038/ncomms6222

40. Fontaine, H. M., Silva, P. R., Neiswanger, C., Tran, R., Abraham, A. D., Land, B. B., Neumaier, J. F., & Chavkin, C. (2021). Stress decreases serotonin tone in the nucleus accumbens in male mice to promote aversion and potentiate cocaine preference via decreased stimulation of 5-HT1B receptors. Neuropsychopharmacology, 1–11. https://doi.org/10.1038/s41386-021-01178-0

41. Graziane, N. M., Polter, A. M., Briand, L. A., Pierce, R. C., & Kauer, J. A. (2013). Kappa opioid receptors regulate stress-induced cocaine seeking and synaptic plasticity. *Neuron*, *77*(5), 942–954. https://doi.org/10.1016/j.neuron.2012.12.034

42. Gruol, D. L., Chavkin, C., Valentino, R. J., & Siggins, G. R. (1983). Dynorphin-A alters the excitability of pyramidal neurons of the rat hippocampus in vitro. *Life Sciences*, *33*, 533–536. https://doi.org/10.1016/0024-3205(83)90558-1

43. Hampsey, E., Jelen, L., & Young, A. H. (2024). Aticaprant: (A κ-opioid receptor antagonist) for major depressive disorder. *Expert Opinion on Emerging Drugs*, *0*(0), 1–12. https://doi.org/10.1080/14728214.2024.2345645

44. Han, J. S., & Xie, C. W. (1984). Dynorphin: Potent analgesic effect in spinal cord of the rat. Scientia Sinica. Series B, Chemical, Biological, Agricultural, Medical & Earth Sciences, 27(2), 169–177.

45. Heikkilä, L., Rimón, R., & Ternius, L. (1990). Dynorphin A and substance P in the cerebrospinal fluid of schizophrenic patients. *Psychiatry Research*, *34*(3), 229–236. https://doi.org/10.1016/0165-1781(90)90001-L

46. Horan, P., Taylor, J., Yamamura, H. I., & Porreca, F. (1992). Extremely long-lasting antagonistic actions of nor-binaltorphimine (nor-BNI) in the mouse tail-flick test. The Journal of Pharmacology and Experimental Therapeutics, 260(3), 1237–1243.

47. Huskinson, S. L., Platt, D. M., Zamarripa, C. A., Dunaway, K., Brasfield, M., Prisinzano, T. E., Blough, B. E., & Freeman, K. B. (2022). The G-protein biased kappa opioid agonists, triazole 1.1 and nalfurafine, produce non-uniform behavioral effects in male rhesus monkeys. *Pharmacology, Biochemistry, and Behavior*, 173394. https://doi.org/10.1016/j.pbb.2022.173394

48. Inan, S., Dun, N. J., & Cowan, A. (2011). Investigation of Gastrin-Releasing Peptide as a Mediator for 5′-Guanidinonaltrindole-Induced Compulsive Scratching in Mice. Peptides, 32(2), 286–292. https://doi.org/10.1016/j.peptides.2010.11.022

49. Inui, S. (2015). Nalfurafine hydrochloride to treat pruritus: A review. Clinical, Cosmetic and Investigational Dermatology, 8, 249–255. https://doi.org/10.2147/CCID.S55942

50. Ito, H., Navratilova, E., Vagnerova, B., Watanabe, M., Kopruszinski, C., Moreira de Souza, L. H., Yue, X., Ikegami, D., Moutal, A., Patwardhan, A., Khanna, R., Yamazaki, M., Guerrero, M., Rosen, H., Roberts, E., Neugebauer, V., Dodick, D. W., & Porreca, F. (2023). Chronic pain recruits hypothalamic dynorphin/kappa opioid receptor signalling to promote wakefulness and vigilance. *Brain*, *146*(3), 1186–1199. https://doi.org/10.1093/brain/awac153

51. Jackson, K. J., Carroll, F. I., Negus, S. S., & Damaj, M. I. (2010). Effect of the selective kappa-opioid receptor antagonist JDTic on nicotine antinociception, reward, and withdrawal in the mouse. Psychopharmacology, 210(2), 285–294. https://doi.org/10.1007/s00213-010-1803-1

52. Jackson, K. J., Jackson, A., Carroll, F. I., & Damaj, M. I. (2015). Effects of orally-bioavailable short-acting kappa opioid receptor-selective antagonist LY2456302 on nicotine withdrawal in mice. Neuropharmacology, 97, 270–274. https://doi.org/10.1016/j.neuropharm.2015.05.023

53. Jawahar, M. C., Murgatroyd, C., Harrison, E. L., & Baune, B. T. (2015). Epigenetic alterations following early postnatal stress: A review on novel aetiological mechanisms of common psychiatric disorders. *Clinical Epigenetics*, *7*(1), 122. https://doi.org/10.1186/s13148-015-0156-3

54. Jones, D. N., & Holtzman, S. G. (1992). Long term kappa-opioid receptor blockade following nor-binaltorphimine. European Journal of Pharmacology, 215(2–3), 345–348. https://doi.org/10.1016/0014-2999(92)90055-9

55. Kam, A. Y. F., Chan, A. S. L., & Wong, Y. H. (2004). κ-Opioid Receptor Signals through Src and Focal Adhesion Kinase to Stimulate c-Jun N-Terminal Kinases in Transfected COS-7 Cells and Human Monocytic THP-1 Cells. Journal of Pharmacology and Experimental Therapeutics, 310(1), 301–310. https://doi.org/10.1124/jpet.104.065078

56. Kelly, E., Conibear, A., & Henderson, G. (2023). Biased Agonism: Lessons from Studies of Opioid Receptor Agonists. Annual Review of Pharmacology and Toxicology, 63(Volume 63, 2023), 491–515. https://doi.org/10.1146/annurev-pharmtox-052120-091058

57. Knoll, A. T., & Carlezon, W. A. (2010). Dynorphin, stress, and depression. Brain Research, 1314C, 56. https://doi.org/10.1016/j.brainres.2009.09.074

58. Koob, G. F., Buck, C. L., Cohen, A., Edwards, S., Park, P. E., Schlosburg, J. E., Schmeichel, B., Vendruscolo, L. F., Wade, C. L., Whitfield, T. W., & George, O. (2014). Addiction as a Stress Surfeit Disorder. Neuropharmacology, 76(0 0), 10.1016/j.neuropharm.2013.05.024. https://doi.org/10.1016/j.neuropharm.2013.05.024

59. Kopruszinski, C. M., Watanabe, M., Martinez, A. L., de Souza, L. H. M., Dodick, D. W., Moutal, A., Neugebauer, V., Porreca, F., & Navratilova, E. (2022). Kappa opioid receptor agonists produce sexually dimorphic and prolactin-dependent hyperalgesic priming. PAIN, 10.1097/j.pain.0000000000002835. https://doi.org/10.1097/j.pain.0000000000002835

60. Kormos, C. M., Ondachi, P. W., Runyon, S. P., Thomas, J. B., Mascarella, S. W., Decker, A. M., Navarro, H. A., Fennell, T. R., Snyder, R. W., & Carroll, F. I. (2018). Potent and Selective Tetrahydroisoquinoline Kappa Opioid Receptor Antagonists of Lead Compound (3R)-N-[1R)-1-(Cyclohexylmethyl)-2-methylpropyl]-7-hydroxy-1,2,3,4-tetrahydroisoquinoline-3-carboxamide (CDTic). *Journal of Medicinal Chemistry*, *61*(17), 7546–7559. https://doi.org/10.1021/acs.jmedchem.8b00674

61. Kreek, M. J., & Koob, G. F. (1998). Drug dependence: Stress and dysregulation of brain reward pathways. Drug and Alcohol Dependence, 51(1), 23–47. https://doi.org/10.1016/S0376-8716(98)00064-7

62. Lalanne, L., Ayranci, G., Kieffer, B. L., & Lutz, P.-E. (2014). The Kappa Opioid Receptor: From Addiction to Depression, and Back. Frontiers in Psychiatry, 5. https://doi.org/10.3389/fpsyt.2014.00170

63. Land, B. B., Bruchas, M. R., Lemos, J. C., Xu, M., Melief, E. J., & Chavkin, C. (2008). The dysphoric component of stress is encoded by activation of the dynorphin kappa-opioid system. The Journal of Neuroscience: The Official Journal of the Society for Neuroscience, 28(2), 407–414. https://doi.org/10.1523/JNEUROSCI.4458-07.2008

64. Land, B. B., Bruchas, M. R., Schattauer, S., Giardino, W. J., Aita, M., Messinger, D., Hnasko, T. S., Palmiter, R. D., & Chavkin, C. (2009). Activation of the kappa opioid receptor in the dorsal raphe nucleus mediates the aversive effects of stress and reinstates drug seeking. Proceedings of the National Academy of Sciences of the United States of America, 106(45), 19168–19173. https://doi.org/10.1073/pnas.0910705106

65. Lee, Y. S., Muthu, D., Hall, S. M., Ramos-Colon, C., Rankin, D., Hu, J., Sandweiss, A. J., De Felice, M., Xie, J. Y., Vanderah, T. W., Porreca, F., Lai, J., & Hruby, V. J. (2014). Discovery of Amphipathic Dynorphin A Analogues to Inhibit the

Neuroexcitatory Effects of Dynorphin A through Bradykinin Receptors in the Spinal Cord. *Journal of the American Chemical Society*, *136*(18), 6608–6616. https://doi.org/10.1021/ja501677q

66. Lemos, J. C., Roth, C. A., Messinger, D. I., Gill, H. K., Phillips, P. E. M., & Chavkin, C. (2012). Repeated Stress Dysregulates κ-Opioid Receptor Signaling in the Dorsal Raphe through a p38α MAPK-Dependent Mechanism. Journal of Neuroscience, 32(36), 12325–12336. https://doi.org/10.1523/JNEUROSCI.2053-12.2012

67. Lijffijt, M., Hu, K., & Swann, A. C. (2014). Stress Modulates Illness-Course of Substance Use Disorders: A Translational Review. Frontiers in Psychiatry, 5, 83. https://doi.org/10.3389/fpsyt.2014.00083

68. Liu, J. J., Chiu, Y.-T., DiMattio, K. M., Chen, C., Huang, P., Gentile, T. A., Muschamp, J. W., Cowan, A., Mann, M., & Liu-Chen, L.-Y. (2019). Phosphoproteomic approach for agonist-specific signaling in mouse brains: mTOR pathway is involved in κ opioid aversion. Neuropsychopharmacology, 44(5), 939–949. https://doi.org/10.1038/s41386-018-0155-0

69. Mann, K., Torup, L., Sørensen, P., Gual, A., Swift, R., Walker, B., & van den Brink, W. (2016). Nalmefene for the management of alcohol dependence: Review on its pharmacology, mechanism of action and meta-analysis on its clinical efficacy. European Neuropsychopharmacology, 26(12), 1941–1949. https://doi.org/10.1016/j.euroneuro.2016.10.008

70. Margolis, E. B., Hjelmstad, G. O., Bonci, A., & Fields, H. L. (2003). κ-Opioid Agonists Directly Inhibit Midbrain Dopaminergic Neurons. The Journal of Neuroscience, 23(31), 9981–9986. https://doi.org/10.1523/JNEUROSCI.23-31-09981.2003

71. Martin, W. R., Eades, C. G., Thompson, J. A., Huppler, R. E., & Gilbert, P. E. (1976). The effects of morphine- and nalorphine- like drugs in the nondependent and morphine-dependent chronic spinal dog. Journal of Pharmacology and Experimental Therapeutics, 197(3), 517–532.

72. McLaughlin, J. P., Li, S., Valdez, J., Chavkin, T. A., & Chavkin, C. (2006). Social defeat stress-induced behavioral responses are mediated by the endogenous kappa opioid system. *Neuropsychopharmacology: Official Publication of the American College of Neuropsychopharmacology*, *31*(6), 1241–1248. https://doi.org/10.1038/sj.npp.1300872

73. McLaughlin, J. P., Marton-Popovici, M., & Chavkin, C. (2003). κ Opioid Receptor Antagonism and Prodynorphin Gene Disruption Block Stress-Induced Behavioral Responses. The Journal of Neuroscience, 23(13), 5674–5683. https://doi.org/10.1523/JNEUROSCI.23-13-05674.2003

74. McLaughlin, J. P., Xu, M., Mackie, K., & Chavkin, C. (2003). Phosphorylation of a Carboxyl-terminal Serine within the κ-Opioid Receptor Produces Desensitization and Internalization. *Journal of Biological Chemistry*, *278*(36), 34631–34640. https://doi.org/10.1074/jbc.M304022200

75. Melief, E. J., Miyatake, M., Bruchas, M. R., & Chavkin, C. (2010). Ligand-directed c-Jun N-terminal kinase activation disrupts opioid receptor signaling. Proceedings of the National Academy of Sciences of the United States of America, 107(25), 11608–11613. https://doi.org/10.1073/pnas.1000751107

76. Melief, E. J., Miyatake, M., Carroll, F. I., Béguin, C., Carlezon, W. A., Cohen, B. M., Grimwood, S., Mitch, C. H., Rorick-Kehn, L., & Chavkin, C. (2011). Duration of action of a broad range of selective κ-opioid receptor antagonists is positively correlated with c-Jun N-terminal kinase-1 activation. Molecular Pharmacology, 80(5), 920–929. https://doi.org/10.1124/mol.111.074195

77. Meng, F., Xie, G. X., Thompson, R. C., Mansour, A., Goldstein, A., Watson, S. J., & Akil, H. (1993). Cloning and pharmacological characterization of a rat kappa opioid receptor. Proceedings of the National Academy of Sciences of the United States of America, 90(21), 9954–9958.

78. Messing, R. B., Portoghese, P. S., Takemori, A. E., & Sparber, S. B. (1982). Antagonism of morphine-induced behavioral suppression by opiate receptor alkylators. Pharmacology, Biochemistry, and Behavior, 16(4), 621–626. https://doi.org/10.1016/0091-3057(82)90426-9

79. Mizrahi, R. (2010). Advances in PET analyses of stress and dopamine. *Neuropsychopharmacology*, *35*(1), 348–349. https://doi.org/10.1038/npp.2009.132

80. Mogil, J. S., Wilson, S. G., Chesler, E. J., Rankin, A. L., Nemmani, K. V. S., Lariviere, W. R., Groce, M. K., Wallace, M. R., Kaplan, L., Staud, R., Ness, T. J., Glover, T. L., Stankova, M., Mayorov, A., Hruby, V. J., Grisel, J. E., & Fillingim, R. B. (2003). The melanocortin-1 receptor gene mediates female-specific mechanisms of analgesia in mice and humans. Proceedings of the National Academy of Sciences, 100(8), 4867–4872. https://doi.org/10.1073/pnas.0730053100

81. Nagase, H., Hayakawa, J., Kawamura, K., Kawai, K., Takezawa, Y., Matsuura, H., Tajima, C., & Endo, T. (1998). Discovery of a Structurally Novel Opioid K-Agonist Derived from 4, 5-Epoxymorphinan. Chemical & Pharmaceutical Bulletin, 46(2), 366–369. https://doi.org/10.1248/cpb.46.366

82. Portoghese, P. S., Lipkowski, A. W., & Takemori, A. E. (1987). Binaltorphimine and nor-binaltorphimine, potent and selective kappa-opioid receptor antagonists. Life Sciences, 40(13), 1287–1292. https://doi.org/10.1016/0024-3205(87)90585-6

83. Redila, V. A., & Chavkin, C. (2008). Stress-induced reinstatement of cocaine seeking is mediated by the kappa opioid system. *Psychopharmacology*, *200*(1), 59–70. https://doi.org/10.1007/s00213-008-1122-y

84. Reichard, K. L., Newton, K. A., Rivera, Z. M. G., Menezes, P. M. S. de, Schattauer, S. S., Land, B. B., & Chavkin, C. (2020). Regulation of Kappa Opioid Receptor Inactivation Depends on Sex and Cellular Site of Antagonist Action. Molecular Pharmacology, 98(5), 548–558. https://doi.org/10.1124/molpharm.120.000124

85. Sayre, L. M., Takemori, A. E., & Portoghese, P. S. (1983). Alkylation of opioid receptor subtypes by alpha-chlornaltrexamine produces concurrent irreversible agonistic and irreversible antagonistic activities. Journal of Medicinal Chemistry, 26(4), 503–506. https://doi.org/10.1021/jm00358a009

86. Schattauer, S. S., Bedini, A., Summers, F., Reilly-Treat, A., Andrews, M. M., Land, B. B., & Chavkin, C. (2019). ROS generation is stimulated by kappa opioid receptor activation through phosphorylated c-Jun-N-terminal kinase and inhibited by p38 MAPK activation. Journal of Biological Chemistry, jbc.RA119.009592. https://doi.org/10.1074/jbc.RA119.009592

87. Schattauer, S. S., Kuhar, J. R., Song, A., & Chavkin, C. (2017). Nalfurafine is a G-protein biased agonist having significantly greater bias at the human than rodent form of the kappa opioid receptor. Cellular Signalling, 32, 59–65. https://doi.org/10.1016/j.cellsig.2017.01.016

88. Schattauer, S. S., Land, B. B., Reichard, K. L., Abraham, A. D., Burgeno, L. M., Kuhar, J. R., Phillips, P. E. M., Ong, S. E., & Chavkin, C. (2017). Peroxiredoxin 6 mediates Gαi protein-coupled receptor inactivation by cJun kinase. Nature Communications, 8(1), 743. https://doi.org/10.1038/s41467-017-00791-2

89. Schattauer, S. S., Miyatake, M., Shankar, H., Zietz, C., Levin, J. R., Liu-Chen, L.-Y., Gurevich, V. V., Rieder, M. J., & Chavkin, C. (2012). Ligand Directed Signaling Differences between Rodent and Human κ-Opioid Receptors *. *Journal of Biological Chemistry*, *287*(50), 41595–41607. https://doi.org/10.1074/jbc.M112.381368

90. Schenk, S., Partridge, B., & Shippenberg, T. S. (1999). U69593, a kappa-opioid agonist, decreases cocaine self-administration and decreases cocaine-produced drug-seeking. Psychopharmacology, 144(4), 339–346. https://doi.org/10.1007/s002130051016

91. Schindler, A. G., Messinger, D. I., Smith, J. S., Shankar, H., Gustin, R. M., Schattauer, S. S., Lemos, J. C., Chavkin, N. W., Hagan, C. E., Neumaier, J. F., & Chavkin, C. (2012). Stress Produces Aversion and Potentiates Cocaine Reward by Releasing Endogenous Dynorphins in the Ventral Striatum to Locally Stimulate Serotonin Reuptake. Journal of Neuroscience, 32(49), 17582–17596. https://doi.org/10.1523/JNEUROSCI.3220-12.2012

92. Schulteis, G., Yackey, M., Risbrough, V., & Koob, G. F. (1998). Anxiogenic-like effects of spontaneous and naloxone-precipitated opiate withdrawal in the elevated plus-maze. *Pharmacology, Biochemistry, and Behavior*, *60*(3), 727–731. https://doi.org/10.1016/s0091-3057(98)00034-3

93. Schwarzer, C. (2009). 30 years of dynorphins—New insights on their functions in neuropsychiatric diseases. Pharmacology & Therapeutics, 123(3), 353–370. https://doi.org/10.1016/j.pharmthera.2009.05.006

94. Shippenberg, T. S., & Herz, A. (1986). Differential effects of mu and kappa opioid systems on motivational processes. NIDA Research Monograph, 75, 563–566.

95. Smith, C. B., Medzihradsky, F., Hollingsworth, P. J., DeCosta, B., Rice, K. C., & Woods, J. H. (1990). Nor-binaltorphimine is a reversible, noncompetitive opioid antagonist in the mouse vas deferens with high affinity for kappa receptors in monkey brain membranes. Progress in Clinical and Biological Research, 328, 65–68.

96. Smith, J. S., Schindler, A. G., Martinelli, E., Gustin, R. M., Bruchas, M. R., & Chavkin, C. (2012). Stress-Induced Activation of the Dynorphin/κ-Opioid Receptor System in the Amygdala Potentiates Nicotine Conditioned Place Preference. The Journal of Neuroscience, 32(4), 1488–1495. https://doi.org/10.1523/JNEUROSCI.2980-11.2012

97. Stoffel, E. C., Ulibarri, C. M., Folk, J. E., Rice, K. C., & Craft, R. M. (2005). Gonadal Hormone Modulation of Mu, Kappa, and Delta Opioid Antinociception in Male and Female Rats. The Journal of Pain : Official Journal of the American Pain Society, 6(4), 261–274. https://doi.org/10.1016/j.jpain.2004.12.006

98. Sundaramurthy, S., Annamalai, B., Samuvel, D. J., Shippenberg, T. S., Jayanthi, L. D., & Ramamoorthy, S. (2017). Modulation of serotonin transporter function by kappa-opioid receptor ligands. Neuropharmacology, 113, 281–292. https://doi.org/10.1016/j.neuropharm.2016.10.011

99. Tejeda, H. A., Counotte, D. S., Oh, E., Ramamoorthy, S., Schultz-Kuszak, K. N., Bäckman, C. M., Chefer, V., O'Donnell, P., & Shippenberg, T. S. (2013). Prefrontal Cortical Kappa-Opioid Receptor Modulation of Local Neurotransmission and Conditioned Place Aversion. Neuropsychopharmacology, 38(9), 1770–1779. https://doi.org/10.1038/npp.2013.76

100. Terenius, L., & Wahlström, A. (1978). STUDIES ON ENDORPHINS IN MAN. In P. Deniker, C. Radouco-thomas, & A. Villeneuve (Eds.), *Neuro-Psychopharmacology* (pp. 453–458). Pergamon. https://doi.org/10.1016/B978-1-4832-8322-7.50077-7

101. Urban, J. D., Clarke, W. P., von Zastrow, M., Nichols, D. E., Kobilka, B., Weinstein, H., Javitch, J. A., Roth, B. L., Christopoulos, A., Sexton, P. M., Miller, K. J., Spedding, M., & Mailman, R. B. (2007). Functional selectivity and classical concepts of quantitative pharmacology. *The Journal of Pharmacology and Experimental Therapeutics*, *320*(1), 1–13. https://doi.org/10.1124/jpet.106.104463

102. Von Voigtlander, P. F., & Lewis, R. A. (1982). U-50,488, a selective kappa opioid agonist: Comparison to other reputed kappa agonists. Progress in Neuro-Psychopharmacology & Biological Psychiatry, 6(4–6), 467–470. https://doi.org/10.1016/s0278-5846(82)80130-9

103. Walker, B. M., & Koob, G. F. (2008). Pharmacological Evidence for a Motivational Role of κ-Opioid Systems in Ethanol Dependence. Neuropsychopharmacology : Official Publication of the American College of Neuropsychopharmacology, 33(3), 643–652. https://doi.org/10.1038/sj.npp.1301438

104. Walker, B. M., Zorrilla, E. P., & Koob, G. F. (2011). Systemic κ-opioid receptor antagonism by nor-binaltorphimine reduces dependence-induced excessive alcohol self-administration in rats. *Addiction Biology*, *16*(1), 116–119. https://doi.org/10.1111/j.1369-1600.2010.00226.x

105. West, A. M., Holleran, K. M., & Jones, S. R. (2023). Kappa Opioid Receptors Reduce Serotonin Uptake and Escitalopram Efficacy in the Mouse Substantia Nigra Pars Reticulata. International Journal of Molecular Sciences, 24(3), 2080. https://doi.org/10.3390/ijms24032080

106. Windisch, K. A., Morochnik, M., Reed, B., & Kreek, M. J. (2021). Nalmefene, a mu opioid receptor antagonist/kappa opioid receptor partial agonist, potentiates cocaine motivation but not intake with extended access self-administration in adult male mice. *Neuropharmacology*, *192*, 108590. https://doi.org/10.1016/j.neuropharm.2021.108590

107. Windisch, K. A., Reed, B., & Kreek, M. J. (2018). Naltrexone and nalmefene attenuate cocaine place preference in male mice. *Neuropharmacology*, *140*, 174–183. https://doi.org/10.1016/j.neuropharm.2018.07.025

108. Wisler, J. W., DeWire, S. M., Whalen, E. J., Violin, J. D., Drake, M. T., Ahn, S., Shenoy, S. K., & Lefkowitz, R. J. (2007). A unique mechanism of β-blocker action: Carvedilol stimulates β-arrestin signaling. Proceedings of the National Academy of Sciences of the United States of America, 104(42), 16657–16662. https://doi.org/10.1073/pnas.0707936104

109. Yarur, H. E., Casello, S. M., Tsai, V. S., Enriquez-Traba, J., Kore, R., Wang, H., Arenivar, M., & Tejeda, H. A. (2023). Dynorphin / kappa-opioid receptor regulation of excitation-inhibition balance toggles afferent control of prefrontal cortical circuits in a

pathway-specific manner. Molecular Psychiatry, 1–13. https://doi.org/10.1038/s41380-023-02226-5

110. Zhang, S., Tong, Y., Tian, M., Dehaven, R. N., Cortesburgos, L., Mansson, E., Simonin, F., Kieffer, B., & Yu, L. (1998). Dynorphin A as a Potential Endogenous Ligand for Four Members of the Opioid Receptor Gene Family. Journal of Pharmacology and Experimental Therapeutics, 286(1), 136–141.

Carlie Neiswanger

(206) 484-1313

carneis@uw.edu

EDUCATION

2018-2024: University of Washington, Seattle, WA

PhD candidate (Graduation date: June 6, 2024)

Department of Pharmacology, School of Medicine

2017-2018: University of Georgia, Athens, GA

Post-Baccalaureate Research Education Program (PREP) Scholar

Focus: Infectious Diseases

2009-2011, 2014-2017: Washington State University, Pullman, WA

B.S., 5/2017

Majors: Neuroscience, Psychology

PUBLICATIONS

Neiswanger, C., Kimball, K., Ruiz, M.V., Lee, J., Land, B., Berndt, A., & Chavkin, C. Microdosing G-biased Partial Agonists Inactivates Kappa Opioid Receptors - an alternative strategy for human trials. (2024) (in preparation).

J. D. Lee, Y. Wang, A. Nguyen, **C. Neiswanger**, S. S. Schattauer, F. Yeboah, S. Zuniga, S. Wait, M. Rappleye, S. Bremner, C. Chun, K. Evitts, A. S. T. Smith, D. L. Mack, J. E. Young, C. I. Chavkin, A. Berndt. Structure-guided design of sensitive genetically encoded peroxide indicator with subsecond response kinetics for continuous and non-continuous detection of intracellular peroxide level. (2024) (in preparation).

Fontaine HM, Silva PR, **Neiswanger C**, Tran R, Abraham AD, Land BB, Neumaier JF, Chavkin C. Stress decreases serotonin tone in the nucleus accumbens in male mice to

promote aversion and potentiate cocaine preference via decreased stimulation of 5-HT_{1B} receptors.
Neuropsychopharmacology. 2022 Mar;47(4):891-901. doi: 10.1038/s41386-021-01178-0. Epub 2021 Sep 25. PMID: 34564712.

Luczo JM, Bousse T, Johnson SK, Jones CA, Pearce N, **Neiswanger CA**, Wang MX, Miller EA, Petrovsky N, Wentworth DE, Bronshtein V, Papania M, Tompkins SM. Intranasal powder live attenuated influenza vaccine is thermostable, immunogenic, and protective against homologous challenge in ferrets. NPJ Vaccines. 2021 Apr 21;6(1):59. doi: 10.1038/s41541-021-00320-9. PMID: 33883559; PMCID: PMC8060263.

CONFERENCE PRESENTATIONS

Neiswanger, C., Kimball, K., Ruiz, M.V., Lee, J., Berndt, A., & Chavkin, C., (2023) Microdosing Partial Agonists Inactivates Kappa Opioid Receptors - An Alternative Strategy for Human Trials (poster). Annual Meeting of the American College of Neuropsychopharmacology, Tampa, FL.

J. D. Lee, Y. Wang, A. Nguyen, **C. Neiswanger**, S. S. Schattauer, F. Yeboah, S. Zuniga, S. Wait, M. Rappleye, S. Bremner, C. Chun, K. Evitts, A. S. T. Smith, D. L. Mack, J. E. Young, C. I. Chavkin, A. Berndt (2022) oRos: a comprehensive suite of fast and sensitive optogenetic H2O2 sensors for the in situ monitoring of redox signaling and oxidative stress in neurons. (Abstract) Society for Neuroscience annual meeting, San Diego, CA.

Neiswanger, C.A., Schattauer, S., Kimball, K., Ruiz, M.V., Lee, J., Berndt, A., & Chavkin, C., (2022) Kappa Receptor Partial Agonists Inactivate KOR through a JNK/ROS Mechanism (talk). Conference on the Therapeutic Potential of Kappa Opioids, Bethesda, MD.

Neiswanger, C.A., Schattauer, S., Kimball, K., Tran, R., Lee, J., Berndt, A., & Chavkin, C., (2022). Kappa opioid receptor partial and biased agonists inactivate KOR through a JNK/ROS mechanism (poster). International Narcotics Research Conference, Valencia, Spain.

Neiswanger, C.A., Schattauer, S., Kimball, K., Tran, R., Lee, J., Berndt, A., & Chavkin, C., (2022). Exploration of kappa opioid receptor signaling (talk). Center for Excellence in Neurobiology of Addiction, Pain, and Emotion, Seattle, WA.

Neiswanger, C.A., Luczo, J. M., & Tompkins, S.M. (2018). Pathogenesis of a novel avian influenza A virus, A/New York/108/2016 (H7N2) (poster). Molecular Parasitology & Vector Biology Symposium by the Center for Tropical and Emerging Global Diseases, Athens, GA.

Neiswanger, C.A., Luczo, J. M., & Tompkins, S.M. (2018). Pathogenesis of a novel avian influenza A virus, A/New York/108/2016 (H7N2) (poster). American Society for Microbiology Microbe, Atlanta, GA.

Knox, C.A. & Craft, R.M. (2017). Sex differences in opioid-cannabinoid interactions on chronic inflammatory pain (poster). Showcase for Undergraduate Research and Creative Activities, Pullman, WA.

Knox, C.A. & Craft, R.M. (2016). Sex differences in opioid-cannabinoid interactions on chronic inflammatory pain (poster). Annual Biomedical Research Conference for Minority Students, Tampa, FL.

(Knox was my name before marriage)

GRANTS AND FELLOWSHIPS

2019-2022, National Institute on Drug Abuse T32 (T32DA007278)

2016, WSU Alcohol and Drug Abuse Research Program undergraduate research fellowship, $2,700

2015, WSU Psychology Department Undergraduate Research Initiative Grant, $750

AWARDS

2023, Conference on the Therapeutic Potential of Kappa Opioids Travel Award

2022, International Narcotics Research Conference Travel Award

2016, Annual Biomedical Research Conference for Minority Students Presentation Award (category: neuroscience)

2016, Annual Biomedical Research Conference for Minority Students Travel Award

---

RESEARCH

Sept 2018- June 2024 **Graduate Student**

Department of Pharmacology, School of Medicine, University of Washington, Seattle, WA

- Behavioral research in mouse models of depression, chronic stress, and addiction
- Ex vivo slice imaging (2p and light microscopes), voltammetry
- Survival viral injections and cannula placement surgeries in multiple brain areas
- Fiber photometry
- Mentorship of undergraduate, post-bac, and junior graduate students
- Mentors: Dr. Charles Chavkin, Dr. Benjamin Land

Aug 2017- July 2018 **PREP Scholar, Post-Bac Research Assistant**

Department of Infectious Disease, Center for Vaccines and Immunology, College of Veterinary Medicine, University of Georgia, Athens, GA

- Participation in the Emory-UGA Center of Excellence for Influenza Research and Surveillance (NIAID-CEIRS)
- Influenza A environmental stability study
- Murine in vivo study investigating pathogenesis and pathology of a human influenza isolate
- Training in mouse handling, cell culture, RNA extraction and amplification, PCR, reverse genetics, egg-grown virus, and aseptic technique
- Multiple manuscripts in progress
- Mentors: Dr. Mark Tompkins, Dr. Jasmina Luczo

Oct 2014- July 2017 **Research Assistant**

Department of Integrated Physiology and Neuroscience, Department of Psychology, College of Veterinary Medicine, Washington State University, Pullman, WA

- Psychopharmacology research in rat models focusing on sex differences and pain
- Study of affective pain and reversal of pain-suppressed behavior via pharmacologic intervention
- Interactions between and effects of opioids and cannabinoids on chronic pain
- Training in rat handling, injections (intraperitoneal, subcutaneous, and intraplantar), survival surgery (gonadectomy), graphing (Sigma Plot), and statistical analysis (SPSS).
- Manuscript in progress
- Mentor: Dr. Rebecca M. Craft

PROFESSIONAL ACTIVITIES AND DEVELOPMENT

Aug 2021- Present **Undergraduate/Post-bac Mentorship**

- Training in various lab techniques, data collection and analysis
- Preparation and application to graduate programs
- Preparation of weekly lab meeting data presentation
- Lead an undergrad-focused journal club

Summer 2019, 2022 **Undergraduate Professional Development panels**

- Design and participate in presentation and Q&A
- Summer program in the NAPE center with a focus on DEI students

July 2019- Present **Pharmacology Equity, Diversity, and Inclusion (PEDI) Committee Member**

- Participate in monthly meetings
- Plan and organize events for graduate student recruitment
- Create actionable items to increase EDI awareness and membership in the department

Sept 2019- March 2020 **Teaching Assistant, Intro Pharmacology**

- Designing and presenting review lectures
- Creating and administering quizzes
- Aiding pharmacy students in gaining a deeper understanding of pharmacology

Aug 2016- May 2017 **Peer Mentor**

Department of Psychology, Washington State University, Pullman, WA

- Mentor freshmen and sophomore undergraduates in the psychology program
- Office hours once a week to help students with class work and successful navigation of the psychology major
- Presentations on how to be a successful student and how to prepare for life after undergraduate work
- Program coordinators: Dr. Dee Posey, Amy Nusbaum, MS

Aug 2016-May 2017 Teaching **Assistant, Introductory Psychology**

Department of Psychology, Washington State University, Pullman, WA

- Proctor and grade exams (written and multiple choice)
- Grade writing assignments with constructive feedback on content, citations, and style
- Program Coordinator: Dr. Samantha Swindell
